

Antimicrobial properties of Ag zeolites and Ag zeolite containing polymers

Sama Salem Belkhair



Manchester
Metropolitan
University

Antimicrobial properties of Ag zeolites
and Ag zeolite containing polymers

Sama Salem Belkhair

*Submitted in the partial fulfilment of the
requirements of Manchester Metropolitan
University for the degree of Doctor of
Philosophy*

Faculty of Science and the Environment
The Manchester Metropolitan University
2016

Declaration

This is a declaration to certify that the material contained in this thesis has not been accepted in substance for any other degree and it is not currently submitted in candidature for any other academic award.

Sama Salem Belkhair

Abstract

Ag zeolites have been studied in this thesis for antibacterial applications in powder form or in composite materials. The influence of the textural characteristics (crystal size and mesoporosity) of silver-exchanged FAU- and BEA-type zeolites on their antimicrobial efficacy was studied. Two pairs of zeolite X and zeolite beta with different sizes as well as a mesoporous zeolite beta were tested against *Escherichia coli* (*E. coli*) and *Candida albicans* (*C. albicans*). Reduction of crystal size resulted in a slight decrease in the killing efficacy against both microorganisms. Zeolite beta showed higher activity than zeolite X despite the lower Ag content in that sample, which was attributed to the higher concentration of silver released from zeolite beta samples to the medium. Introduction of mesoporosity had a beneficial effect on the antimicrobial efficacy. Cytotoxicity measurements using peripheral blood mononuclear cells indicated that Ag zeolite X was more toxic compared to Ag beta, particularly the nanosized sample.

The influence of the form of silver (metallic or ionic) on the antimicrobial efficacy was determined using Ag-loaded EMT zeolites. The killing efficacy of pure EMT, Ag⁺-EMT and Ag⁰-EMT against *E. coli* was studied semi-quantitatively. The antibacterial activity increased with increasing Ag content for both types of samples (Ag⁺-EMT and Ag⁰-EMT). The Ag⁰-EMT samples show slightly enhanced antimicrobial efficacy compared to that of Ag⁺-EMT, however, the differences are not substantial and the preparation of Ag nanoparticles is not viable considering the complexity of preparation steps.

A multidisciplinary approach has been applied to the preparation of antibacterial Ag zeolite/silicone elastomer composites aimed at products that satisfy a range of requirements, namely good mechanical properties after zeolite

incorporation and strongly antibacterial. The composites showed strong efficacy against *E. coli* and *Staphylococcus epidermidis* (*S. epidermidis*). Organic functionalisation of the zeolite with organo-silanes prior blending with the matrix usefully improved composite mechanical properties and reduced colour development in Ag zeolite containing silicone elastomers.

The same approach was applied for the preparation of dental acrylic resins. Antibacterial dental resin containing Ag zeolites at loadings of 0.2, 0.4, 0.7 and 2 wt.% were prepared. The composites showed strong efficacy against *E. coli* and no viable *E. coli* were detected after 5 hours of incubation. The presence of Ag zeolites within the acrylic resin resulted in resin discolouration, which was more pronounced at high Ag zeolite loadings. A sustained Ag release over long periods of time (54 days) was observed with a greater Ag release in artificial saliva compared to that in distilled water. Dental resins loaded with Ag-free zeolites followed by post-fabrication insertion of Ag by ion-exchange were prepared to overcome discolouration. The materials prepared using this approach had a similar colour to that of the original polymer as determined by the colour measurements. These composites showed strong efficacy against *E. coli* and no viable *E. coli* cells were detected after 5 hours of incubation.

Acknowledgments

There are many people who have helped and supported me during this work and to whom I owe a great deal of thanks. Firstly, I would like to express my sincere gratitude to my Director of Studies Dr. Lubomira Tosheva for giving me the opportunity to undertake this project. Her support and guidance through this project has been invaluable. I would also like to thank my co-supervisors Dr. Christopher Liauw and Professor Joanna Verran for their help and the expert knowledge they have brought to the research. I would also like to thank my parents Mufeda Gadour and Salem Belkhair for all the love, care and continuous encouragement. I would not have succeeded in completing this research without your support. Thank you. This one is for both of you! Finally, special thanks goes to my husband Seraj Ellafi and my siblings Mohammed, Mustafa, Sarean and Moadd Belkhair for all your love, guidance, patience, support and prayers throughout my work

Table of contents

Declaration	3
Abstract	4
Acknowledgments	6
Table of Contents	7
List of Figures	12
List of Tables	18
List of Abbreviations	20
Chapter 1. Introduction	23
1.1. Zeolites	23
1.2. Synthesis of nanozeolites	25
1.3. Synthesis of hierarchical zeolites	27
1.4. Silver as antimicrobial agent	29
1.5. Antimicrobial applications of Ag zeolites	30
1.6. Antimicrobial composites containing zeolites	34
1.7. Silicone elastomers	35
1.8. Dental acrylic resins	36
1.9. Antimicrobial composites	38
1.9.1. Antibacterial silicone elastomers	38
1.9.2. Antibacterial dental acrylic resins	39

1.10. Zeolite functionalisation	40
1.11. Characterisation methods	41
1.11.1. Scanning electron microscopy	41
1.11.2. Energy-dispersive X-ray spectroscopy	43
1.11.3. X-ray diffraction	43
1.11.4. Gas adsorption	44
1.11.5. Fourier transform infrared spectroscopy	46
1.11.6 Raman spectroscopy	46
1.11.7. Dynamic light scattering	48
1.11.8. Thermogravimetric Analysis	48
1.11.9. ICP-AES	49
1.11.10. Mechanical testing	49
1.12. Microorganisms and methods for determination of the antibacterial activity	50
1.12.1. Gram-positive bacteria	51
1.12.2. Gram-negative bacteria	51
1.12.3. Fungi	52
1.12.4. Bacterial growth	53
1.12.5. Methods for determination of the antibacterial activity	54
1.12.5.1 Viable plate count method	54

1.12.5.2 Minimum inhibitory and minimum bactericidal concentration	55
1.12.5.3 Cytotoxicity tests	55
1.13. Aims and objectives	57
1.13.1 Aims	57
1.13.2 Objectives	57
Chapter 2. Experimental	58
2.1. Synthesis of zeolites	58
2.1.1 Synthesis of zeolite X	58
2.1.2 Synthesis of zeolite beta	58
2.1.3 Synthesis of EMT zeolites	59
2.2. Preparation of Ag zeolites	60
2.2.1 Ag-X and Ag-beta zeolites	60
2.2.2 Ag-EMT zeolites	61
2.3. Functionalised Ag-zeolites	61
2.4. Synthesis of polymer composites	62
2.4.1 Silicone elastomers	62
2.4.2 Dental acrylic resins	62
2.5 Antimicrobial tests	64
2.5.1 Antimicrobial activity of Ag-zeolites (X and beta)	64
2.5.2 Cytotoxicity tests	66

2.5.3 Antimicrobial activity of Ag-zeolites composites	67
2.5.4 Ag release of silicone elastomers loaded with AgX zeolite	69
2.5.5 Ag release of dental resins loaded with AgX zeolite	69
2.5.6 Charging of preformed dental acrylic composites with silver	70
2.5.7 Ag release of charged NaX dental acrylic components with silver	70
2.6 Characterisation methods	71
2.6.1 Zeolite characterisation	71
2.6.2 Polymer characterisation	73
Chapter 3. Results and discussion	75
3.1. Ag zeolite powders and their antimicrobial efficacy	75
3.1.1 The antimicrobial properties of Ag ⁺ -EMT and Ag ⁰ -EMT zeolites	75
3.1.2 Conclusions	81
3.2. Influence of the zeolite textural characteristics on the antimicrobial efficacy of Ag-zeolites	81
3.2.1 Zeolite characteristics	82
3.2.2 Cytotoxicity tests	90
3.2.3 Antimicrobial tests	92
3.2.4 Conclusions	99
3.3. Silver zeolite-loaded silicone elastomers	99
3.3.1 Zeolite characteristics	100
3.3.2 Silicone elastomers	111

3.3.3 Antimicrobial assessment of silicone elastomers loaded with AgX	115
3.3.4 Conclusions	120
3.4. Silver zeolite-loaded dental acrylic resins	122
3.4.1 Dental acrylic resins	122
3.4.2 Antimicrobial testing of dental acrylic samples	125
3.4.3 Ag charged NaX dental acrylic samples	132
3.4.4 Conclusions	136
Chapter 4. Conclusions	137
Chapter 5. Future work	139
References	141
Appendices	150
Appendix 1 Publications and presentations based on the results presented in this thesis	150
Appendix 2 Paper 1	151
Appendix 3 Paper 2	152

List of Figures

Figure 1. Framework structures of zeolite FAU, EMT and BEA.

Figure 2. The chemical structure of 3-(Trimethoxysilyl)propyl methacrylate.

Figure 3. The chemical structure of vinylsilane.

Figure 4. Overview of the different signals generated when an electron beam interacts with a specimen.

Figure 5. The diffraction of X-rays (constructive interference).

Figure 6. The five types of adsorption isotherms; a is the amount of gas adsorbed and P/P_0 is the partial pressure.

Figure 7. Schematic illustration of the Rayleigh, Stokes and Anti-Stokes scattering processes.

Figure 8. Tensile stress-strain diagram.

Figure 9. Growth curve for bacteria with its four distinct phases, Lag (A), Log (B), stationary (C), and death (D).

Figure 10. Spot inoculation of *E. coli* (in duplicate) onto thio-neutralising agar (left) and nutrient agar (right) at 1 minute intervals, following exposure to Ag-free EMT zeolite (control). Each sector corresponds to one minute sampling time; the first sample is taken directly after mixing (0 min).

Figure 11. Spot inoculation of *E. coli* onto thioglycollate agar plates (in duplicate) following 1 minute interval exposure to Ag^+ -EMT and Ag^0 -EMT zeolite samples. Each sector above corresponds to one minute sampling time; the first sample is taken directly after mixing (0 min).

Figure 12. Spot inoculation of *E. coli* onto thioglycollate agar plates (in duplicate) following 1 minute interval exposure to Ag⁺-EMT and Ag⁰-EMT zeolite samples. Each sector above corresponds to one minute sampling time; the first sample is taken directly after mixing (0 min).

Figure 13. Spot inoculation of *E. coli* onto thioglycollate agar plates (in duplicate) following 1 minute interval exposure to Ag⁺-EMT and Ag⁰-EMT zeolite samples. Each sector above corresponds to one minute sampling time; the first sample is taken directly after mixing (0 min).

Figure 14. SEM images of (a) X1, (b) X2, (c) B1, (d) B2 and (e) B3 samples.

Figure 15. DLS particle size distribution for samples B1 and B2.

Figure 16. XRD patterns of the zeolites X and beta used in this work.

Figure 17. Nitrogen adsorption isotherms of zeolites X.

Figure 18. Nitrogen adsorption isotherms of caclined zeolites beta.

Figure 19. Cytotoxic effect of silver zeolite samples of different concentrations on freshly isolated cultured PBMCs. Asterisks (*) indicate significant differences in comparison with the control (* $p < 0.05$, ** $p < 0.01$, *** $p < 0.001$).

Figure 20. Spot inoculation of *C. albicans* (left) and *E. coli* (right) onto thioglycollate agar plates (in duplicate) following 1 minute interval exposure to the Ag free zeolite samples. Each sector on the plates above corresponds to one minute sampling time; the first sample (top) is taken directly after mixing (0 min).

Figure 21. Spot inoculation of *E. coli* onto thioglycollate agar plates (in duplicate) following 1 minute interval exposure to X1 (a), X2 (b), B1 (c), B2 (d) and B3 (e) zeolite samples at concentration of 0.5 mg/ml. Each sector on the plates above

corresponds to one minute sampling time; the first sample (top) is taken directly after mixing (0 min).

Figure 22. Spot inoculation of *C. albicans* onto thioglycollate agar plates (in duplicate) following 1 minute interval exposure to X1 (a), X2 (b), B1 (c), B2 (d) and B3 (e) zeolite samples at concentration of 0.1 mg/ml. Each sector on the plates above corresponds to one minute sampling time; the first sample (top) is taken directly after mixing (0 min).

Figure 23. Spot inoculation of *E. coli* onto thioglycollate agar plates (in duplicate) following 1 minute interval exposure to X1 (a), X2 (b), B1 (c), B2 (d) and B3 (e) zeolite samples at concentration of 0.05 mg/ml. Each sector on the plates above corresponds to one minute sampling time; the first sample (top) is taken directly after mixing (0 min).

Figure 24. Spot inoculation of *C. albicans* onto thioglycollate agar plates (in duplicate) following 1 minute interval exposure to X1 (a), X2 (b), B3 (c), B4 (d) and B5 (e) zeolite samples at concentration of 0.5 mg/ml. Each sector on the plates above corresponds to one minute sampling time; the first sample (top) is taken directly after mixing (0 min).

Figure 25. SEM images at two different magnification of (a and c) zeolite Na-X and (b and d) typical SEM images of organically modified AgX crystals.

Figure 26. XRD patterns of Na-X and Ag-containing zeolite. Miller indices are given in *Fd3m*.

Figure 27. Nitrogen adsorption/desorption isotherms at -196 °C of NaX and Ag-containing zeolites.

Figure 28. DRIFTS spectra of Na-X, Ag-X, Ag-X/M and Ag-X/V zeolites demonstrating the structure remained unchanged confirming preservation of the zeolite structure in the modified samples.

Figure 29. Digital images of: Left) V-AgX in distilled water and Right) V-AgX in chloroform showing dispersion of the vinylsilane modified zeolite in chloroform.

Figure 30. a) Raman spectra of NaX, AgX, V-AgX and M-AgX; spectra are vertically offset for clarity. The arrows mark the additional peaks observed in all Ag-exchanged samples. b) Position and FWHM of the strong peak near 510 cm^{-1} as determined by fitting the spectra.

Figure 31. TGA curves of NaX and AgX samples.

Figure 32. Far-IR absorption spectra of zeolite X (NaX) and Ag-exchanged zeolite X (AgX) as well as of reference mechanical mixtures of zeolite X with 10 wt.% Ag(I) oxide (NaX + 10 wt.% Ag_2O) and Ag(II) oxide (NaX + 10 wt.% AgO). The arrows mark the spectral bands that can discriminate monovalent and divalent Ag^{n+} . Spectra are vertically offset for clarity.

Figure 33. Digital images of silicone elastomers containing NaX, AgX, M-AgX and V-AgX zeolites. The middle image shows the neat SE. The arrows point to zeolite aggregates present in samples NaX/SE and AgX/SE.

Figure 34. Typical SEM images of cryo-fractured surfaces of SE/zeolite composite containing: (a) unmodified zeolite (NaX or AgX) and (b) organo-silane modified Ag zeolite (M-AgX and V-AgX gave similar images).

Figure 35. Antimicrobial testing of Silicone elastomer (Si elastomer), NaX/SE (zeolite), AgX/SE (Ag-zeolite), V-AgX/SE (V) and M-AgX/SE (M) against *E. coli*.

Figure 36. Antimicrobial testing of Silicone elastomer (Si elastomer), NaX/SE (zeolite), AgX/SE (Ag-zeolite), V-AgX/SE (V) and M-AgX/SE (M) against *S. epidermidis*.

Figure 37. Antimicrobial testing of Silicone elastomer (Si elastomer), NaX/SE (zeolite), AgX/SE (Ag-zeolite), V-AgX/SE (V) and M-AgX/SE (M) against *C. albicans*.

Figure 38. Digital images DA acrylic resins; from left to right: DA (control), DA containing Ag-zeolite at 0.2 wt.% loading, DA containing Ag-zeolite at 0.4 wt.%, DA containing Ag-zeolite at 0.7 wt.% and DA containing Ag-zeolite at 2 wt.% loading.

Figure 39. Antimicrobial testing of DA (Dental resin), DA / Ag-X (2 wt.%), DA / Ag-X (0.7 wt.%), DA / Ag-X (0.4 wt.%), and DA / Ag-X (0.2 wt.%) against *E. coli*, demonstrating the successful conferment of antimicrobial activity to the DA after addition of the silver.

Figure 40. Antimicrobial testing of DA (Dental resin), DA / Ag-X (2 wt.%), DA / Ag-X (0.7 wt.%), DA / Ag-X (0.4 wt.%), and DA / Ag-X (0.2 wt.%) against *C. albicans*.

Figure 41. Ag release of DA and DA containing Ag-zeolite in 20 ml distilled water

Figure 42. Ag release of DA and DA containing Ag-zeolite in 20 ml artificial saliva

Figure 43. Colour measurement test of DA and DA containing Ag-zeolite before and after Ag release test.

Figure 44. Antimicrobial testing of DA (Dental resin), DA / Ag-X (2 wt.%), DA / Ag-X (0.7 wt.%), DA / Ag-X (0.4 wt.%), and DA / Ag-X (0.2 wt.%) against *E. coli*, after 54 days submersion in distilled water.

Figure 45. Viable bacterial cell counts of *E. coli* in the presence of DA and DA containing zeolite-silane charged from AgNO₃ solution.

Figure 46. Digital image of DA acrylic resins; from left to right: DA (control), DA containing zeolite-silane at 2 wt.% loading (before charging) and c) DA containing zeolite-silane at 2 wt.% loading (after charging).

List of Tables

Table 1. Summary of experimental procedures used, concentrations, Ag wt.% and microorganisms tested in antimicrobial testing of Ag-zeolites.

Table 2. Synthesis conditions for the zeolites used in this work.

Table 3. Summary of polymer composites.

Table 4. Summary of concentrations used in Ag-zeolite (zeolite = X or beta) antimicrobial tests.

Table 5. ICP results of Ag⁺-EMT and Ag⁰-EMT samples.

Table 6. Gas adsorption data for Ag⁺-EMT and Ag⁰-EMT samples.

Table 7. Crystal sizes of the zeolites used determined by SEM.

Table 8. EDX results of zeolites.

Table 9. EDX results of Ag-zeolite.

Table 10. BET surface area (S_{BET}), micropore volume (V_{μ}), mesoporous volume (V_{meso}) and external surface (S_{ext}) of the Ag zeolite samples used.

Table 11. Ag released (ppm) after the 7-minute tests using *E. coli*.

Table 12. Ag content, BET surface area (S_{BET}), micropore volume (V_{μ}) and external surface area (S_{EXT}) of zeolite and modified zeolite samples.

Table 13. Mechanical testing data of SE samples prepared in this work.

Demonstrating no deterioration in the mechanical properties of composite samples compared to these of the neat silicone elastomer was observed.

Table 14. The interaction between the interfaces can be explained from their Swelling degree of: (a) Silicone, (b) Silicone/Na-X, (c) Silicone/Ag-X, (d) Silicone/Ag-X/M and (e) Silicone/Ag-X/V.

Table 15. Colour measurement test of DA and DA containing Ag-zeolite.

Table 16. Mechanical properties of the dental acrylic resin samples prepared.

Table 17. Colour measurement test of DA and DA containing Ag-zeolite before and after Ag release test.

Table 18. Ag release of DA and DA containing zeolite-silane charged from AgNO_3 solution in 20 ml distilled water.

Table 19. Colour measurement test of DA and DA containing zeolite-silane before and after charging from AgNO_3 solution.

List of Abbreviations

AgX/DA	Dental acrylic containing Ag-zeolite
AgX/SE	Silicone elastomer containing Ag-zeolite
BDDT	Brunauer, Deming, Deming and Teller (BDDT) system
BEA	A three-letter code describing the zeolite Beta structure
BET	Brunauer-Emmett-Teller
BJH	Barrett-Joyner-Halenda Analysis
<i>C. albicans</i>	<i>Candida albicans</i>
CFU	Colony Forming Units
CRT	Cathode ray tube
DA	Dental acrylic
DA / Ag-X (0.2 wt.%)	Dental acrylic containing functionalised Ag-zeolite at 0.2 wt.% loading
DA / Ag-X (0.4 wt.%)	Dental acrylic containing functionalised Ag-zeolite at 0.4 wt.% loading
DA / Ag-X (0.7 wt.%)	Dental acrylic containing functionalised Ag-zeolite at 0.7 wt.% loading
DA / Ag-X (2 wt.%)	Dental acrylic containing functionalised Ag-zeolite at 2 wt.% loading
DA/ zeolite-silane (1 wt.%)	Dental acrylic containing functionalised zeolite X at 1 wt.% loading

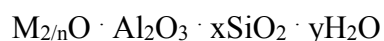
DA/ zeolite-silane (2 wt.%) functionalised zeolite X at 2 wt.% loading	Dental acrylic containing
DLS	Dynamic light scattering
DRIFTS	Diffuse reflectance infrared Fourier transform spectroscopy
<i>E. coli</i>	<i>Escherichia coli</i>
EDS	Energy-dispersive X-ray spectroscopy
EMT	A three-letter code describing the zeolite EMT structure
FAU	A three-letter code describing the zeolite X structure
FTIR	Fourier transform infrared spectroscopy
HTV	High temperature vulcanization
IR	Infrared spectroscopy
IUPAC	International union of pure and applied chemistry
M-AgX/SE zeolite X at 2 wt.% loading	Silicone elastomer containing functionalised methacrylate silane
MMMs	Mixed matrix membranes
MTW	A three-letter code describing the zeolite MTW structure
NaX/DA	Dental acrylic containing zeolite X at 2 wt.% loading
NaX/SE	Silicone elastomer containing zeolite X at 2 wt.% loading
NIOSH	National Institute for Occupational Safety and Health
REL	Recommended Exposure Limit

RTV	Room temperature vulcanization
<i>S. epidermidis</i>	<i>Staphylococcus epidermidis</i>
SE	Silicone elastomer
SEM	Scanning electron microscopy
TGA	Thermogravimetric analysis
V-AgX/SE	Silicone elastomer containing functionalised vinylsilane zeolite
X at 2 wt.% loading	
XRD	X-ray diffraction

Chapter 1. Introduction

1.1 Zeolites

Zeolites are naturally occurring aluminosilicate minerals firstly discovered by Alex Cronstedt in 1756.^{1, 2} Their name originates from the classic Greek words meaning boiling stone, describing Cronstedt's observation of steam formation upon gently heating the mineral stilbite. There are more than 45 natural zeolites (e.g. clinoptilolite), and 229 synthetic zeolites to date.³ Based on pore diameters, materials are classified according to the International Union of Pure and Applied Chemistry (IUPAC) as microporous (less than 2.0 nm), mesoporous (between 2.0 nm and 50 nm) and macroporous (more than 50 nm).⁴ Zeolites are microporous materials with pore sizes in the range 0.3-1.2 nm. They are built of oxygen-linked tetrahedral units of Si⁴⁺ or Al³⁺ that form a three-dimensional structure comprising channels and voids occupied by alkali or alkali-earth cations and water molecules. Zeolites may be represented by the empirical formula



In this formula, M is the counterion, n is the valence of the cation, x is the SiO₂/Al₂O₃ and y is the number of molecules per unit cell in the hydrated zeolite. Zeolites are classified according to their framework structure with a unique three-letter code, which is not related to their composition. For example, zeolites X and Y have different Si/Al ratio but the same FAU-type structure. Zeolite X has lower Si/Al ratio and correspondingly higher ion-exchange capacity in comparison with zeolite Y. Other zeolite structures used in this work are the BEA-type (zeolite beta) and the EMT-type (EMT) zeolites. Based on the Si:Al ratio the zeolite compound is further categorised as low Si:Al zeolite, like zeolite X, intermediate Si:Al zeolite e.g.

mordenite and high Si:Al zeolite like zeolite beta.⁵ In addition to this, zeolites are further sub-divided based on the number of T atoms present, where T is Si or Al. Depending on the zeolite pore openings, they are classified as small pore opening zeolites (8-member ring), medium or intermediate pore opening zeolites (10 member ring) and large pore opening zeolites (12 member ring).⁶ For instance, the zeolite beta pore structure is characterised with a three dimensional system having 12 member ring channels ($5.5 \times 5.5 \text{ \AA}$ and $7.6 \times 6.4 \text{ \AA}$). Other examples of large pore zeolites are FAU- and EMT-type zeolites. EMT-zeolite is considered as the hexagonal form of FAU zeolite.⁷ The structural feature of EMT zeolite represent two distinct cage like structures also known as the hypercages ($7.3 \times 7.3 \text{ \AA}$) and hypocages ($7.5 \times 6.5 \text{ \AA}$), on the other hand only one supercage with a size of $7.4 \times 7.4 \text{ \AA}$ is observed in the case of FAU-zeolite.^{8,9}

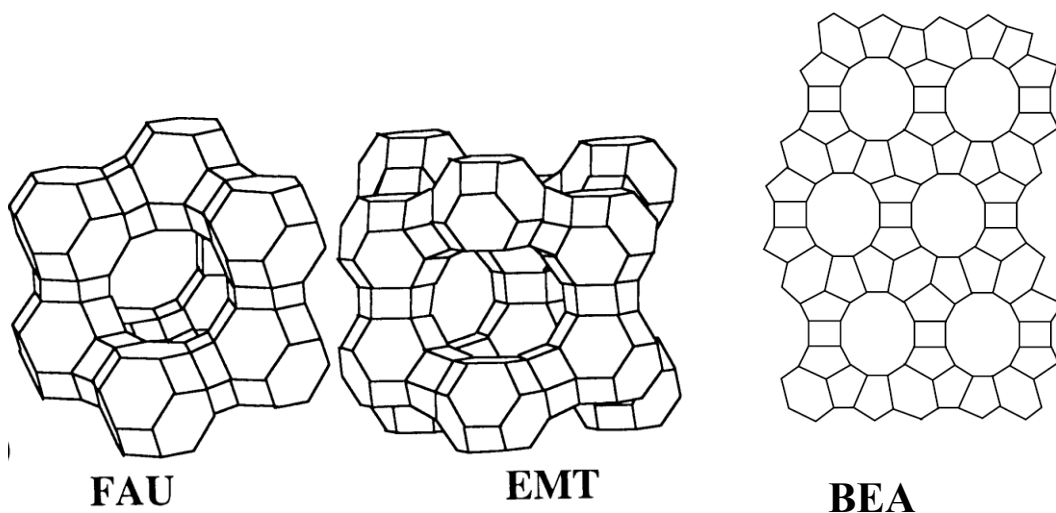


Figure 1. Framework structures of zeolite FAU, EMT and BEA.¹⁰

Zeolites are synthesised by hydrothermal treatment of reactive aluminosilicate gels or solutions in a basic environment. Zeolite syntheses are generally conducted at temperatures between $100\text{-}200 \text{ }^\circ\text{C}$ in stainless steel autoclaves. Crystallisation times vary from hours to days. Sometimes, organic

molecules such as tertaalkylammonium cations are added to act as structure-directing agents or templates in the synthesis of zeolites. Calcination at high temperatures (500 °C) for several hours is applied to remove the templates and result in opening of the zeolite pore structure. The zeolite crystallisation involves two steps: nucleation and crystallisation. Nucleation is a process, where small aggregates of precursors give rise to nuclei, which become larger with time.¹¹⁻¹⁵ Crystallisation is the formation of the zeolite crystals. The main factors affecting zeolite formation include temperature, time, composition of reactant mixture and nature of precursors. Zeolite traditional applications include ion exchange, adsorption and catalytic processes. The counter cations for instance can be ion-exchanged by other cations, which is used in laundry detergents to soften water (to remove Ca^{2+} and Mg^{2+} cations).¹

In the past two decades, there have been significant efforts to develop synthetic methods for: (i) preparing zeolites with crystal sizes of less than 100 nm (nanozeolites) and (ii) hierarchical zeolites containing secondary porosity in the meso/macro pore range.¹⁶⁻²⁵ Nanozeolites comprise one of the major developments in the zeolite area since their first synthesis in the early 1990s.²² Nanozeolites exhibit large external surface area and reduced diffusion paths compared to micron sized zeolites.^{19, 26-28} There are examples of their superior performance compared to conventional micron-sized zeolites in traditional applications such as catalysis.²⁹ In addition, they have shown potential for many emerging applications.³⁰

1.2 Synthesis of nanozeolites

Conventionally, zeolites are prepared in the form of micron sized crystals. After understanding the potential of micron sized zeolites in the petrochemical industry, there were great efforts conducted to modify the characteristics of existing zeolite

materials to enhance performance. Reduction of zeolite sizes is amongst the most important and most studied approaches. Increasing the relative surface area by decreasing the particle size for example, increases the percentage of surface atoms exposed and reduces diffusion paths.¹⁹ Nanosized zeolites in the form of stable colloidal suspensions were first prepared in 1993 in the presence of structure-directing agents.³¹ Since then, intense research in the area of nanozeolites has been conducted to prepare nanozeolites of different zeolite types. However, the number of different zeolites prepared in nanoform is somewhat limited, and most synthesis techniques use templates, which are not industrially friendly due to their high costs.

FAU-type zeolites are commonly used in the petrochemical industry and therefore it is vital to develop industrially favourable methods to obtain FAU-type nanozeolites.¹⁴ Previously, FAU nanocrystals were prepared by the addition of tetramethylammonium hydroxide and 15-crown-5 ether along with a reduced sodium oxide content.^{32, 33} Eliminating the use of organic templates gives rise to more efficient green synthesis methods. Nanosized zeolite X crystals with a size of 150 to 200 nm were synthesized at room temperature in the absence of organic template for the duration of 3 weeks.¹⁴ However, these crystals were aggregated due the increased sodium content. A template free synthesis method using a reactive gel system with a three stage temperature control procedure, nanosized zeolite Y with a 850 nm diameter was achieved.³⁴ In another work with a two stage crystallisation, zeolite Y with a size of 120-200 nm were synthesised using a template free approach. Kim *et al.* synthesised relatively small zeolite Y particles with a template free, shorter crystallisation times and optimised gel compositions.³⁵ FAU nanocrystal with a particle size below 100 nm were synthesised using a structure directing agent.³⁶

Similarly to FAU-type zeolite, EMT zeolites could be used as catalysts in the petroleum industry but high cost is a major obstacle for the preparation EMT zeolites.^{37, 38} Traditionally, EMT-type zeolites are prepared by the addition of an expensive structure directing agent, namely 18-crown-6 ether. Recently, a template free approach was developed for the synthesis of nanosized EMT zeolites.³⁹ EMT zeolites with a size of 50- 70 nm were synthesised under ambient conditions at 30 °C.

BEA-type zeolites also play an important role in catalysis. Traditionally, the synthesis of zeolite BEA involves the use of structure-directing agents such as tetraethylammonium.^{40, 41} An alternative structure-directing agent used in BEA synthesis is 4,4'-trimethylenebis(N-methyl-N-benzylpiperidinium).⁴² Altering the Si/Al ratio in the aluminium silicate gel from 14 to 42 yielded nanosized zeolite BEA with a size of 30 to 50 nm at a synthesis temperature of 100 °C for 72 h.⁴³ Even higher yields of nanozeolite beta (57 nm) were observed from 18 to 21 Si/Al ratios at 90 °C.⁴⁴ Using a template free approach, zeolite beta with a size of 400 nm was synthesized at 100 °C.⁴⁵

1.3 Synthesis of hierarchical zeolites

Hierarchical zeolites are another key area attracting considerable attention due to the presence of larger pores often leading to improved catalytic activity as well. To date, several different approaches have been used to synthesise hierarchical zeolites.²¹ They include removal of framework atoms, dual templating with surfactants, hard templating methods, silanisation methods and other mixed approaches. The physical characteristics of the secondary porosity depend on the synthesis methods used.

The first approach includes the removal of atoms such as Si or Al from the zeolite structure to develop mesoporosity. The developed mesoporosity is dependent on the atom removed from the structure. Although it gives rise to additional mesoporosity, a large mass of the zeolite is dissolved and lost during synthesis. In addition, the removal of the framework atoms can create vacancies and cause the zeolite structure to collapse and also alter the acidic properties of the zeolite. Alternatively, dual templating with surfactants is extensively employed, and is an alternative procedure to the conventional synthesis methods.⁴⁶ The technique involves introducing a template for the synthesis of the zeolite and a surfactant for the introduction of mesoporosity. The hard templating synthesis method involves the use of sacrificial templates giving rise to the secondary porosity in the zeolite products. The hard templates are removed after the synthesis by combustion or dissolution. Employing this synthesis method has disadvantages including the hard template being completely destroyed and high costs involved in scaling up. The next approach involves the introduction of organosilanes (silanisation) to give rise to additional mesoporosity.⁴⁷⁻⁴⁹ Organosilanes react with silanol groups and form functionalised organosilane silica. After calcination, the space previously occupied by the organosilane is directly proportional to the developed mesoporosity.

Silanisation and T atom removal strategies has resulted in zeolite ZSM-5 with superior properties in comparison to the hard templating technique.⁵⁰ Lately, many mixed approaches have been applied combining different methods to introduce mesoporosity. One approach involves post synthesis treatment involving surfactant and a base.^{51, 52} Another involves the local rearrangement of zeolite framework.⁵³⁻⁵⁷

1.4 Silver as antimicrobial agent

The constant rise of antibiotic-resistant bacteria and lack of new antibiotics to treat infectious diseases are causing significant health concerns worldwide. Silver has the ability to act on a wide range of microorganisms, including bacteria, fungi and moulds.⁵⁸ Its antimicrobial properties have been known since ancient times and were excessively used in World War II to prevent wound infections.^{59, 60} Silver-based materials have emerged as one of the most promising antibacterial alternatives.⁶¹⁻⁶⁶ Many forms of silver include silver as an ion (e.g., silver halides, silver sulphides, silver nitrates, etc.), others contain metallic silver (e.g., silver nanoparticles), silver complexes and colloidal silver have been employed in many materials to reduce bacterial colonisation. Silver additives (e.g., AgION, Zeomic, etc.) have even been used within textiles, food packaging, clothing and deodorants to eliminate bacteria. The mechanism of antibacterial action, issues and challenges in the use of silver as antibacterial agent have been discussed in several excellent reviews.^{58, 62, 67-70} The silver mechanism of action with microbes have been discussed in many studies and different mechanisms have been proposed. Firstly, it is proposed in the Ag mechanism of action that bacterial cells, when in contact with silver, take in the silver ion, which, binds with negatively charged components and cause structural defects in bacteria that affect the bacterial cells viability.⁷¹⁻⁷⁴ The second mechanism suggests that when Ag^+ is released to an aqueous or humid environment, it forms strong bonds with electron donor groups containing sulphur, oxygen, nitrogen and interact with thiol groups ($-\text{SH}$) in the biomolecules causing the bacteria cell death.⁷⁵⁻⁷⁷ The mode of action of silver raises a degree of controversy, and is yet not understood clearly. Silver can enter the body via inhalation⁷⁸ (dust and fumes), contact with jewellery and in applications such as burn cream. Also, silver

can enter the human body through the use of acupuncture needles,⁷⁹ medical devices,⁸⁰ dental amalgams⁸¹ or accidental puncture wounds. The National Institute for Occupational Safety and Health (NIOSH) established a Recommended Exposure Limit (REL) of 0.01 mg m⁻³ per 8 hours for silver compounds.⁸² For biomedical application, the determination of the cytotoxicity of Ag zeolites is of paramount importance, but such studies are rarely carried out. Greulich et al. have reported that the toxic effect of silver towards bacterial and mammalian cell is similar.⁸³ Zeolites themselves have shown cytotoxicity depending on the zeolite type, dose and cells used.^{84, 85} Ultrasmall, 8-18 nm EMT and LTL, zeolites have demonstrated absence of cytotoxicity at concentrations between 100 and 400 µg mL⁻¹.⁸⁶ Two recent review discuss aspects of nanozeolite cytotoxicity in more detail.^{87, 88}

1.5 Antimicrobial applications of Ag zeolites

An ion-exchange procedure with the counter-balancing cations in zeolites allows ions such as silver (Ag⁺) to be easily incorporated into the zeolite. Silver metal has emerged as one of the most promising metals for the preparation of antibacterial zeolites. The antimicrobial property owned by silver have been established for decades, and Ag materials are effective against a wide range of microorganisms (Table 1).^{71, 72, 89-94} Incorporating silver within a porous material such as zeolite allows gradual release of silver to the environment.^{89, 95} Experiments with Ag zeolite coatings submersed in distilled water for a year indicated that the coatings retained their antibacterial activity and were capable of killing *E. coli* upon repeated exposures.⁹⁶ Direct comparison of different studies is often difficult because of the different testing methods used. There are a number of established synthesis methods for the introduction of silver into zeolites, but commonly it is introduced via

ion-exchange from silver nitrate solution. ZSM-5 containing only 0.2 wt.% Ag loading has been reported to be active against *Staphylococcus aureus*,⁹⁷ higher Ag loadings, 2 wt.% and above, have been classically used.^{89, 92, 95, 97-101} Zhou *et al.* have demonstrated that the Ag exchange procedure can be optimised to achieve higher silver loadings compared to reported values.¹⁰¹ The antimicrobial activity of Ag zeolites could be further improved by introducing a second metal and Zn/Ag containing zeolite Y showed good activity against bacteria and yeast.¹⁰² The antifungal properties of Ag mordenite have been extensively studied for six microorganisms, moulds and yeasts.¹⁰⁰ Further, the antimicrobial properties of Ag-zeolites were dependent on the zeolite structure (pore sizes, pore channel systems) rather than the amount of silver exchanged in the zeolite.¹⁰³ Zeolites with a three-dimensional pore system (beta) had proved to exhibit greater degree of antibacterial activity compared to one-dimensional zeolites (MTW). The possible reason for this result is that the three dimensional pore structure offers greater efficiency with respect to the Ag released in the medium.^{97, 103} It has also been noted that a variation in the Si/Al ratio within the same zeolite-type structure, e.g., zeolite X (Si/Al ratio = 1.64) and zeolite Y (Si/Al ratio = 2.83), FAU-type structure, was found to influence the minimum inhibitory concentration against bacteria, correspondingly.⁸⁹ The results were attributed to the presence of metallic silver in zeolite X.⁸⁹

The zeolite crystal size is another parameter proposed to effect the antibacterial efficiency but a direct comparison has not been reported to date. A reduction of zeolite crystal size has been found to effect the antibacterial activity.⁹⁵ The antibacterial tests indicated that the micron sized (1.5–5 μm) zeolite killed *Enterococcus faecalis*, *E. coli* and *Pseudomonas aeruginosa* about 1.3-2 times more rapidly compared to the nanosized (50-400 nm) zeolite. However, the effect of the

zeolite characteristics, in particular particle size, on the antibacterial properties was not the main focus of this work. Ag-exchanged zeolite A with a particle size between 1 and 3 μm showed higher antibacterial activity when challenged with *E. coli* in comparison with zeolite A with a particle size between 2 and 5 μm , correspondingly.¹⁰⁴ The results were attributed to the differences in varying size distribution of the zeolites.¹⁰⁴ Sotiriou and Pratsinis have argued that smaller sized particles can release silver ions at a comparatively faster rate, leading to a toxic effect due to an increased silver concentration.¹⁰⁵ The Ag form (Ag^+ or Ag^0) of Ag-zeolites has been found to effect the antibacterial activity.^{97, 106, 107} The antibacterial activity of Ag zeolites increased with increasing the Ag content in parent ETS-10, EMT and A, correspondingly, zeolites. In these works, six Ag zeolite samples were tested, three after Ag ion-exchange at different levels, and three after subsequent silver reduction. The samples prepared after Ag reduction showed higher activity, although the conclusions from these studies were somewhat controversial.^{106, 107} Although several studies have reported the antibacterial properties of Ag-zeolites following reduction of the ion-exchanged silver,^{89, 99, 108} a comparative study between the two different forms of silver (Ag^+ or Ag^0) has not been reported. The antibacterial activity of six Ag zeolite samples were tested, three after Ag ion-exchange at different levels, and three after subsequent silver reduction. The samples prepared after Ag reduction showed higher activity.¹⁰⁷ Further, it has been demonstrated that the activity of silver nanoparticles was due to the aerobic release of silver ions and that Ag^0 did not have any bactericidal properties.¹⁰⁹⁻¹¹¹ From the above it seems clear that the antimicrobial efficiency of silver zeolites depends on a number of factors. Particularly important are (i) the silver form (Ag^+ or Ag^0) and content; and (ii) the zeolite structure, crystal size and Si/Al ratio.

Table 1. Summary of experimental procedures used, Ag wt.% and microorganisms tested in antimicrobial testing of Ag-zeolites.

Zeolite	Ag wt. %	Method	Microorganisms tested	Ref
Zeolite BEA	0.7	Viable plate count	<i>E. coli</i>	103
Zeolite MTW	1.3			
Zeolite A	2.2			
Zeolite Y	9.7	Minimum Inhibition Concentration	<i>E. coli</i>	89
Zeolite X	9.8			
ZSM-5	na	Viable plate count	<i>S. aureus</i>	97
Mordenite (Pellet)	15–20 wt. %			
Mordenite (granular)	35 wt. %			
FAU (micron sized)	15.2 (Ag/Cu wt. %)	Viable plate count	<i>E. coli</i> <i>Ent. Faecalis</i> <i>Ps. aeruginosa</i>	95
FAU (nanosized)	13.9 (Ag/Cu wt. %)			
Zeolite X	33.2	Minimum Inhibition Concentration	<i>S. aureus</i> <i>E. coli</i> <i>P. aeruginosa</i> <i>Bacillus cereus</i> <i>Candida albicans</i> <i>Candida glabrata</i> <i>Aspergillus niger</i> <i>Penicillium vinaceum</i>	104
Zeolite A	37.3			

1.6 Antimicrobial composites containing zeolites

Mixed matrix membranes (MMMs) combine the easy processability and low cost of the polymeric materials with the high stability and permeability and/or selectivity of the inorganic filler. The novelty of the concept of MMMs was to combine the major properties of an inorganic filler with a polymer to overcome the shortcomings of both types of materials. Zeolites are often used as inorganic fillers due to their attractive properties, such as; (i) rigid framework with high chemical, mechanical and thermal stability and (ii) high surface areas and micropore systems with slow antimicrobial release rates.¹¹² Multifunctional materials based on Ag zeolites, can be already found in the literature.¹¹³ In organic-inorganic composites, Ag-zeolites are introduced to reduce as well as prevent bacterial colonisation on surface of polymeric materials. Although inorganic fillers introduce enhanced properties such as thermal and mechanical characteristics, poor interfacial interaction is observed between zeolites and the polymer interface. Poor interfacial interaction leads to defects at the interface such as voids.^{114, 115} To overcome the existing defects, different factors such as zeolite particle size, zeolite loading and zeolite surface characteristics have to be optimised.¹¹⁶ However, to eliminate the interfacial defects (voids), introducing a coupling agent, which creates a chemical bridge between the filler and the matrix is considered a vital step to improve the compatibility between the phases. Ag-zeolites have been studied as additives in various biocompatible polymers at loadings of 1-10 wt%.^{91, 117-133} The work of Pehlivan and co-workers showed that the presence of a coupling agent significantly improved the filler-matrix adhesion, however, the antimicrobial efficiency of the MMMs prepared were not reported in their work.¹²² Silanes are recognised to extensively improve filler-matrix adhesion studied for the preparation of zeolite

containing composites.^{129, 134, 135} In spite of numerous research representing the need of surface modification of inorganic filler to eliminate the occurrence of interfacial incompatibility (leading to poor dispersion in the matrix), Ag zeolites have rarely been modified prior to composite fabrication.^{118, 119, 121, 123-125} Often, only antimicrobial properties have been studied without determining how the mechanical properties of the composites changed upon Ag zeolites loading.^{119, 123, 124} The beneficial role of Ag zeolite compound as additives in a number of medical appliances like catheters may be cited as examples to deliver microbial resistance. It is observed that on routine use of catheters, microbial growth on the surface of the catheters is a common problem and impregnation with Ag zeolite has been effective to address the above stated problem to a significant extent.¹³⁶ In the case of removable dentures fabricated from dental acrylic resins, it has been observed that such dentures are very susceptible to bacterial colonisation and incorporation of the antimicrobial additives compounds has solved the problem to a considerable extent.¹³⁷⁻¹⁵⁰ Oral candidiasis is the most common infection involving oral mucosal tissues in complete denture wearers.¹⁵¹ Although incorporating antimicrobial additive such as Ag-zeolites have the potential to bring direct benefit to denture wearers, there has been limited studies in this area.

1.7 Silicone elastomers

Silicone elastomers, also known as ‘polydimethylsiloxanes’ are elastic substances which contain linear silicone polymers crosslinked in a three-dimensional network.¹⁵² Elastomers display natural rubber-like properties; once stretched the elastomer reverts to its original shape. Elastomer main characteristics are: (i) the elastomers consists of long chains, (ii) a flexible Si-O-Si backbone and

(iii) the crosslinks prevent the chains from sliding.¹⁵³ In general, silicones are known for their low temperature and high temperature resistance, biocompatibility, and hydrophobic behaviour.¹⁵⁴

The traditional approach to form elastomers is to crosslink silicones. There are a number of routes to crosslink silicones. The most popular routes include room temperature vulcanisation (RTV) and high temperature vulcanisation (HTV). RTV systems are able to cure at room temperature and HTV systems cure at temperatures above 100 °C. The RTV system is mainly comprised of two component materials and cure at room temperature with a catalyst (RTV-2) or cure with water at room temperature (RTV-1).¹⁵⁵ The RTV-2 system (used in this study) are either condensation (polydimethylsiloxanes are reacted with a crosslinker) or addition cure systems. The principle of the addition reaction process (used in this study) involves 2-polydimethylsiloxanes crosslinked using a catalyst. Most common addition curing RTV systems are available in mixing ratios of 1:1, 9:1 or 100:1. Variable mixing ratios are possible. The system starts to cure once a platinum compound is added as a catalyst.¹⁵⁶ Silicone elastomers are widely used, in medical device production such as catheters, tubing for dialysis and transfusion equipment.⁹⁸

1.8 Acrylic resins

Denture bases are fabricated with poly(methylmethacrylate) (PMMA) resins with a degree of crosslinking.¹⁵⁷ The PMMA resin consists of long chains of methylmethacrylate (MMA) repeated units. Free radical polymerisation of MMA repeated units result in the formation of PMMA. Dental acrylic resins have been used since 1936 due their low cost, satisfactory aesthetic and biocompatibility in oral

environments. Dental resins are useful in dentistry because they can be shaped and moulded and then transformed to a solid that can take a permanent shape when they polymerise. The 'dough-technique' is used to fabricate dentures, whereby a powder-liquid system is used. The powder consists of the polymer: polymethylmethacrylate beads (produced by suspension polymerisation), initiator (approx. 0.5 % benzyl peroxide) and pigment (iron or cadmium salts).¹⁵⁸ The liquid component (methylmethacrylate major component) is added to the powder (typically 1:2 ratio) to form a dough which can be moulded. The International Organisation for Standardisation (ISO 20795-1:2013) specifies requirements for denture base polymers (BS EN ISO 20795-1:2013). The ideal requirements of denture base polymers are listed below:¹⁵⁷

Physical properties: Denture base polymers should match the appearance of natural soft tissues. The glass transition temperature should take into an account of temperature ranges in the oral cavity. The material must be radiopaque to enable detection of denture if swallowed.

Chemical properties: In the oral cavity, the polymer should be inert. Absorption of oral fluids can cause an alteration in the mechanical properties. This may cause crazing and dimensional change. The polymer should be insoluble, chemically inert and of low water absorption.

Biological properties: The polymer upon set should be non-toxic and non-irritant to the patient. If absorption of fluid occurs, the denture base should prevent bacterial colonisation.

Mechanical properties: Denture base polymers should have high yield stress, modulus of elasticity and sufficient flexural strength, to resist the occurrence of midline fracture.

1.9. Antimicrobial composites

1.9.1. Antibacterial silicone elastomers

Silicone elastomers are usually associated with a widespread range of applications but in particular medical devices. A major concern associated with medical devices are microbial infections.¹⁵⁹ Silicone elastomers contain a strong O-Si-O backbone, the backbone gives silicone elastomers its unique performance properties biocompatibility, high flexibility, ease of fabrication, chemical and thermal resistance. A significant number of studies have focused on surface modification, whereby biocide(s) are chemically attached to the polymer's surface to prevent and reduce bacterial colonisation. Surface modifications with organosilanes, quaternary salts and crosslinking polymers have given rise to silicone elastomers with antibacterial activity.¹⁶⁰⁻¹⁶⁴ For instance, quaternary salts were used to reduce and prevent biofilm formation.¹⁶³ The significant antibacterial activity observed was attributed to the positive charge on the quaternary ammonium which strongly binds to the negative bacterial cell wall causing structural damage. Another strategy involves impregnating a hydrogel network of cross-linked poly(2-hydroxyethyl methacrylate) embedded in silicone elastomers for a long term sustained drug release at loadings of 1-25 wt%.^{165, 166} Often, only the antibacterial properties have been studied without assessment of the mechanical properties of the antimicrobial elastomers. The modification of silicone elastomer with Ag zeolites has rarely been

studied. A study using Ag/nano TiO₂ incorporated in silicone elastomers has shown that the materials had great antimicrobial efficiency when challenged with *Staphylococcus aureus*.¹⁶⁷ Loadings of up to 10 wt.% showed increased antibacterial activity with increased loading. Again, mechanical properties were not reported.

1.9.2. Antibacterial dental acrylic resin

Dentures are installed in patients to restore dental and other functions affected by tooth decay, including facial prosthetic appearance. However, the insertion of prosthetic devices in the oral cavity affects the oral microflora resulting in accumulation of microorganisms on the surface of denture acrylic resins. This can lead to a number of oral diseases, which would require medical treatment and eventually replacement of the denture. Thus, the introduction of antimicrobial agents in dentures that do not influence the denture characteristics would be highly beneficial. Such dentures will have the potential to reduce the need to take medication and reduce additional costs linked to denture replacements. Silver is the most popular metal of choice for preparation of antibacterial polymers. However, limited research is available on incorporating Ag additives into dental acrylic resins.¹²⁶ A few studies using Ag nanoparticles have been published in the literature.^{147, 148, 168, 169} Different concentrations of Ag in dental acrylic gave rise to antibacterial activity.¹⁶⁸ Introducing Ag nanoparticles with sizes ranging from 1 to 100 nm showed a high antimicrobial efficiency towards *C. albicans*.¹⁴⁸ Holtz *et al.* incorporated Ag vanadate containing Ag nanoparticles at 0-10 wt.% loading into dental resins.¹⁶⁹ The composite showed strong efficiency against *Staphylococcus aureus*, *Pseudomonas aeruginosa* and *C. albicans*. Ag nanoparticles at loadings of

0.2 and 0.5 wt.% incorporated in dental acrylic resins showed antibacterial efficiency against *Streptococcus mutans* with 52.4% and a 97.5%, correspondingly, bacterial inhibition.¹⁴⁷

The use of Ag-zeolites as an antimicrobial additive for biocompatible dental acrylic resins has rarely been used. The impregnation of silver-zinc containing zeolite at a loading 2.5 wt.% in dental acrylic resins displayed significantly high activity against microorganisms.¹²⁶ However, the mechanical properties of the composite significantly decreased upon increasing the Zn/Ag zeolite loadings. Further, a significant reduction in the flexural strength of Zn/Ag zeolite incorporated in dental acrylic resins at a 10 wt.% loading was determined.¹⁴⁶ Although incorporating antimicrobial additives is of great benefit in reducing bacterial colonisation, reduction in flexural strength can risk fracture in oral cavity. An alternative method to Ag additives is to employ polymer poly(2-tertbutylaminoethyl) methacrylate, in which the amine in the methacrylate backbone reduced bacterial colonisation.¹³⁹

1.10. Zeolite functionalisation

A strategy to overcome poor filler-matrix adhesion is *via* chemical treatment (such as silane treatment).¹⁷⁰ Y_nSiR_{4-n} is the general formula for silanes, where R are easily hydrolysable groups (such as methoxy or ethoxy) and Y is a functional organic group (non-hydrolysable groups), capable of interaction with surface silanol groups, respectively.¹⁷¹ Silylation is conducted either through hydrolysis or a condensation reactions such as as:

Hydrolysis reaction:



Condensation reaction:



The coupling agents used in this study to modify zeolite samples are 3-(Trimethoxysilyl)propyl methacrylate (Figure 2) and vinyl silane (Figure 3).

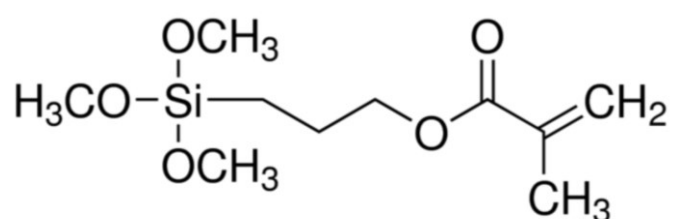


Figure 2. The chemical structure of 3-(Trimethoxysilyl)propyl methacrylate.

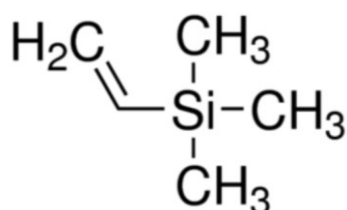


Figure 3. The chemical structure of vinylsilane.

1.11. Characterisation methods

1.11.1. Scanning electron microscopy

Scanning electron microscopy (SEM) is an analysis technique, which is commonly used in zeolite studies to determine the zeolite crystal size, morphology and the presence of impurities. The SEM consists of an electron gun, electron lenses, scan coils and detectors.¹⁷² The electron gun generates a beam of electrons from a cathode or filament made of tungsten or LaB₆. The electrons escape at high voltage from the

filament. The interaction with the sample and the electron beam generates different signals, see Figure 4.

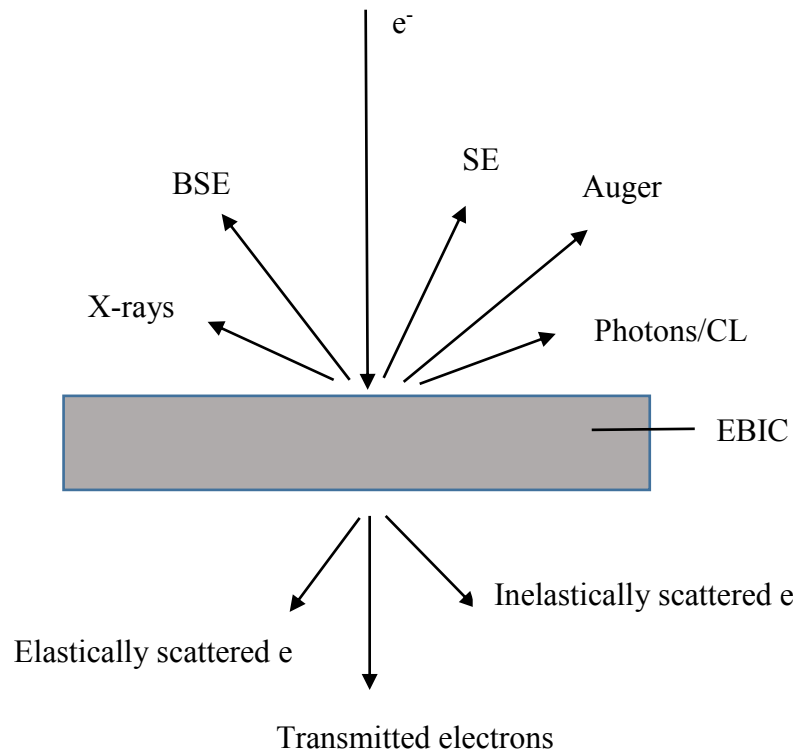


Figure 4. Overview of the different signals generated when an electron beam interacts with a specimen.

In SEM, secondary electrons generated are used for the fabrication of images. The fine beam of electrons is scanned across the specimen by the scan coils and the number of secondary electrons produced from each point of the sample is counted by a detector. At the same time, the spot of a cathode ray tube (CRT) is scanned across the screen and the brightness of the spot is determined by the amplified current from the detector. The electron beam and the CRT spot are both scanned in a similar way to a television receiver, i.e. in a rectangular set of straight lines (a raster).

1.11.2. Energy-dispersive X-ray spectroscopy

Energy-Dispersive x-ray spectroscopy (EDS or EDX) is a chemical microanalysis procedure used in combination with the scanning electron microscope. Energy-Dispersive X-ray spectroscopy finds its application in estimating the atomic % of an element present within a compound. The atomic % of elements present in the periodic table starting from sodium to uranium can be detected by the utilisation of the the EDS technique.¹⁷³ One or multiple peaks can be related to each element. Hence for the purpose of calculation of the concentration of the element present within a compound, it is required to evaluate the line intensities of every element present in the sample and also for the same element in calibration standards of known concentrations.

1.11.3. X-ray diffraction

X-ray diffraction (XRD) is a method used to identify the phase(s) present and to determine the degree of crystallinity. In this technique, X-rays are focused through a specimen; they are diffracted in all possible directions by the atoms in the structure. When destructive interference occurs, the waves will be refracted in all directions such as in amorphous materials. In a constructive interference, atoms in a crystal are arranged in a regular pattern, and the waves will be scattered in a very few directions (Figure 5).

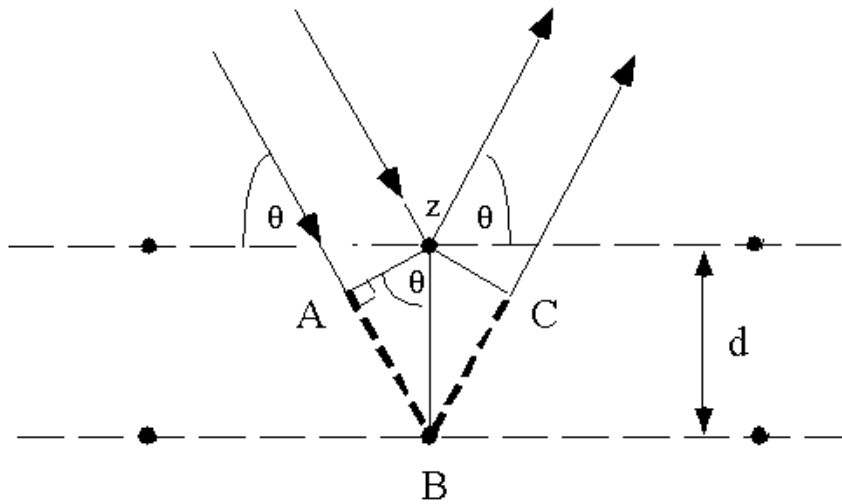


Figure 5. The diffraction of X-rays (constructive interference).

Braggs Law states that these waves could be used to evaluate the distance between the planes. Constructive interference is achieved when the length $AB + BC$ is similar to the entire whole number of wavelength.¹⁷⁴ To determine the distance between two crystal planes, Bragg's law is used:

$$2d \sin \theta = n\lambda$$

where θ is the deflection angle, d is the lattice spacing, λ is the wavelength and n is the order of reflection.¹⁷⁵

1.11.4. Gas adsorption

Gas adsorption is used to estimate the surface area of solids. Adsorption isotherms give the amount of gas adsorbed by a solid at a constant temperature. Usually nitrogen is used as an adsorptive gas and the isotherms are measured at -196°C . The monolayer capacity can be determined from gas adsorption data using different models. The most commonly used model is the BET (Brunauer, Emmet and

Teller) model and the surface area calculated using this model is called the BET surface area.

Based on the shape of the adsorption isotherms measured for different types of solids, the adsorption isotherms have been classified into five types according to the Brunauer, Deming, Deming and Teller (BDDT) system (Figure 6).¹⁷⁶

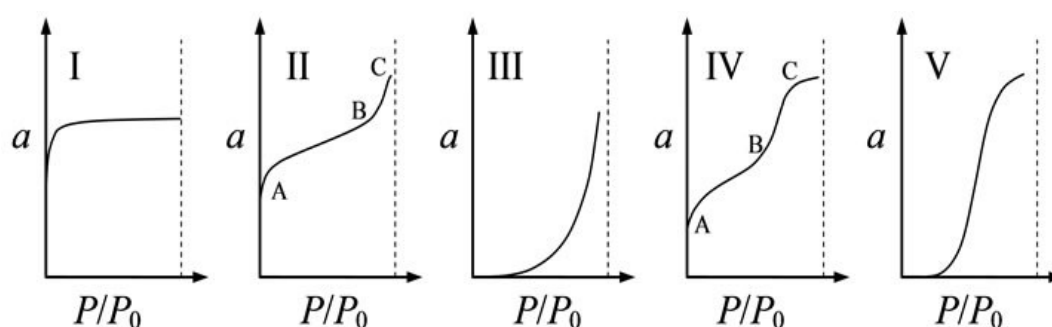


Figure 6. The five types of adsorption isotherms; a is the amount of gas adsorbed and P/P_0 is the partial pressure.

Type I – characteristic of microporous adsorbents such as zeolites and metal organic frameworks.

Type II – nonporous or macroporous adsorbents; at point A monolayer coverage is complete and multilayer adsorption begins; point A can be used for a rough estimation of the surface area – the larger the y-axis value corresponding to point B is the larger the surface area would be.

Type IV – typical of mesoporous adsorbents such as ordered mesoporous materials; it is characterised with a hysteresis loop formed as a result of the different adsorption / desorption behaviour at certain relative pressures associated with capillary condensation of the gas in mesopores.

Type III and V (rare) – adsorptive molecules have greater affinity for one another than they do for the solid; valueless in surface area and pore analysis.

1.11.5. Fourier transform infrared spectroscopy

Fourier transform infrared spectroscopy or FTIR is a technique that finds its application in the process of obtaining infrared spectrum of absorption, emission, photoconductivity or Raman scattering phenomena of an experimental sample (solid/liquid/gas). The major components of the FTIR spectrophotometer are a light source, beam splitter, static and movable mirror. The process involves passing a light beam over an experimental sample. The beam of light emitted from the light source has a wavelength falling into the region of infrared to electromagnetic spectrum. Partial absorption of the infrared wavelength occurs with some part of the wavelength being transmitted. The obtained data or reading indicates the molecular absorption of bonds in a particular chemical group and hence the molecular fingerprint of the experimental sample is obtained.¹⁷⁷ Diffuse reflectance infrared Fourier transform spectroscopy or DRIFTS is a type of Fourier transform infrared spectroscopy (FTIR). The advantage of DRIFTS over standard FTIR methods no sample preparation required. It eliminates pellet pressing thus eliminating the risk of modifying the chemical nature of the sample before analysis. Also, DRIFTS is more surface specific in the 1200-400 cm^{-1} middle-IR region.¹⁷⁸

1.11.6. Raman Spectroscopy

Raman Spectroscopy is a technique used to observe molecular vibrations, rotations, and other low-frequency modes in a system. In this technique, samples are

irritated with a monochromatic light source (i.e. laser). Upon interaction with the molecule, a photon may be elastically scattered; this gives rise to the Rayleigh line. Interactions may, however, be inelastic. The molecules in the sample can undergo a quantum transition causing their electrons to be excited to a virtual energy state, with the result the photon loses energy and is scattered to a lower frequency ($\Delta\nu$ negative). This scattering process is known as Anti-Stokes scattering (Figure 7). If the molecule is already in an energy level above its lowest, an encounter with a photon may cause it to undergo a transition to a lower energy, in which case the photon is scattered with increased frequency ($\Delta\nu$ positive). This scattering process is known as Stokes scattering.^{179, 180} Thus, we see that a Raman spectrum consists of the intensity of the scattered radiation plotted as a function of wavenumber. Molecular vibrations induced by inelastic scattering can only be Raman active if there is a change in the polarisability of the molecule. The symmetry of a molecule determines which vibrations are Raman active. Symmetric vibrations are much more intense when compared to anti-symmetric vibrations in Raman spectroscopy.¹⁸¹

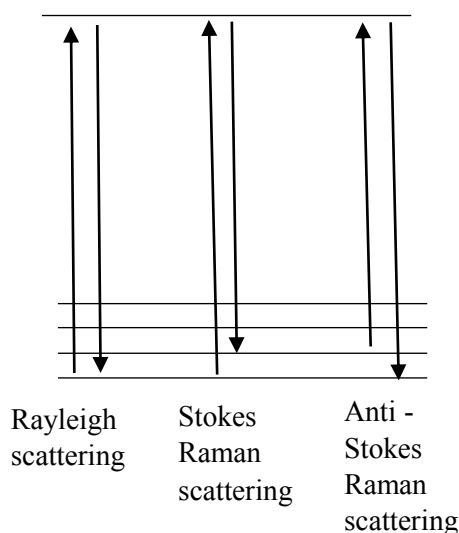


Figure 7. Schematic illustration of the Rayleigh, Stokes and Anti–Stokes scattering processes.

1.11.7. Dynamic light scattering

Dynamic light scattering or DLS is a procedure that is applied to estimate the size distribution profile of minute particles present as suspension or polymers in a particular solution. The initial step of this process involves sample irradiation and this is subsequently followed by the phenomena of light scattering also known as the Rayleigh scattering phenomena. The colloidal particles undergo random kinetic motion or Brownian movement due to continuous collision with the surrounding particles and also with the medium. The value obtained by the process of DLS is represented as the Z-average value. With reference to the Rayleigh scattering phenomena it may be stated that the amount of light scattered by a single molecule of the experimental sample is directly proportional to the sixth power of the radius of the experimental sample.¹⁸²

1.11.8. Thermogravimetric Analysis

Thermogravimetric analysis (TGA) is an analytical technique used to determine the mass change as a function of temperature. A TGA analyser consists of an extremely accurate balance ($\pm 0.0005\text{g}$) mounted inside a furnace, which continually records the mass of a sample during the experiment. Alternatively, when temperature is kept constant and the change of mass is measured it is known as isothermal or static thermogravimetric. The data obtained gives information about properties such as thermal stability, moisture content or solvent and decomposition temperature and rate.¹⁸³ TGA is used for zeolite analysis to determine water content, organic template content and phase transformations.

1.11.9. ICP-AES

The process of inductively coupled plasma atomic emission spectroscopy (ICP-AES) is also designated as inductively coupled plasma optical emission spectroscopy or ICP-OES is an example of an analytical method that is utilized for the detection of trace metals. The primary steps involved in ICP-AES include sample nebulisation by spraying the sample with aerosol or argon gas.¹⁸⁴ The aerosol is introduced into the plasma. The electron of the experimental sample attains an excited state and jump to the higher energy level. On returning to the ground state it is observed that the experimental sample emits radiation of electromagnetic radiation. By subsequent separation of the photon wavelength the concentration of the experimental samples can be estimated. It is evident that the emission intensity is variable in nature and all elements except argon can be detected by the process of ICP-AES. Considering the case of alkalis with presence of elements like sodium, potassium, rubidium and caesium are difficult to be detected by this procedure due to weak emission property. The detection limits range from 1-100 $\mu\text{g dm}^{-3}$.¹⁸⁵

1.11.10. Mechanical testing

The process of mechanical testing of an experimental object can be executed with the help of tensometer. This instrument can be utilised in estimation of the tensile strength and Young's modulus of a sample. The tensile strength can be represented as force applied per unit area sufficient to break the experimental sample (Figure 8). The process applied by tensometer involves the loading of the sample and subsequent application of force. A hydraulic arm is present in the tensometer. As

force is exerted over the experimental sample tensometer measure the tensile strength of the sample.¹⁸⁶

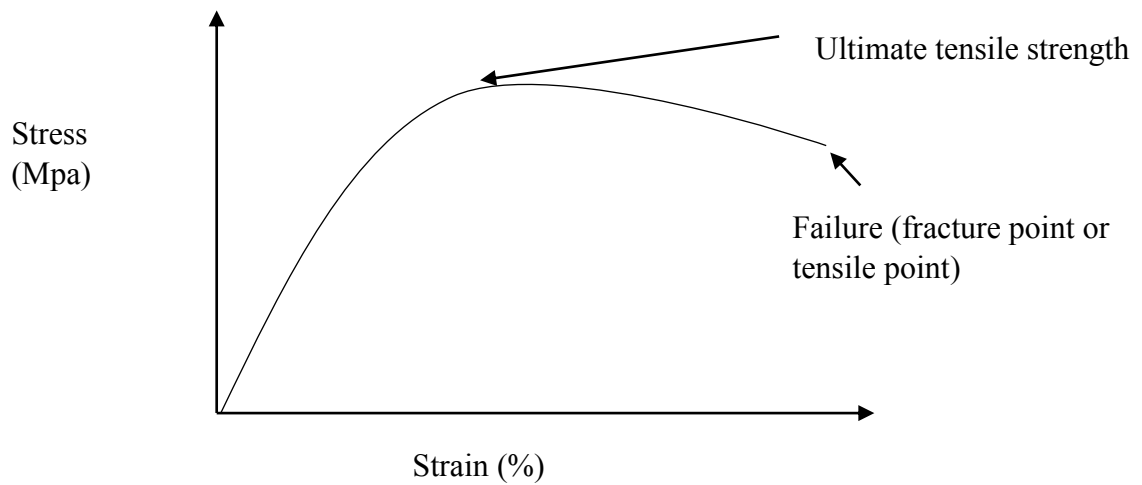


Figure 8. Tensile stress-strain diagram

The process applied by tensometer involves the loading of the sample and subsequent application of force. For tensile testing, dumbbell specimens are cut. The exact shape and width of the specimen is dependent on the material used. The tensile strength of samples of variable size and dimensions can be estimated with the application of this mechanical testing procedure.¹⁸⁷

1.12. Microorganisms and methods for determination of the antibacterial activity

Bacteria are unicellular organisms that are too small to be seen with the human eye (cell diameter range approximately 0.5 μm - 20 μm), and therefore fall under the classification of microorganisms. Bacteria are examples of the prokaryotic cell. In general, prokaryotic cells are those that do not have a membrane bound nucleus. Bacteria can be distinguished into two subgroups based on structural characteristic: Gram-positive and Gram-negative bacteria.¹⁸⁸ The names derive from the Danish

scientist Christian Gram, who, in 1884 developed a rapid staining technique that can differentiate bacteria as belonging to one of the two basic types based upon colour reactions. In Grams staining procedure cells are stained with crystal violet and iodine then washed with alcohol, which decolourises Gram negative bacteria. As for Gram positive bacteria they retain the deeper purple of the crystal violet-iodine complex.

1.12.1. Gram-positive bacteria

In Gram positive bacteria, the shape and integrity of the cell is maintained by a thick single layer of peptidoglycan. As much as 90% of the Gram-positive wall is composed of peptidoglycan. Some Gram-positive bacteria have a single layer of peptidoglycan, many others have several layers of peptidoglycan stacked one upon another. They also contain acidic molecules called teichoic acids in their cell walls which provides rigidity. Gram-positive bacteria take up the crystal violet stain used in the Gram staining test, and then appear to be purple-coloured when seen through a microscope. In contrast to the Gram-negative bacteria, the Gram positive cell wall is typically much thicker. *S. epidermidis* are one of over 40 species belonging to the genus *Staphylococcus*. *S. epidermidis* is a Gram positive cocci, about 1–2 µm in diameter after overnight incubation. Species of *Staphylococcus* commonly occur on the skin surface. *S. epidermidis* has gained significant interest with prosthetic implants infections such as hip and knee replacements¹⁸⁹ and medical devices.¹⁹⁰

1.12.2. Gram-negative bacteria

Gram-negative bacteria have a much thinner inner 2-7 nm peptidoglycan layer and outer membrane (7-8 nm thick), making the walls less sturdy. In Gram

staining procedure, Gram-negative bacteria lose the crystal violet stain and appear pale pink when seen through a microscope. *E. coli*, a Gram negative bacteria, is a rod shaped bacterium, about 3µm in length and 1µm in diameter.¹⁹¹ In contrast to the Gram-positive bacteria, *E. coli* does not present a coat of peptidoglycan in the cell wall. *E. coli* is the organism commonly contaminating catheter and in particular catheter related urinary tract infections.¹⁹²

1.12.3. Fungi

Fungi are large, diverse, and widespread group of organisms, consisting of mold, mushrooms, and yeasts. Fungi reproduce by asexual means in one to three ways: (1) by the growth and spread of hyphal filaments; (2) by the asexual production of spores; or (3) by simple cell division, as in budding yeasts.¹⁹³ *C. albicans* is fungi that grows as a yeast. Asexual reproduction occurs among yeast. In this process, the parent cell divides, either equally or unequally, to produce one or more offspring's that develop into mature forms. Binary fission is a type of cell division. Although some fungi also reproduce asexually by budding. In budding, a new individual is formed either at the surface or in an internal cavity. *C. albicans* is a recognised human pathogen and is usually associated with infections involving implants of the oral cavity.¹⁹⁴

1.12.4. Bacterial growth

When a culture of bacteria is added to a fresh medium and the cell concentration is periodically measured, then a curve describing the change in cell number against time can be drawn. This curve is called the growth curve (Figure 9).

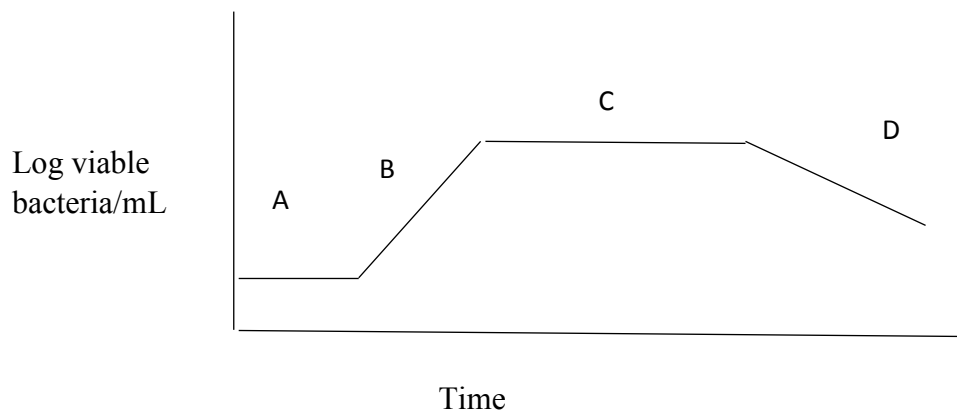


Figure 9. Growth curve for bacteria with its four distinct phases, Lag (A), Log (B), stationary (C), and death phase (D).

The typical growth curve of a bacterial culture (or other microorganisms, such as yeasts) begins with the lag phase. The lag phase represents what appears to be the transition period for bacteria transferred to a new environment. At this stage, the bacteria are producing the necessary enzymes so that they can grow in the new environment. While there is a no increase in cell numbers, there is a significant increase in the size of individual cells, with increases in cell protein, DNA and overall metabolic activity. In the log phase, the number of cells increase, cell division occurs at a maximal rate. At some point, the growth rate begins to taper off and the stationary phase starts. Here the growth and death rates are more nearly identical and a fairly constant population of viable cells is achieved. After a short period, the death phase is observed. During this period the number of viable cells

decreases, this situation will continue until the number of cells is very low and remain almost constant for a time.

1.12.5. Methods for determination of the antibacterial activity

There are a number of ways of to measure the antimicrobial efficiency of antimicrobial agents (Contact kill, Inductively Coupled Plasma Atomic Emission Spectroscopy (ICP-AES) or ion release, Minimum Inhibitory Concentration (MIC), Minimum Bactericidal Concentration (MBC) and Zone Of Inhibition (ZOI)., each with their own advantage for specific purposes.^{72, 89-91, 95, 96} To assess the efficiency of Ag zeolite antimicrobial (used in this work) activity, a viable bacterial counting technique was used, which involves the removal of the bacteria from the surface by sonication and quantifying them by colony counting on agar plates. The viable plate count method used in this work was selected according to ISO 22196 standard.

1.12.5.1. Viable plate count method

Viable counts are carried out to count the number of living microorganisms in a sample that are capable of developing colonies on a suitable solid agar medium.¹⁹⁵ Serial dilutions of the bacterial suspension are conducted to ensure an appropriate number of colonies are counted. The serial dilution are transferred to a sterile solid agar medium either by a spread method or pour plate method. The agar plate are incubated so that the bacteria can reproduce. The formation of visible colonies generally takes 16 to 24 hours, depending on the microorganism used. For accuracy, it is recommended not to count colonies fewer than 30 or more than 300. It

is assumed that each colony arises from an individual bacterial cell. Therefore by the counting the number of colonies that develop, the colony forming units (CFUs) can be calculated according to the formula:

$$\text{CFU mL}^{-1} = \frac{\text{Number of colonies} \times \text{Dilution Factor}}{\text{Volume plated in mL}}$$

A drawback of the viable count procedure, is that there is no set of incubation condition and medium compositions that permit the growth of all bacteria types. Tiny colonies can be missed during the counting stage. The results are the probable number of bacteria, and not the exact number since more than one organism may produce a single colony. Also, accurate results require many replications.¹⁹⁶

A surface viable count ‘miles and misra method’ is a technique used in microbiology, allowing quick comparison of the antimicrobial efficacy of samples with a similar nature. A faster and more economical alternative to standard plate count method. This technique was used to compare Ag zeolite powder samples.

1.12.5.2. Minimum inhibitory and minimum bactericidal concentration

Minimum inhibitory concentration (MIC) is the concentration that will inhibit the growth of challenging microbe after incubation. Diffusion assays, containing a serially decreasing amount of antimicrobial agent are added to suitable growth medium with inoculated bacteria. After incubation all samples are examined for growth. The last concentration which produces no visible growth is scored as MIC. Determining the minimum bactericidal concentration (MBC) requires inoculating a second set of assays agar plates with inocula taken from assays without bacterial growth. After incubation, plates without growth represent the

antibacterial agent concentrations that kill the test microorganisms. The technique is used to confirm resistance and in vitro activity of new antimicrobials.

1.12.5.3. Cytotoxicity tests

Cytotoxicity refers to an agents that disrupt or destroy cells. A cytotoxic agent may be genotoxic (causing DNA damage), mutagenic (causing gene mutation) or it may be harmful for cell organelles (e.g. cell membrane) or it may even be teratogenic. The test conducted to quantify the toxicity level of a biological experimental sample is designated as Cytotoxicity test. This procedure involves the quantification of viable cells after a specific period of incubation. This test is found to be very effective in analysing the toxic effect on living cells. Induced cellular necrosis or apoptosis are the significant steps of this particular test.¹⁹⁷ A surrogate marker is applied in order to highlight the viable cellular population when compared with the untreated control sample. While it can be measured in a number of different ways, assessing cell viability through the use of vital dyes (formazan dyes), protease biomarkers or by measuring ATP content are some of the most commonly used methods in determining cytotoxicity.¹⁹⁸

1.13. Aims and objectives

1.13.1 Aim

The primary aim of this thesis was to investigate the antibacterial applications of Ag zeolites in powder form (Section 1.5) or as additives to polymers (Section 1.6).

1.13.2 Objective

- To identify convenient screening technique allowing the comparison of the antimicrobial efficacy of samples, for which great differences in the antimicrobial properties are not expected.
- To apply the technique developed to compare the antimicrobial efficacy of Ag zeolites (powder form) of different crystal size and also to study the influence of mesoporosity.
- To assess the efficiency of antimicrobial Ag zeolite containing polymers.
- To characterise polymer before and after addition of zeolites: mechanical properties, compatibility between the zeolite and the organic matrix depending on the presence or absence of organic modification of the zeolites, discolouration and Ag loading.
- To overcome discolouration problems of the polymers when loaded with Ag zeolites.

Chapter 2. Experimental

2.1. Synthesis of zeolites

2.1.1 Synthesis of zeolite X

Three samples of zeolite X were prepared in this work and denoted as X1, X2 and X3 for convenience. Sample X1 was prepared from a gel with the molar composition $5.5\text{Na}_2\text{O} : 1.0\text{Al}_2\text{O}_3 : 4.0\text{SiO}_2 : 190\text{H}_2\text{O}$ using NaAlO_2 (Fischer), NaOH (Alfa Aesar), fumed silica (Aerosil 200, Degussa) and distilled water.¹⁹⁹ The mixture was stirred at room temperature for 24 h, transferred to a polypropylene reactor and hydrothermally treated at $60\text{ }^\circ\text{C}$ for 4 days. After the synthesis, the sample was purified by three-time centrifugation and redispersion in distilled water and dried at $60\text{ }^\circ\text{C}$ overnight.

Sample X2 was prepared from a gel with the molar composition $8\text{NaOH} : 0.2\text{Al}_2\text{O}_3 : 1.0\text{SiO}_2 : 200\text{H}_2\text{O}$ as described previously.¹⁴ The precursor gel was transferred to a Teflon-lined autoclave and treated at $110\text{ }^\circ\text{C}$ for 3 h.

Sample X3 was prepared from a gel with the molar composition $8\text{NaOH} : 0.2\text{Al}_2\text{O}_3 : 1.0\text{SiO}_2 : 200\text{H}_2\text{O}$ as described previously. The precursor gel was transferred to a Teflon-lined autoclave and treated at $80\text{ }^\circ\text{C}$ for 24 h.

2.1.2 Synthesis of zeolite beta

Three zeolite beta samples were synthesised in this work, samples B1, B2 and B3. Zeolite beta samples B1 and B2 were synthesised from a clear precursor solution with the molar composition $0.3\text{Na}_2\text{O} : 9\text{TEAOH} : 0.5\text{Al}_2\text{O}_3 : 25\text{SiO}_2 : 489\text{H}_2\text{O}$ using aluminium isopropoxide (Alfa Aesar), silica sol (Bindzil 30/220, EKA Chemicals),

tetraethylammonium hydroxide (20 wt.% aqueous solution, Alfa Aesar) and distilled water. Sample B1 was prepared by hydrothermal treatment at 150 °C for 48 h, whereas for sample B2 the crystallisation was performed at 170 °C for 38 h. Both samples were purified by three-time centrifugation and redispersion in distilled water and dried at 60 °C. The organic template was removed by calcination at 550 °C for 5 h after heating to that temperature at a rate of 10 °C min⁻¹.

A mesoporous zeolite beta sample, sample B3, was synthesised according to the procedure reported by Zhu *et al.* employing poly(diallyldimethylammonium chloride) (PDADMA) (20 wt.% in water, Aldrich) as a template.²⁰⁰ A gel was prepared with the molar composition 45SiO₂ : Al₂O₃ : 10Na₂O : 2258H₂O : 7.5 PDADMA using fumed silica (Aerosil 200), sodium aluminate, NaOH and PDADMA. The gel was stirred for 12 h at room temperature, transferred to an autoclave and crystallised at 180 °C for 96 h. The powder obtained was collected by filtration, dried at 100 °C, and calcined at 550 °C for 5 h as described above to remove the organic template.

2.1.3 Synthesis of EMT zeolites

The EMT-type zeolite, sample E, was prepared from a clear precursor suspension with the molar composition 5.15SiO₂ : 1Al₂O₃ : 18.45Na₂O : 240.3H₂O. The suspension was continuously stirred for 10 min at room temperature and then kept at 30 °C for 36 h. This sample was kindly provided by Prof. Svetlana Mintova from the University of Caen, France.²⁰¹

Table 2. Synthesis conditions for the zeolites used in this work.

Ref	Sample	Zeolite	Molar composition	Hydrothermal treatment
199	X1	X	5.5Na ₂ O : 1.0Al ₂ O ₃ : 4.0SiO ₂ : 190H ₂ O	60 °C/4 d
14	X2	X	8NaOH : 0.2Al ₂ O ₃ : 1.0SiO ₂ : 200H ₂ O	110 °C/3 h
	X3	X	8NaOH : 0.2Al ₂ O ₃ : 1.0SiO ₂ : 200H ₂ O	80 °C/24 h
41	B1	Beta	0.3Na ₂ O : 9TEAOH : 0.5Al ₂ O ₃ : 25SiO ₂ : 489H ₂ O	150 °C/48 h
	B2	Beta	0.3Na ₂ O : 9TEAOH : 0.5Al ₂ O ₃ : 25SiO ₂ : 489H ₂ O	170 °C/38 h
200	B3	Beta	45SiO ₂ : Al ₂ O ₃ : 10Na ₂ O : 2258H ₂ O : 7.5 PDADMA	180 °C/96 h
202	E	EMT	18.45Na ₂ O : 1.0Al ₂ O ₃ : 5.15SiO ₂ : 3H ₂ O	30 °C/36 h.

2.2. Preparation of Ag zeolites

2.2.1 Ag-X and Ag-beta zeolites

For the preparation of the Ag-exchanged silver zeolites, the as-made zeolites X or calcined beta zeolites were added to 0.05 M silver nitrate solution (AgNO₃, Alfa Aesar) at a weight ratio of 1 to 20. The slurry was stirred for 72 h at room temperature. The Ag-exchanged zeolite (AgX) were filtered or centrifuged, washed repeatedly with distilled water and dried at 60 °C overnight.

2.2.2 Ag-EMT zeolites

The Ag- EMT zeolites, were provided by Prof. Svetlana Mintova from the University of Caen, France. The ion-exchange process was performed as follows: 20 mL silver perchlorate solutions with a concentration of 0.05 M were added to three dispersed EMT zeolite suspensions (7.5 wt.%, 12 mL) and kept for 2 h, 4 h and 6 h. The ion-exchanged samples were purified three times *via* high-speed centrifugation and redispersed in distilled water. The silver nanoparticles (Ag NPs) in the EMT zeolite suspensions (2 wt.%, 7 mL) were obtained under microwave reduction (120 °C, 10 min, 1000 W) in the presence of a triethylamine as a reducing agent ($\text{N}(\text{C}_2\text{H}_5)_3$, 2 mL). The reduced suspensions were again purified three times and finally dispersed in water. The as-made zeolite suspensions before and after reduction are abbreviated as Ag^+ -EMT 2 h, Ag^+ -EMT 4 h and Ag^+ -EMT 6 h and Ag^0 -EMT 2 h, Ag^0 -EMT 4 h, and Ag^0 -EMT 6 h, respectively, according to the different ion-exchange times used (2, 4 and 6 hours).

2.3 Functionalised Ag-zeolites

Organic modification of the AgX zeolites (sample X3) was performed as appropriate prior to their use as additives in polymers. For the preparation of the functionalised silver zeolites, 2 g of AgX were mixed with 20 g of 10 wt.% solution of 3-(trimethoxysilyl) propylmethacrylate (GE Bayer silicone) or triethoxyvinylsilane (97%, Sigma-Aldrich) in cyclohexane (Fischer) and stirred for 30 min at room temperature. The zeolite was then washed several times with cyclohexane by decanting. The modified zeolites were dried at 50 °C for 72 h. All procedures were

performed in the dark using foil to cover glassware. The two organically-functionalised samples were labelled as Ag-X / M and Ag-X / V, respectively.

2.4 Synthesis of polymer composites

2.4.1 Silicone elastomers

Silicone elastomers (SE) were prepared from samples of M511 maxillofacial (Technovent, UK). The elastomers were prepared using a mixture consisting of 29.106 g of Part A (Silicone polymer with Si-H groups) and 3.234 g of part B (vinyl functionalised dimethyl silicone polymer, plus Pt catalyst). The system components were mixed for 60 s under vacuum using Multivac 4 (Degussa AG, Germany). After a resting time of 15 min, the uncured SE was spread into a 13 cm x 13 cm x 1 cm metal mould using a pallet knife. The mould was placed on a vibrating table for 10-15 minutes to bring the air bubbles to the surface, the bubbles were burst using a thin wire. The moulding was cured at room temperature for 24 h. After curing, the SE was removed from the steel mould and stored in a polythene bag. A melinex sheet was used in the mould to ease the recovery of the cured SE. Zeolite-containing silicone elastomers were prepared similarly after adding 2 wt.% zeolites (X3) to the uncured SE mixture. SE containing NaX, AgX, M-AgX and V-AgX were prepared and stored as described.

2.4.2 Dental acrylic resins

For the preparation of dental acrylic (DA) composite, a mixture containing 14.4 g of liquid component (mainly methyl methacrylate with added crosslinking

agent (ethylene glycol dimethacrylate)) (Davis Schottlander & Davis Ltd, UK) and 35.0 g powder poly(methyl methacrylate) (Davis Schottlander & Davis Ltd, UK) were mixed slowly in an acrylic mixing jar. After a resting time of 15 min, a mould releasing agent (CIL 1711E) (Chemical Innovations Limited, Preston, UK) was sprayed onto two melinex sheets covering the surface of the mould for easy removal. The mixture was packed into eight, 10 mm x 110 mm x 3 mm moulds within its packing time, and the flask was screwed down tightly. The closed mould was then placed in hydraulic press pump to remove excess flash. The moulding was cured at 95 °C for 9 hours in a dry heat curing unit (Milnes Bros, UK). When flasks cooled down to room temperature, test pieces were deflashed and removed carefully from moulds. Each specimen was sawed into 10 mm x 20 mm x 3 mm coupons suitable for antimicrobial testing. The Ag-zeolite (X3) sample was added at a 2 wt.%, 0.7 wt.%, 0.4 wt.% and 0.2 wt.% to the uncured DA. The Ag-zeolites samples were organically modified with 3-(trimethoxysilyl)propyl methacrylate prior to addition to the uncured DA. A summary of the polymer composites is presented in Table 3.

Table 3. Summary of polymer composites.

Polymer type	Zeolite	Coupling agent	Amount inorganic added	of filler	Sample code
Silicone elastomer	X3	-	-		SE
	X3	-	2.0 wt. %		NaX/SE
	X3	-	2.0 wt. %		AgX/SE
	X3	Vinylsilane	2.0 wt. %		V-AgX/SE
	X3	3-(trimethoxysilyl) propylmethacrylate	2.0 wt. %		M-AgX/SE
Dental acrylic	X3	-	-		DA
	X3	-	2wt. %		NaX/DA
	X3	-	2 wt. %		AgX/DA
	X3	3-(trimethoxysilyl) propylmethacrylate	2 wt. %		DA / Ag-X (2 wt. %)
	X3	3-(trimethoxysilyl) propylmethacrylate	0.7 wt. %		DA / Ag-X (0.7 wt. %)
	X3	3-(trimethoxysilyl) propylmethacrylate	0.4 wt. %		DA / Ag-X (0.4 wt. %)
	X3	3-(trimethoxysilyl) propylmethacrylate	0.2 wt. %		DA / Ag-X (0.2 wt. %)
	X3	3-(trimethoxysilyl) propylmethacrylate	2.0 wt. %		DA / M-NaX 2 wt. %
	X3	3-(trimethoxysilyl) propylmethacrylate	1.0 wt. %		DA/ DA / M-NaX 1 wt. %

2.5 Antimicrobial tests

2.5.1 Antimicrobial activity of Ag-zeolites (X, Beta and EMT)

A single colony of *E. coli* (ATCC 8739) from a freshly cultured nutrient agar (Oxoid, UK) plate was removed using a sterile loop and inoculated in a 100 mL of sterile nutrient broth (Oxoid, UK). The broth was incubated for 18–24 hours at 37 °C in a rotary shaker incubator set at 150 rpm. The liquid culture was centrifuged at 3000 rpm for 10 minutes to form a pellet. The supernatant was discarded and the pellet was re-suspended in distilled water. An optical density of 1.0 at 540 nm wavelength was obtained (Jenway 6305 Spectrophotometer, UK), equalling approximately 10^8 colony-forming units (CFU) per mL. 25 μ L of the bacterial

suspension was added to 20 mL of 0.5, 0.1, 0.05 mg mL⁻¹ suspension and vortexed immediately for 30 seconds (Table 4) for zeolite X and beta. For EMT-type zeolite, 25 mL of the bacterial suspension was added to 5 mL of 0.5 mg mL⁻¹ suspension of Ag⁺-EMT and Ag⁰-EMT. The Ag-free sample was used for control experiments. The samples were incubated at 37 °C in a rotary shaker incubator set at 150 rpm and a sample was taken every 60 seconds using a 50 dropper over a period of 0–7 minutes with continuous vortexing in between time intervals. A single drop (20 µL) of sample was added to an eighth of thioglycollate agar plate for culturing the *E. coli*. The thioglycollate (thio-neutralising) agar was prepared by mixing thioglycollate broth with 1.2 wt. % technical agar (Oxoid, UK). All tests were carried out in duplicate. The plates were incubated overnight at 37 °C.

The same procedure was applied for *C. albicans* (NCYC 1363) but the overnight growth was performed in sabouraud dextrose liquid medium. An optical density of 1.0 at 540 nm wavelength was obtained (Jenway 6305 Spectrophotometer, UK), equalling approximately 10⁵ CFU per mL. The dilutions were made as above and plated out onto thioglycollate (thio-neutralising) agar. The release of silver from the zeolite samples was measured in the mother liquor immediately after the 7 minute test. The liquid culture was centrifuged at 3000 rpm for 10 minutes to form a pellet. The pellet was discarded and the supernatants were analysed on a Thermo Scientific ICAP6300 DUO inductively coupled plasma optical emission spectrometer (ICP-OES) using the Ag 328.1 nm analytical wavelengths.

Table 4. Summary of concentrations used in Ag-zeolite (zeolite = X or beta) antimicrobial tests.

Amount of Ag-zeolite added (mg)	Volume of sterile water (mL)	Concentration of Ag-zeolite suspension (mg/mL)
1	20	0.05
2	20	0.1
10	20	0.5

2.5.2 Cytotoxicity tests

The cytotoxicity tests, were conducted by Dr Nasser Al Shanti from the University of Manchester Metropolitan University, UK. The peripheral blood mononuclear cells (PBMCs) were isolated from donated blood of healthy individuals (n=3, one female and two males, age between 20-25 years old) as previously described.²⁰³ An in house ethical approval protocol (Manchester Metropolitan University) was followed. The blood (20 mL) was carefully layered on the same volume of Ficoll-Paque PLUS (GE Healthcare Life Sciences, Buckinghamshire, UK). After 40 min centrifugation at $400 \times g$ at 18–20 °C, the peripheral blood mononuclear cells layer was carefully removed and washed twice with RPMI-1640 medium. Isolated PBMCs (3×10^5 per well) were cultured in flat-bottomed 24-well plates.²⁰⁴ The PBMCs were grown in RPMI-1640 medium containing Ag zeolite (X1, X2, B1 and B2) samples of different concentrations (1, 0.5, 0.1, 0.05 and 0.001 mg mL^{-1}), 10% (v/v) human AB serum and 1% penicillin/streptomycin at 37 °C in 5% CO₂. Three experiments (blood from three volunteers) were performed for each zeolite concentration with eight readings obtained for X1 and X2 samples (one duplicate and two triplicates) and seven readings obtained for B1 and B2 samples as well as the untreated cells (two duplicates and one triplicate). The amount of Ag zeolite needed to obtain the above

concentrations was firstly added to PBS and vortexed. After two weeks, the samples were centrifuged and the supernatant was used in the cytotoxicity tests. All cultures were supplemented with 50 U mL⁻¹ human recombinant interleukin-2 (IL-2) (R&D Systems Abingdon, UK).

Flow cytometry, which is widely used to determine apoptotic population using pre-G1,²⁰⁵ was employed to measure the cytotoxic effect of silver zeolites on PBMCs apoptosis, following 48 h days in culture. The PBMCs were harvested and washed in PBS prior to fixing at -20°C in 75% ethanol. After a minimum of 24 h, the PBMCs were washed twice in PBS and re-suspended with gentle vortexing in propidium iodide labelling buffer (50 µg mL⁻¹ propidium iodide, 0.1% sodium citrate, 20 µg mL⁻¹ ribonuclease A, 0.3% Nonidet P-40, pH 8.3) at approximately 1 x 10⁶ cells mL⁻¹. The PBMCs were analysed using a Becton Dickinson FACSCalibur flow cytometer. Data were analysed using Cell Quest software (Becton Dickinson, Oxford, UK). Statistical significance of the results for zeolite-treated cells and untreated cells was determined with a one-way ANOVA followed by Tukey-Kramer multiple post hoc analysis. All results are presented as mean ± standard deviation of the mean (N= 7 or 8 as discussed above). Results were considered as statistically significant when p< 0.05.

2.5.3 Antimicrobial activity of Ag-zeolites composites

A single colony of *E. coli* (ATCC 8739) or *S. epidermidis* (NTCC 11046) from a freshly cultured nutrient agar (Oxoid, UK) plate was removed using a sterile loop and inoculated in sterile nutrient broth (Oxoid, UK). Broth was incubated for 18-24 hours at 37 °C on a rotary shaker at 150 rpm. The liquid culture was

centrifuged at 3000 rpm for 10 minutes to form a pellet. The supernatant was discarded and the pellet was re-suspended in sterile ringers solution (Oxoid, UK). An optical density of 1.0 at 540 nm wavelength was obtained, equalling approximately 10^8 colony-forming units (CFU) per mL. A 1:10 dilution was performed in ringers solution and this suspension (approximately 10^6 CFU/mL) was used to inoculate the surfaces. The dimension of the composites test pieces was 20 mm x 10 mm. The specimens were sterilised by autoclaving at 121 °C for 15 minutes. Each sample was placed in a separate sterile Petri dish. Antimicrobial activity of test specimens was carried out according to ISO 22196 standard. The standardized bacterial suspension (50 µl) was pipetted onto the sample surface. A 20 mm x 10 mm polyethylene film was placed on top and gently pressed down to ensure the bacteria spread evenly on the surface; care was taken to ensure the bacteria did not leak beyond the edges of the film. Immediately after inoculation, surfaces were placed individually into 10 ml neutralising agent (14.6% sodium thiosulphate and 10% sodium thioglycolate in 100 ml distilled water, 5 ml was filter sterilized into 495 ml sterile distilled water)²⁰⁶ and vortexed for 30 seconds ensuring the polyethylene film detached. Bacteria were enumerated by serial dilutions (1:10) and plating followed by CFU determination. A 100 µl were spread onto nutrient agar plate and plates were incubated overnight at 37 °C. The remaining surfaces in Petri dishes were incubated at 37 °C and tested as above at 5 and 24 hours. All tests were carried out in triplicate. The same procedure was applied for *C. albicans* (NCYC 1363) but grown overnight in sabouraud dextrose liquid medium (Oxoid, UK). The 1:10 dilutions were made as above and 100 µl were plated out onto sabouraud dextrose agar. The surfaces were incubated at 37 °C and tested at 0, 24 and 48 hours. Comparing this to the known initial number

of viable cells (10^6) inoculated onto the surface allowed a quantitative measure of the level of cell death caused by the Ag in the polymer sample.

2.5.4 Ag release of silicone elastomers loaded with AgX zeolite

For determining the amount of silver leached from the surface to a liquid medium, 10 mL of HPLC grade water (Fischer, UK) was placed in sterile plastic universals containing one of each of the silver, modified silver and control surfaces. Surfaces were incubated at 37 °C in a reciprocating shaker at 150 rpm and at 1 h, 5 h, 24 h, 48 h and 72 h, the surfaces were transferred to a fresh universal containing HPLC grade water. Test surfaces were tested in triplicate and all samples were frozen at -85 °C prior to analysis. The samples were analysed on a Varian Vista AX CCD inductively coupled plasma atomic emission spectrometer (ICP-AES) using the Ag 328.1 nm analytical wavelength. Silver content was calculated from calibration curves (0.01 to 2 ppm).

2.5.5 Ag release of dental resin loaded with AgX zeolite

For determining the amount of silver leached from the surface (DA containing Ag-zeolites) to a liquid medium, 20 mL of sterile distilled water was placed in glass universals containing one of each of the surfaces. Surfaces were incubated at 37 °C in a reciprocating shaker at 150 rpm for different periods 4, 8, 12, 26, 40 and 54 days the surfaces were transferred to a fresh universal containing sterile distilled water after each time interval. Test surfaces were tested in triplicates. The amount of silver leached from the surface to artificial saliva was also monitored. The same protocol was used as above. Artificial saliva was synthesised as follows

0.4 g Sodium chloride (Fischer scientific, UK), 0.4g Potassium chloride (BDH Laboratory supplies poole, UK), 1.192 g di-sodium hydrogen orthophosphate dodecahydrate (Fischer scientific, UK) and 0.218 g potassium dihydrogen orthophosphate (Fisher chemical, UK) added to 1000 ml sterile distilled water.

2.5.6 Charging of preformed dental acrylic composites with silver

The Dental acrylic samples (Ag free) were charged with 20 ml of 0.01 M silver nitrate solution (Alfa Aesar) using the same conditions of the original samples at room temperature for 24 hours in a reciprocating shaker at 150 rpm.²⁰⁷

2.5.7 Ag release of charged NaX dental acrylic components with silver

For determining the amount of silver leached from the surface to a liquid medium, 10 mL of sterile distilled water was placed in glass universals containing one of each of the surfaces. Surfaces were incubated at 37 °C in a reciprocating shaker at 150 rpm and at 1 and 20 days (DA charged from AgNO₃ samples), the surfaces were transferred to a fresh universal containing sterile distilled water. Test surfaces were tested in triplicate. The samples were analysed on a Thermo scientific (Icap6300 DUO) inductively coupled plasma atomic emission spectrometer (ICP-AES) using the Ag 328.1 nm analytical wavelength. Silver content was calculated from calibration curves (0.01 to 10 ppm).

2.6 Characterisation methods

2.6.1 Zeolite characterisation

Zeolite crystal size (Sample X3) was determined using a Carl Zeiss Ltd 40VP Supra Scanning Electron Microscope (SEM). The morphology of the zeolites (Sample X1, X2, B1, B2 and B3) and dispersion quality within the SE/zeolite composites was studied using a JEOL 5600LV SEM. The particle sizes of samples B1 and B2 were also verified by dynamic light scattering (DLS) using a Zetasizer Nano ZS instrument with a 173° backscattering angle geometry. Semi-quantitative chemical analysis was performed on uncoated sample pellets by energy-dispersive X-ray spectroscopy (EDX) using an Apollo 40 SDD detector (EDAX Inc.). An average of five absolute measurements was used to provide the final values. X-ray diffraction (XRD) patterns were collected with a PANalytical X'Pert X-ray diffractometer (XRD) employing Cu K α radiation (40 kV and 30 mA) and a PIXcell detector. Nitrogen adsorption isotherms of the zeolite samples prior to silver ion-exchange were recorded on a Micromeritics ASAP 2020 surface area analyser at -196 °C. Samples were degassed at 110 °C overnight prior to analysis. Surface areas (S_{BET}) were calculated using the BET equation, whereas external surface areas (S_{EXT}) and micropore volumes (V_{μ}) were determined by the t-plot method. Total pore volumes (V_{p}) were obtained from the volume adsorbed at a relative pressure of 0.99 and mesopore volumes (V_{meso}) were calculated from the difference between V_{p} and V_{μ} . BJH pore-size distributions were determined from the desorption branch of the isotherms. Thermogravimetric analysis was performed with a TGA4000 instrument from PerkinElmer. Samples were heated to 900 °C at a heating rate of 10 °C min⁻¹ in air. Powder samples diluted in KBr were examined by diffuse reflectance Fourier transformed infrared (DRIFT) spectroscopy using a Thermo Nicolet Nexus FT-IR

spectrometer fitted with a Spectra-Tech DRIFTS cell (Thermo Fisher Scientific, Waltham USA). DRIFT spectra were measured between 400 and 4000 cm^{-1} with an instrumental spectral resolution of 4 cm^{-1} using 160 scans. Raman-scattering experiments were performed on NaX and AgX zeolite powders with a Horiba Jobin-Yvon T64000 triple-grating spectrometer equipped with a LN_2 -cooled Symphony CCD detector and an Olympus BH41 microscope with a 50 x long-working distance objective. Spectra in the range 15–4000 cm^{-1} were collected in backscattering geometry using the 514.5 nm line of an Ar^+ -ion laser (Coherent Innova 90C FreD). The laser power on the sample surface was 5.9 mW, whilst the diameter of the laser spot on the sample surface was approximately 2 μm . No polarization, orientation, or spatial dependence of the Raman spectra was detected, indicating that the average linear crystallite size is much smaller than linear size of the probed sample volume. The achieved spectral resolution was 1.9 cm^{-1} , while the precision in the peak positions was 0.35 cm^{-1} . The measured spectra were baseline corrected for the continuum photoluminescence background, temperature-reduced to account for the Bose–Einstein occupation factor and then the spectral range 15–650 cm^{-1} was fitted with Lorentz functions to accurately determine the peak positions, full widths at half maximum (FWHMs) and intensities.

To check whether Ag enters the zeolite structure in mono- or divalent ionic form, Fourier transform infrared (FTIR) spectroscopic experiments in the far-IR range (50–550 cm^{-1}) were conducted on NaX and AgX powders as well as on reference mechanical mixtures of NaX with 10 wt% commercial Ag(I) (99.99%, Alfa Aesar) and Ag(II) (98%, Alfa Aesar) oxides.

FTIR spectra were measured in transmission with a Bruker IFS66 v/S equipped with a Globar white source, a DTGS detector, and a 6 μm Si/Mylar beam splitter. In

order to avoid artificial absorption bands from rotation transitions of atmospheric molecules, in particular from H₂O molecules, the far- IR spectra were measured in the sample compartment under a vacuum of 3 mbar. Samples have been prepared as ethanol suspensions, placed onto Si windows (Korth, 400 mm thick, wedged) and the ethanol evaporated off. A background spectrum was collected from a clean Si window. The mirror scanning velocity was 5 kHz and the instrumental spectral resolution was 4 cm⁻¹. Spectra were averaged over 32 scans. An attempt was made using synchrotron IR radiation (IR2 beamline at ANKA/KIT) to collect far-IR spectra from individual zeolite particles NaX, AgX, M-AgX, and V-AgX before and after their incorporation into elastomers. An IR microscope, sealed in a home-made compartment and purged with N₂ gas was used for the analysis. Although the humidity was reduced to ~3%, the spectral range below 300 cm⁻¹ was still confounded by the H₂O rotation bands, which prevented definitive interpretation.

2.6.2 Polymer characterisation

Hexane (Fisher) swelling measurements on the composite samples were carried out at ambient temperature. Sample dimensions were 10 mm x 20 mm x 1 mm and the immersion was for 24 h. After immersion, excess hexane was removed from samples before weighing using filter paper. Degree of swelling was calculated using the following equation:

$$\text{Swelling degree (\%)} = \frac{\text{Weight before} - \text{Weight after}}{\text{Weight before}} \times 100$$

For tensile testing, dumbbell specimens with a width of 3.6 mm were cut from the approximately 1 mm thick SE sheets. A universal testing machine, Hounsfield H10KS tensometer, was used and the tensile tests were carried out at a crosshead

speed of 500 mm min⁻¹. The dumbbell specimens were placed within the tensile grip, with a separation of 20 mm between them. Prior to testing, the thickness of each specimen was measured using a digital caliper at the centre and at the ends. The tensometer measured extension of samples and a 100 N load cell measured the applied force. Five composite samples per compound were tested.

Colour changes in the dental acrylic composites were tested by using the colorimeter (Gretag Macbeth Spectro-Eye, X-Rite, England, UK). In reflectance mode against white background, Sample specimens (10 x 20 mm) were measured in three randomly selected areas. Absolute values of the three coordinates (L*, a*, b*) were achieved. Before the measurement, in order to prevent colour variation, the white background was standardised. For each specimen, three repeated measurements were taken to evaluate the colorimetric values, i.e. b* (yellow-blue proportion), a*(red-green proportion), and L*(brightness). By using the colorimetric values, the differences with the zero value were measured from the means value of ΔL^* , Δa^* and Δb^* . From this particular difference, the difference in colour ΔE for each and every sample was measured by using the below equation:

□

$$(\Delta E=[(\Delta L^*)^2+(\Delta a^*)^2+(\Delta b^*)^2]^{1/2})$$

$$\Delta L^* = L_1 - L_0, \Delta a^* = a_1 - a_0, \Delta b^* = b_1 - b_0$$

L₁, a₁, b₁: sample, L₀, a₀, b₀: control.

Chapter 3. Results and discussion

3.1 Ag zeolite powders and their antimicrobial efficiency

3.1.1. The antimicrobial properties of Ag⁺-EMT and Ag⁰-EMT zeolites

In the present work, the antibacterial properties of an EMT type zeolite, ion-exchanged with silver before and after silver reduction were tested and directly compared. The EMT-type zeolite (diameter of 10 to 20 nm) stabilised in water suspensions was synthesised in the absence of an organic template.³⁹ The high porosity, low Si/Al ratio, high concentration of sodium and ultrasmall crystal size of the EMT-type zeolite permitted the introduction of high levels of silver using short ion-exchange times in the range of 2–6 h (Table 5). The bacterium selected in this study for determination of the antimicrobial properties of Ag-EMT samples was *Escherichia coli*, which is one of the most popular microorganisms in Ag-zeolite studies.^{89, 97-101, 103, 108} The killing efficacy of pure EMT, Ag⁺-EMT and Ag⁰-EMT against *E. coli* was studied semi-quantitatively. 25 mL of the bacterial suspension was added to 5 mL of 0.5 mg mL⁻¹ suspension of Ag⁺-EMT and Ag⁰-EMT. The Ag-free EMT sample was used for control experiments. The samples were incubated at 37 °C in a rotary shaker incubator set at 150 rpm and a sample was taken every 60 seconds using a 50 dropper over a period of 0–7 minutes. The zeolite concentrations used in the tests were based on previous work on Ag-FAU zeolites.⁹⁵

Table 5. ICP-OES results of Ag⁺ leaching from Ag⁺-EMT and Ag⁰-EMT samples immersed in distilled water.

Sample	Ag (wt.%)
Ag ⁺ -EMT 2 h	1.1
Ag ⁰ -EMT 2 h	1.2
Ag ⁺ -EMT 4 h	8.0
Ag ⁰ -EMT 4 h	9.1
Ag ⁺ -EMT 6 h	14.0
Ag ⁰ -EMT 6 h	14.1

Experiments with Ag-free EMT zeolite (control) using both nutrient agar and thio-neutralising agar indicated that the number of viable *E. coli* cells was unaffected, independent of the growth medium used (Figure 10).

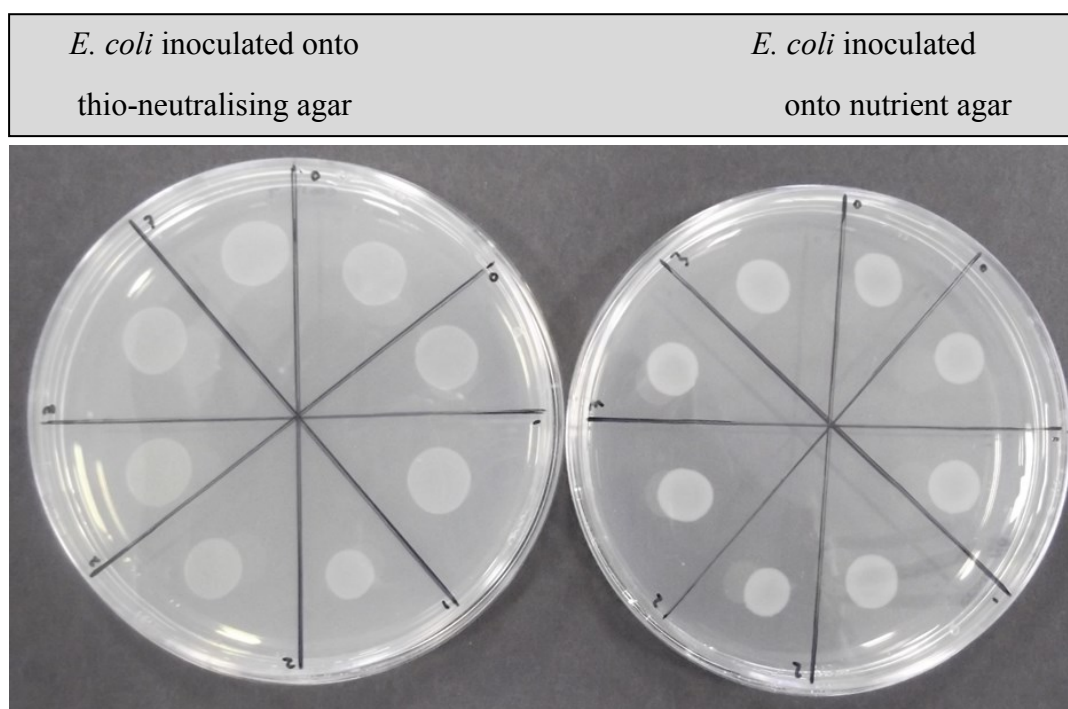


Figure 10. Spot inoculation of *E. coli* (in duplicate) onto thio-neutralising agar (left) and nutrient agar (right) at 1 minute intervals, following exposure to Ag-free EMT

zeolite (control). Each sector corresponds to one minute sampling time; the first sample is taken directly after mixing (0 min).

Initial experiments were conducted using nutrient agar as the growth medium for *E. coli*. However, no viable cells were detected from any of the Ag-containing EMT samples, even after sampling immediately following the addition of *E. coli* to the Ag-containing samples (0 min). It has been assumed that accurate testing of an antimicrobial agent includes the use of a substance to neutralise the effects of the antimicrobial agent before plating on agar. The use of such a neutraliser has been widely accepted by regulatory agencies. Further experiments continued using a thioglycollate agar in order to neutralise the effects of the Ag.^{206, 208}

In the presence of Ag⁺-EMT 4 h and Ag⁺-EMT 6 h samples, the number of viable *E. coli* cells visually decreased over time and no viable cells were detected at 3 and 1 minutes of incubation, respectively (Figure 11, left). For the Ag⁰-EMT 4 h and 6 h samples, no viable *E. coli* was seen at 2 and 1 minutes, respectively (Figure 11 and Figure 12, right). The approximate killing times increased to 6 min in the presence of Ag⁺-EMT 2 h samples. In Ag⁺-EMT 2 h and Ag⁰-EMT 2 h samples, the number of viable *E. coli* cells visually decreased over time and no viable cells were detected after 7 minutes of incubation for both samples (Figure 13).

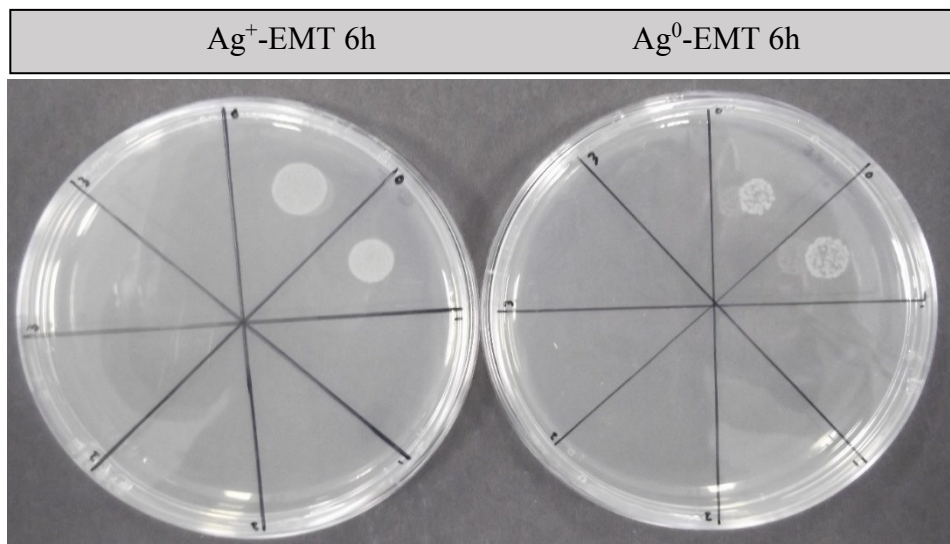


Figure 11. Spot inoculation of *E. coli* onto thioglycollate agar plates (in duplicate) following 1 minute interval exposure to Ag⁺-EMT and Ag⁰-EMT zeolite samples. Each sector above corresponds to one minute sampling time; the first sample is taken directly after mixing (0 min).

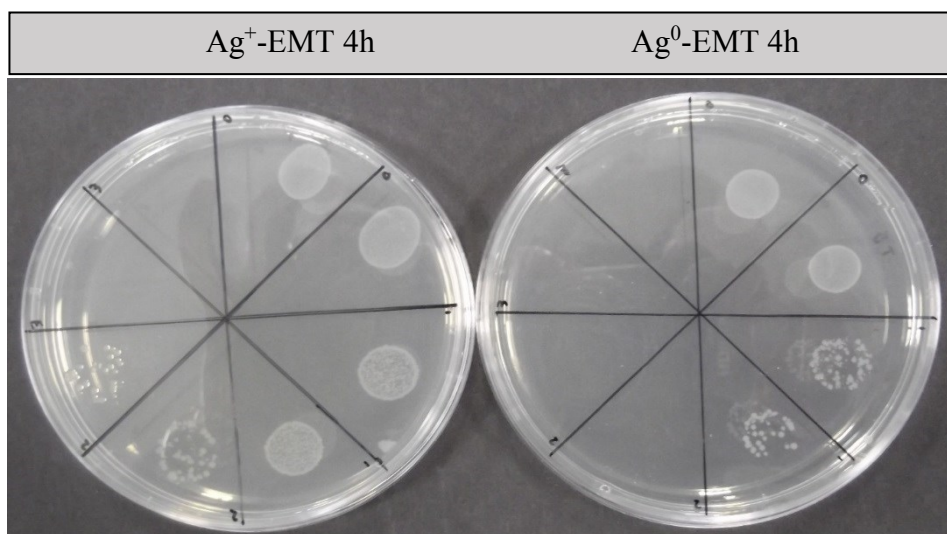


Figure 12. Spot inoculation of *E. coli* onto thioglycollate agar plates (in duplicate) following 1 minute interval exposure to Ag⁺-EMT and Ag⁰-EMT zeolite samples. Each sector above corresponds to one minute sampling time; the first sample is taken directly after mixing (0 min).

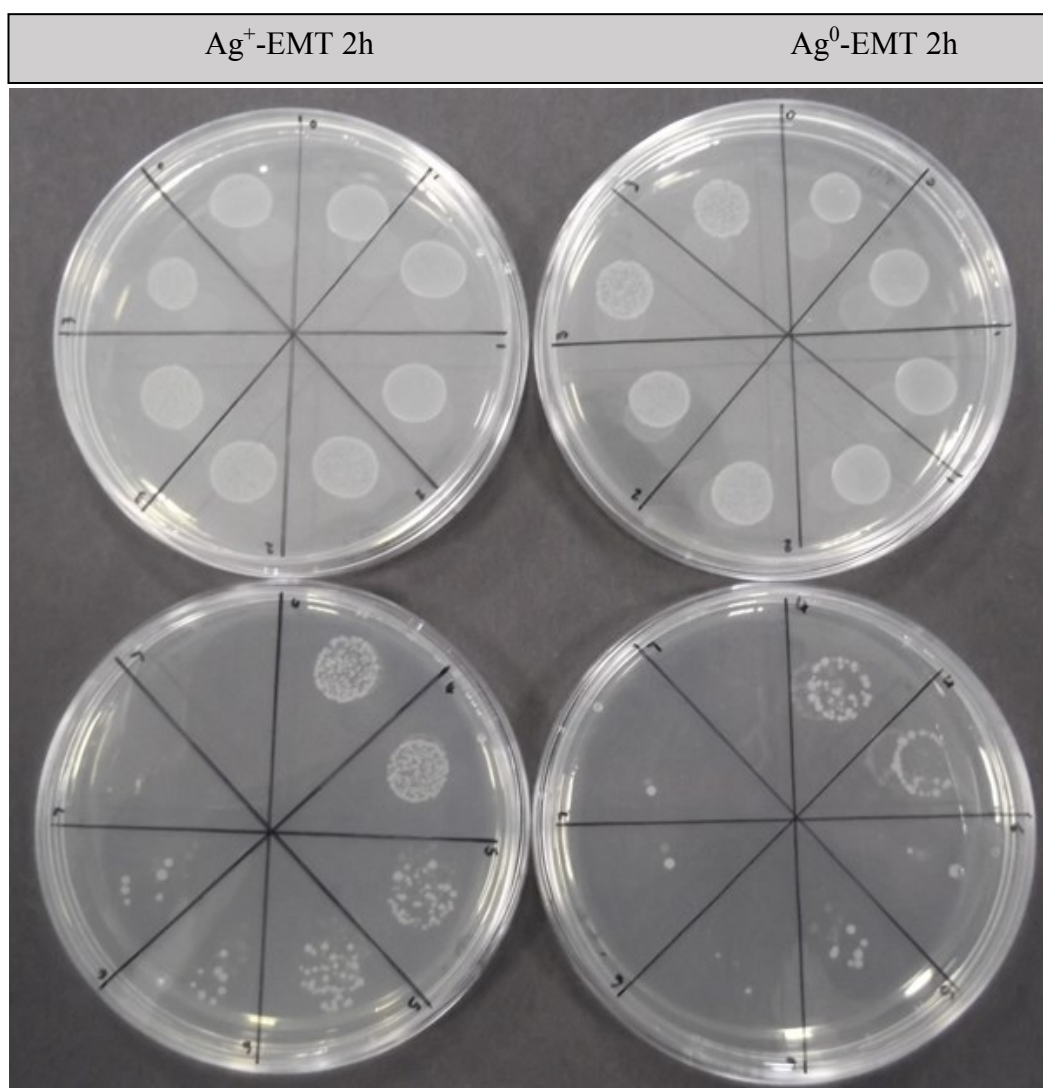


Figure 13. Spot inoculation of *E. coli* onto thioglycollate agar plates (in duplicate) following 1 minute interval exposure to Ag⁺-EMT and Ag⁰-EMT zeolite samples. Each sector above corresponds to one minute sampling time; the first sample is taken directly after mixing (0 min).

The antibacterial experiments performed indicated that the use of a neutralising agar to quench the antimicrobial activity of silver on bacteria following the exposure was of great importance for the results obtained, which again emphasized the difficulty in comparing results from different studies because of the

different test conditions used;^{67, 89, 97-101, 103, 108} The Ag⁰-EMT samples were slightly more active compared to Ag⁺-EMT samples across the different Ag loadings used in this work. The latter observation is surprising considering that the antibacterial properties of Ag⁰ are associated with its oxidation to Ag⁺ in an aqueous environment.^{67, 109} Possible explanations for these results could be the increased amount of surface silver nanoparticles in Ag⁰-EMT samples combined with the higher interparticle mesopore volume (Table 6). As a result, an improved Ag mobility resulting in higher Ag⁺ concentration in solution is achieved. Nevertheless, the difference in the killing times for reduced and non-reduced silver in the EMT samples was not significant. The results indicated instant killing of *E. coli* upon exposure to Ag⁺-EMT and Ag⁰-EMT 6 h zeolite suspensions demonstrating the potential of these materials for antibacterial applications.

Table 6. Specific surface area (^aS_{BET}), micropore volume (^bV_{mic}), external surface (^cS_{ext}) and mesoporous volume (^dV_{meso}) for Ag⁺-EMT and Ag⁰-EMT samples.

Sample	S _{BET} ^a (m ² g ⁻¹)	V _{mic} ^b (cm ³ g ⁻¹)	S _{ext} ^c (m ² g ⁻¹)	V _{meso} ^d (cm ³ g ⁻¹)
EMT	592	0.17	201	0.70
Ag ⁺ -EMT 2 h	487	0.15	127	0.36
Ag ⁰ -EMT 2 h	517	0.16	136	0.42
Ag ⁺ -EMT 4 h	447	0.13	135	0.35
Ag ⁰ -EMT 4 h	425	0.12	173	0.42
Ag ⁺ -EMT 6 h	366	0.10	151	0.38
Ag ⁰ -EMT 6 h	326	0.09	130	0.39

3.1.2. Conclusions

The EMT zeolite nanocrystals with high silver content showed excellent antimicrobial activity against *Escherichia coli*. The Ag⁰-EMT (2, 4 and 6 h) samples show slightly better antimicrobial efficacy compared to that of Ag⁺-EMT (2, 4 and 6 h) analogue samples due to increased mesoporosity. However, the differences are not significant and reduction of ion-exchanged Ag⁺ within the zeolite to Ag nanoparticles is not viable considering the complexity of preparation steps. The results in this study demonstrate that *E. coli* cells are instantly killed upon exposure to water suspensions of ultrasmall Ag⁺-EMT and Ag⁰-EMT 6 h zeolites. Antibacterial tests also showed that neutralising Ag to halt the Ag activity following incubation with microorganisms is essential for the reliability of the tests.

3.2 Influence of the zeolite textural characteristics on the antimicrobial efficacy of Ag zeolites

This section investigated the effect of textural characteristics (crystal size and mesoporosity) of Ag exchanged FAU- and BEA- type zeolites on antimicrobial efficacy. Two pairs of zeolite X (X1 and X2) and zeolite beta (B1 and B2) with different sizes, as well as a mesoporous zeolite beta sample (B3) were tested against *E. coli* and *C. albicans* using our previously developed semi-quantitative procedure. *E. coli* was used as a model for Gram-negative bacteria.⁷⁶ *C. albicans*, a recognised human pathogen¹⁹⁴ was used as an yeast microorganism.

3.2.1 Zeolite characteristics

SEM was used to determine the crystal size distributions of the samples used (Figure 14) and data are presented in Table 7. Sample X1 contained crystals with sizes of about 200 nm, whereas the crystal sizes of sample X2 were one order of magnitude larger (Figure 14 a,b). The size of the crystals in sample B2 was about two times larger compared to the crystals in sample B1 (Figure 14 c,d). This result was also confirmed by the DLS measurement (Figure 15) with Z-average sizes of 254 and 576 nm, correspondingly. DLS could not be used to analyse sample X1 because the polydispersity index for that sample was > 0.1 , indicating aggregation. Sample B3 contained crystals with sizes 550-750 nm and also impurities of amorphous material (Figure 14 e).

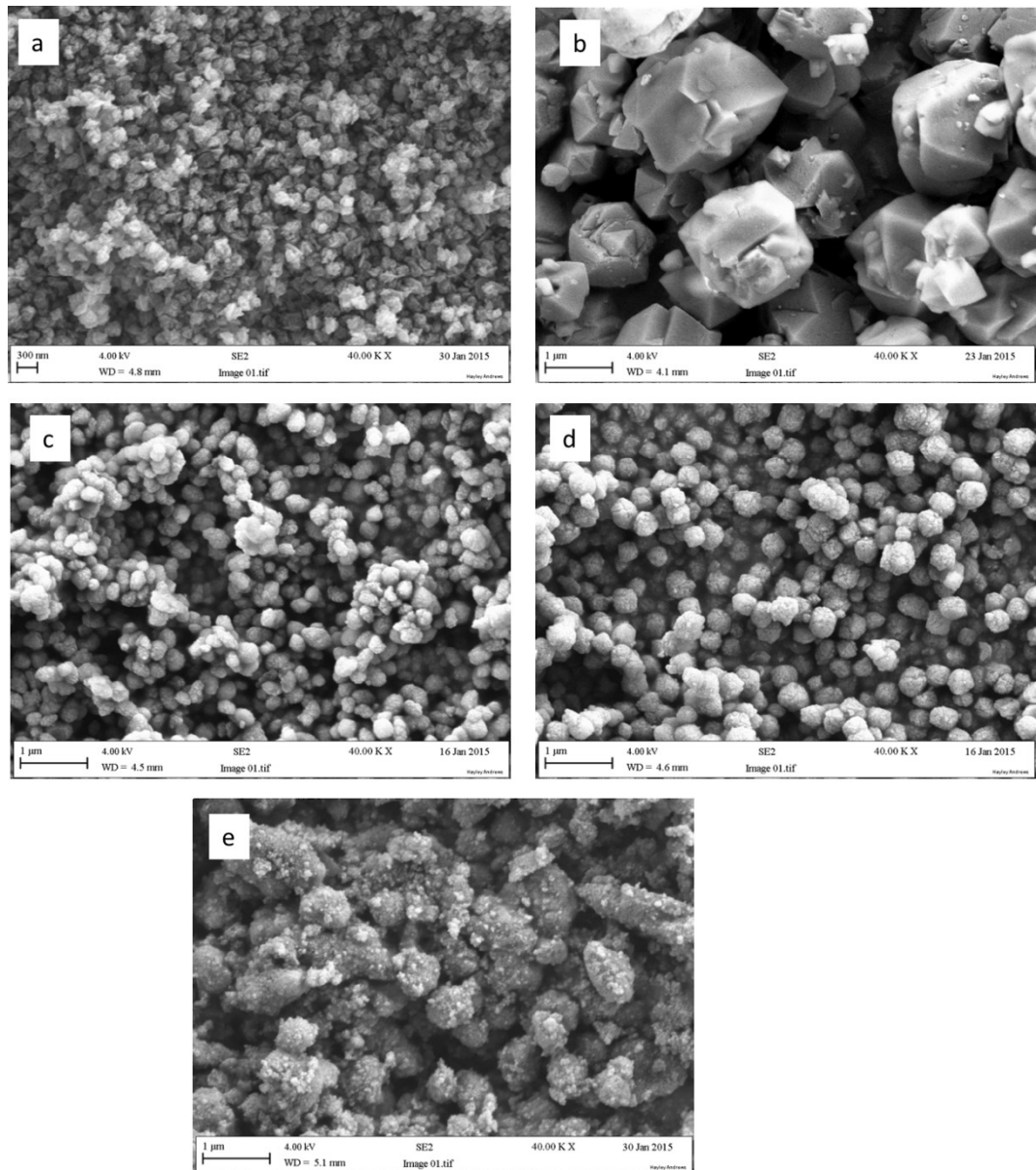


Figure 14. SEM images of (a) X1, (b) X2, (c) B1, (d) B2 and (e) B3 zeolites displaying the morphology and crystal size.

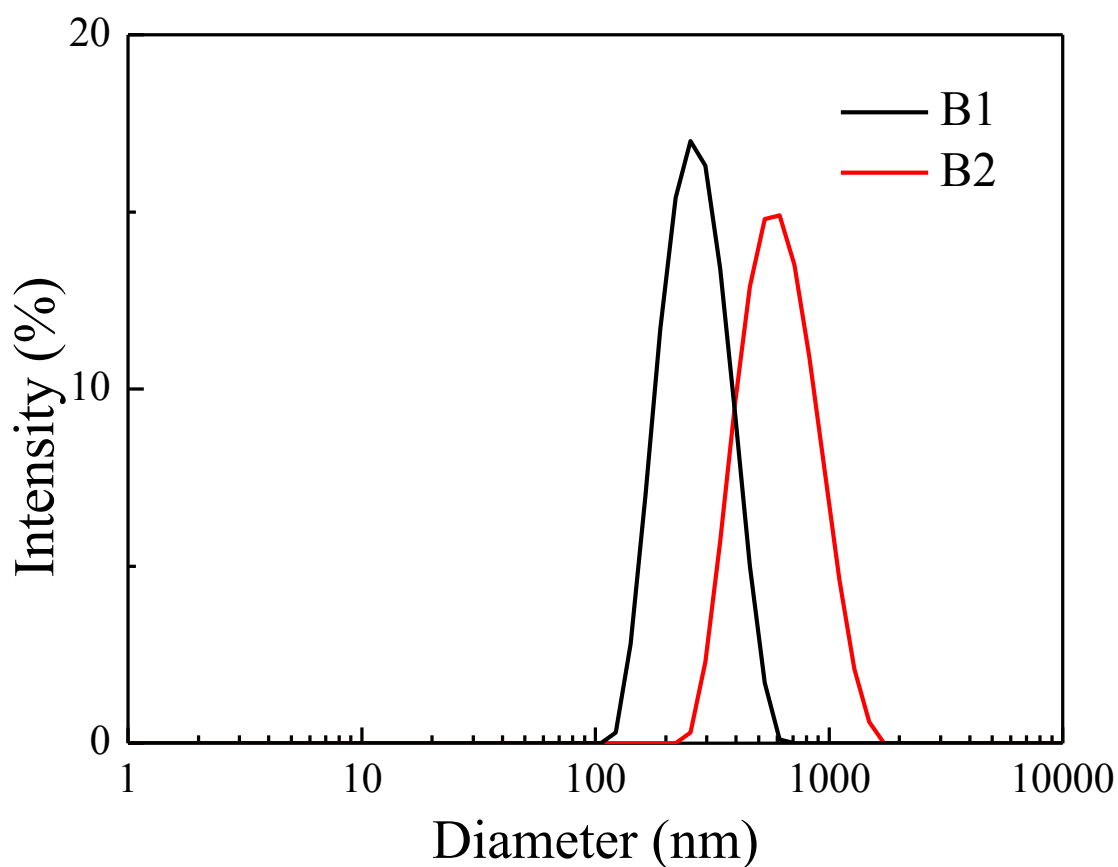


Figure 15. DLS particle size distribution for zeolite samples B1 and B2.

Table 7. Crystal sizes of the zeolite samples used determined by SEM.

Sample	Zeolite type	Crystal size (SEM)
X1	X	180-230 nm
X2	X	1.1-2.2 μm
B1	Beta	200-300 nm
B2	Beta	400-500 nm
B3	Beta	550-750 nm

The samples were further analysed by XRD (Figure 16). The XRD analysis confirmed the presence of zeolite X or zeolite beta, correspondingly, and the absence of other crystalline phases (Figure 16). Changes in the relative intensities in the XRD patterns of the Ag-exchanged zeolite X were observed compared to a NaX sample (Figure 16). The relative intensity variations are related to the change in the charge-balancing cations from Na to Ag.⁸⁹ The peak intensities of the X1 sample were considerably lower compared to these of X2 and the peaks were broader. Both effects can be attributed to the reduction of crystal sizes in X1 to nano-dimensions.¹⁷ Also, no additional peaks due to the presence of silver were detected. The reduction of crystal sizes in X1 to nano-dimensions X2 resulted in similar micropore volumes (Table 10), which were typical of a highly crystalline FAU-type zeolite.⁸⁷ Samples B1 and B2 were highly crystalline, whereas sample B3 contained a large amount of amorphous material as judged by the low intensity of the zeolite beta XRD peaks and the presence of an amorphous halo between 15 and 30 ° 2θ.

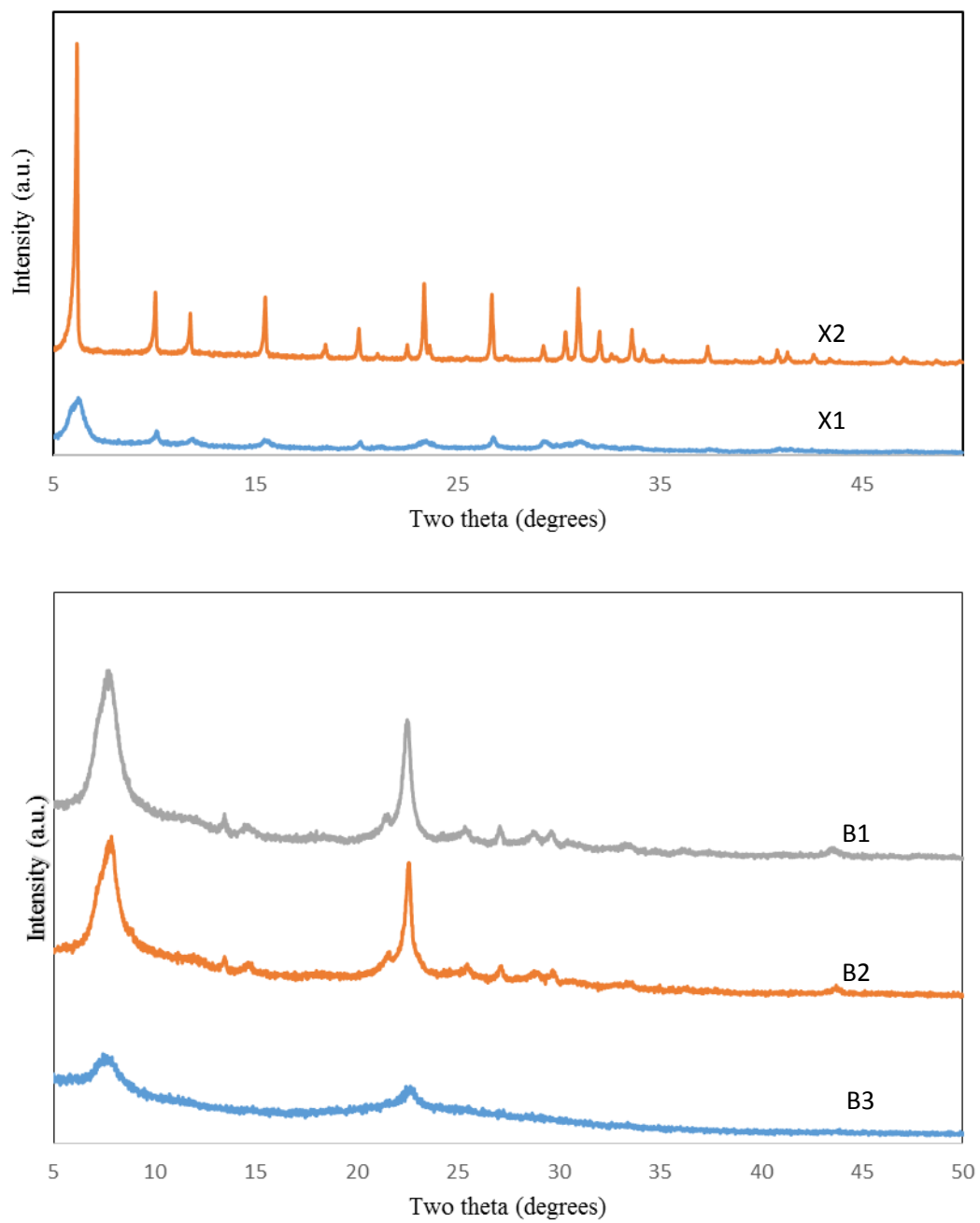


Figure 16. XRD patterns of the zeolites X and beta samples showing the phase of samples.

EDX was used to analyse the Si, Al, Na and Ag content in all samples. EDX results are presented in Tables 8 and 9. The Si/Al molar ratio remained constant in all samples. The Ag content slightly decreased as a result of the organic functionalisation (see Table 9). The reduction of crystal sizes in X1 to X2 resulted in similar micropore volumes (Table 10), which were typical of a highly crystalline FAU-type zeolite.⁸⁷ Samples B1 and B2 were highly crystalline, whereas sample B3 contained a large amount of amorphous material as judged by its lower micropore volume in agreement with the XRD results (Figure 16 and Table 10). Differences in the textural characteristics of the different samples were observed according to nitrogen adsorption data (Figure 17 and 18). All zeolites showed type I isotherms with a hysteresis loop at high relative pressures due to intraparticle textural porosity associated with small particle sizes.⁸⁷ The external surface areas increased with a decrease in the particle size accordingly (Tables 7 and 10). Sample B3 showed a type IV isotherm typical of mesoporous materials.

Table 8. Chemical analysis EDX results of zeolites.

Sample	Zeolite	Elemental composition (wt.%)				Si/Al ratio
		O	Na	Al	Si	
X1	X	40.0	15.5	20.5	24.0	1.2
X2	X	41.4	15.5	19.7	23.4	1.2
B1	Beta	45.9	-	3.8	50.3	13.3
B2	Beta	45.0	-	3.1	51.9	16.9
B3	Beta	45.2	0.8	3.8	50.1	13.0

Table 9. Chemical analysis EDX results of Ag zeolites.

Sample	Zeolite	Elemental composition (wt.%)					Si/Al ratio
		O	Na	Al	Si	Ag	
X1	X	35.5	12.1	19.4	22.6	10.8	1.2
X2	X	35.5	12.1	19.2	22.5	10.7	1.2
B1	Beta	44.4	-	3.7	49.5	2.4	13.5
B2	Beta	43.5	-	3.0	51.2	2.3	17.2
B3	Beta	49.6	0.7	3.7	43.1	2.9	11.5

Table 10. BET surface area (S_{BET}), micropore volume (V_{μ}), mesoporous volume (V_{meso}) and external surface (S_{ext}) of the Ag zeolite samples used.

Sample	Zeolite	$S_{\text{BET}} \text{ m}^2 \text{ g}^{-1}$	$V_{\mu} \text{ cm}^3 \text{ g}^{-1}$	$V_{\text{meso}} \text{ cm}^3 \text{ g}^{-1}$	$S_{\text{ext}} \text{ m}^2 \text{ g}^{-1}$
X1	X	690.5	0.30	0.51	62.3
X2	X	686.5	0.31	0.63	42.5
B1	Beta	639.4	0.22	0.50	185.9
B2	Beta	529.6	0.20	0.31	107.5
B3	Beta	535.6	0.05	1.00	418.4

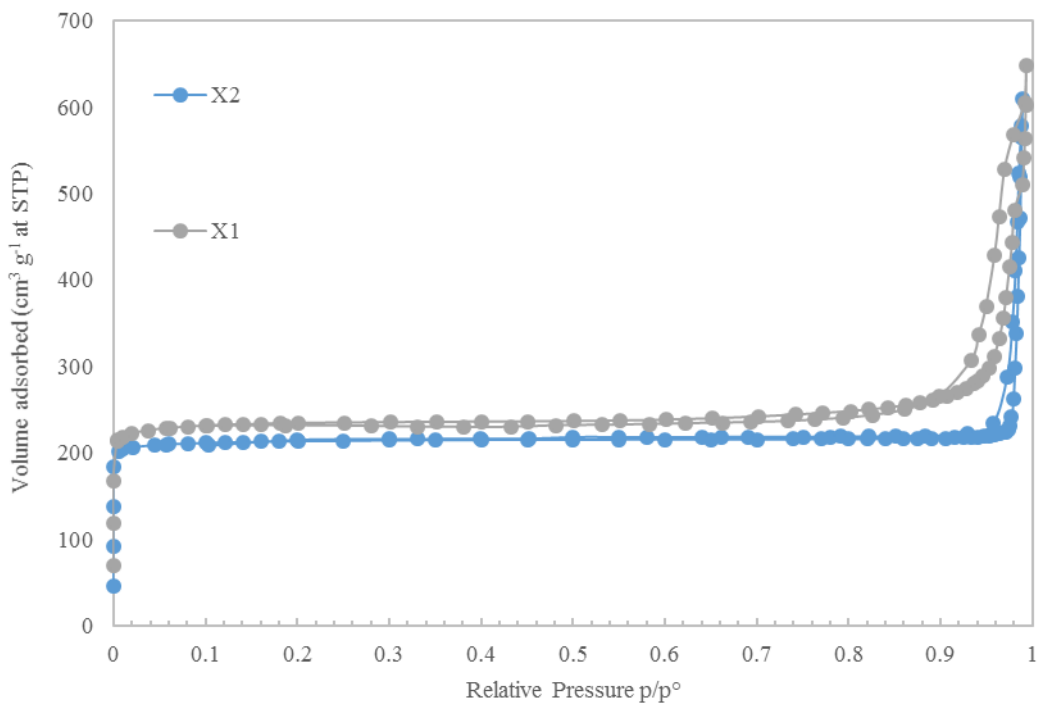


Figure 17. Nitrogen adsorption/desorption isotherms of zeolite X samples demonstrating the nature of the samples' pore structure.

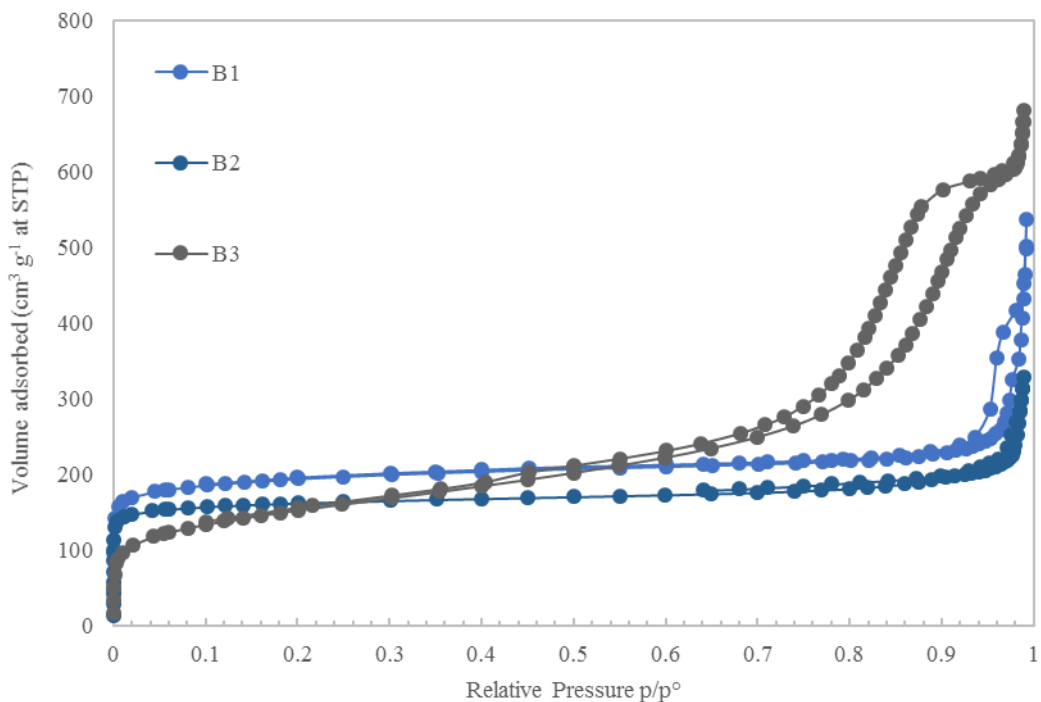


Figure 18. Nitrogen adsorption isotherms of caclined zeolites Beta. Nitrogen adsorption/desorption isotherms of caclined zeolites Beta samples demonstrating the nature of the samples' pore structure.

3.2.2 Cytotoxicity tests

For cytotoxicity tests, PBMCs were cultured for 2 days under the conditions described in experimental (Section 2.5.2.). At the end of cell treatments, PBMCs were subjected to flow cytometry analysis for Pre-G1 (apoptosis marker) and results are shown in Figure 19. According to the results, all zeolites were non-toxic at concentrations of 0.05 mg mL^{-1} and below. Moreover, zeolite beta B1 and B2 samples were non-toxic even at higher concentrations, 0.5 and 0.1 mg L^{-1} , respectively. The higher toxicity of zeolite X samples could not be explained by the amount of Ag released, which was lower compared to that for beta (Table 11). Thus, a possible explanation might be the higher aluminium content and associated

cytotoxicity of the zeolite itself, which effect was more pronounced for the nanosized X1 sample.⁸⁴ For biomedical applications, the determination of the cytotoxicity of Ag zeolites is of paramount importance, but such studies are rarely carried out. The cytotoxicity results indicated that Ag zeolite X was more toxic compared to Ag beta, particularly the nanosized sample.

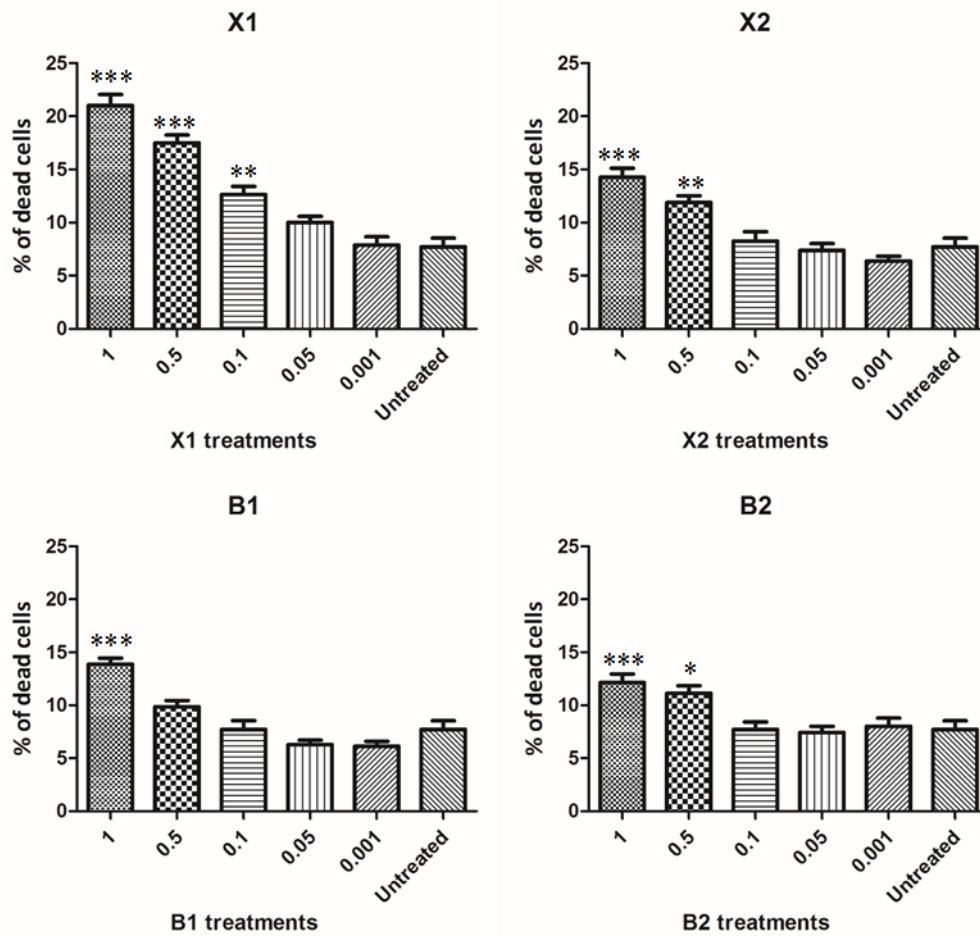


Figure 19. Cytotoxic effect of silver zeolite samples of different concentrations on freshly isolated cultured PBMCs. Asterisks (*) indicate significant differences in comparison with the control (* $p < 0.05$, ** $p < 0.01$, *** $p < 0.001$).

3.2.3 Antimicrobial tests

The zeolite samples were directly compared in terms of their antimicrobial efficacy using our previously developed qualitative procedure (Chapter 3.1). There have been reports in the literature, based on different testing methods, suggesting that larger zeolite crystals might have higher activity.^{95, 97} However, comparing the antimicrobial efficacy as a function of crystal size was not an objective in these studies. The Ag zeolite samples at different concentrations were tested against *E. coli* and *C. albicans*. The Ag-free samples used as controls did not show any antimicrobial activity (Figure 20). The results for zeolite concentrations of 0.5 mg mL⁻¹ and both microorganisms are shown in Figures 21 (*E. coli*) and 24 (*C. albicans*). The number of viable *E. coli* colonies visually decreased with time for both zeolite X samples (Figure 21). However, a substantial number of viable cells were still present in the presence of the nanosized X1 sample after 7 min, whereas no viable cells could be seen at the 7 min sampling time for the micron-sized sample X2. Similar trends were observed for the zeolite beta B1 and B2 samples, although these samples were more efficient and killed *E. coli* within 2 min. The mesoporous zeolite beta (B3) showed the highest efficacy with a killing time of only 1 min. The experiments performed with two additional concentrations, 0.05 mg mL⁻¹ (Figure 23) and 0.1 mg mL⁻¹ (Figure 22) showed similar results except that the killing time increased with increasing the zeolite concentration.



Figure 20. Spot inoculation of *C. albicans* (left) and *E. coli* (right) onto thioglycollate agar plates (in duplicate) following 1 minute interval exposure to the Ag free zeolite samples. Each sector on the plates above corresponds to one minute sampling time; the first sample (top) is taken directly after mixing (0 min).

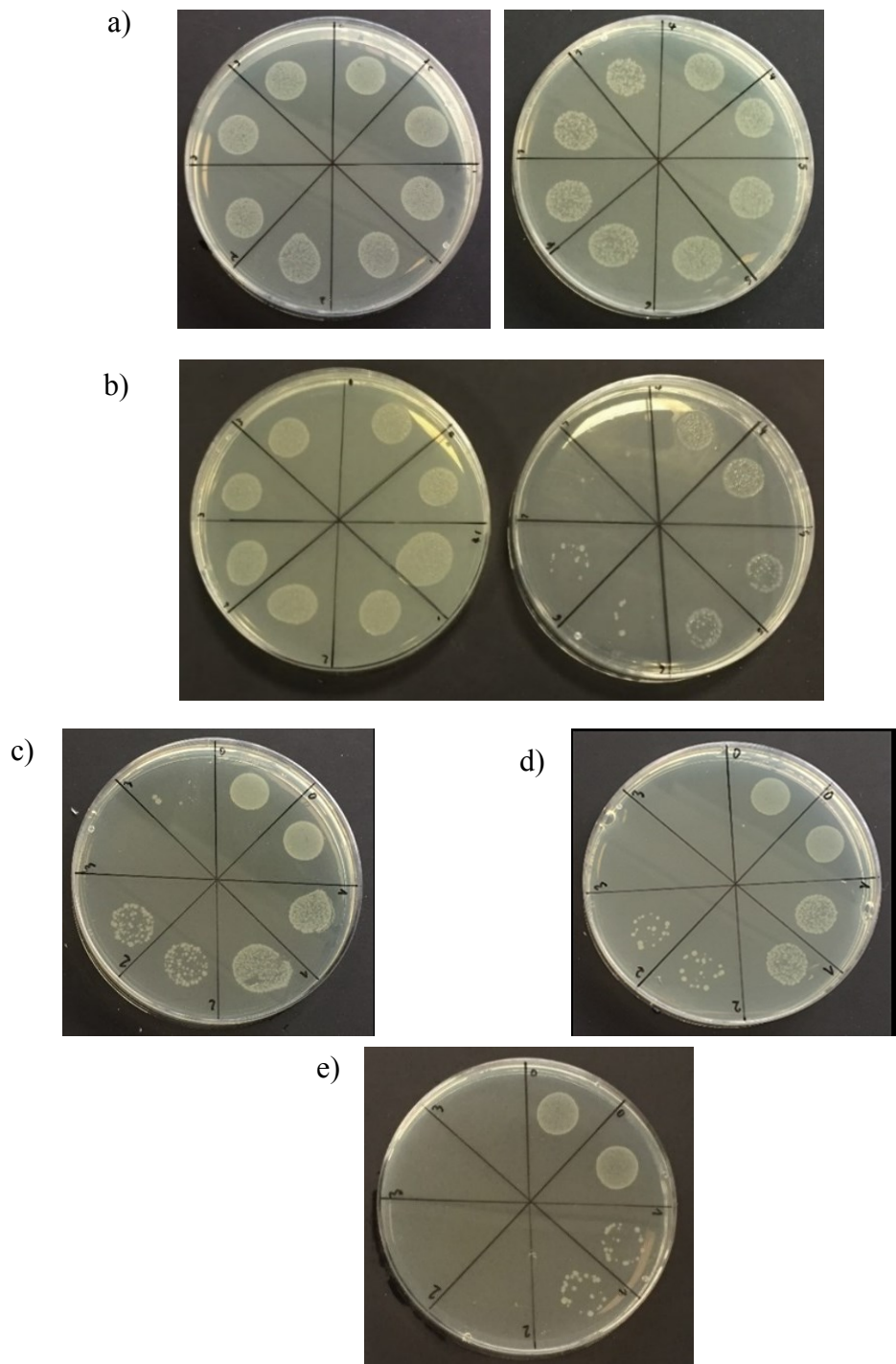


Figure 21. Spot inoculation of *E. coli* onto thioglycollate agar plates (in duplicate) following 1 minute interval exposure to X1 (a), X2 (b), B1 (c), B2 (d) and B3 (e) zeolite samples at concentration of 0.5 mg/ml. Each sector on the plates above corresponds to one minute sampling time; the first sample (top) is taken directly after mixing (0 min).

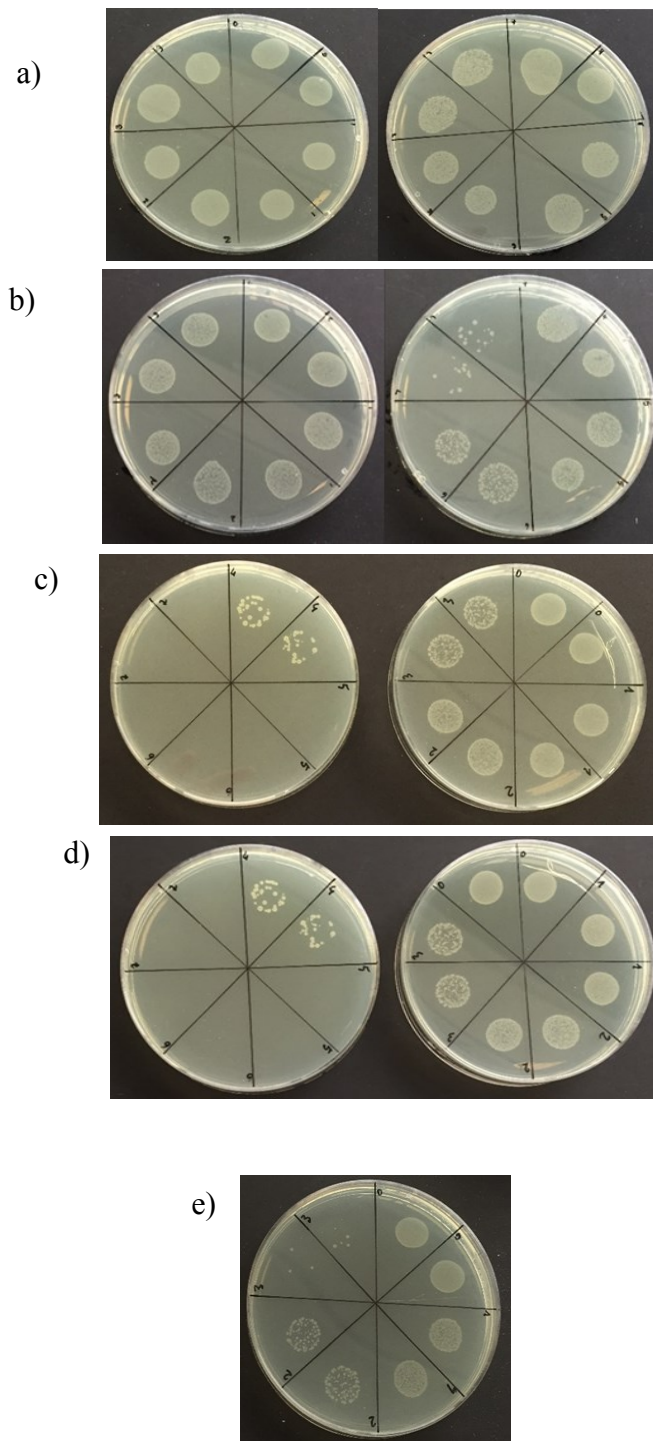


Figure 22. Spot inoculation of *C. albicans* onto thioglycollate agar plates (in duplicate) following 1 minute interval exposure to X1 (a), X2 (b), B1 (c), B2 (d) and B3 (e) zeolite samples at concentration of 0.1 mg/ml. Each sector on the plates above corresponds to one minute sampling time; the first sample (top) is taken directly after mixing (0 min).

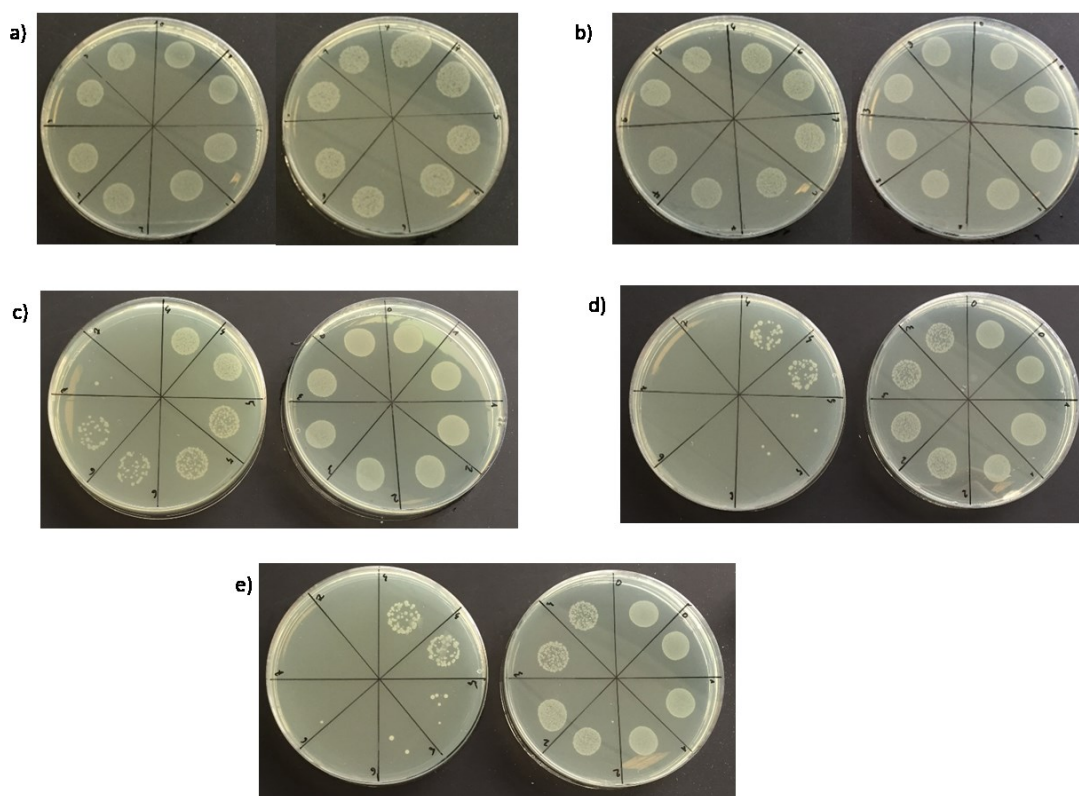


Figure 23. Spot inoculation of *E. coli* onto thioglycollate agar plates (in duplicate) following 1 minute interval exposure to X1 (a), X2 (b), B1 (c), B2 (d) and B3 (e) zeolite samples at concentration of 0.05 mg/ml. Each sector on the plates above corresponds to one minute sampling time; the first sample (top) is taken directly after mixing (0 min).

The 0.5 mg mL⁻¹ zeolite concentration was also tested against *C. albicans* (Figure 24). Although less conclusive, the results also suggest that micron-sized zeolites are more efficient against yeast. Zeolite beta was again more active compared to zeolite X. However, differences between zeolite samples were difficult to discern and quantitative analysis would be more appropriate to further study the activity of the samples against *C. albicans*. Additionally, because of the much larger

C. albicans cells and their lower concentrations compared to *E. coli*, the results for the two microorganisms cannot be directly compared.

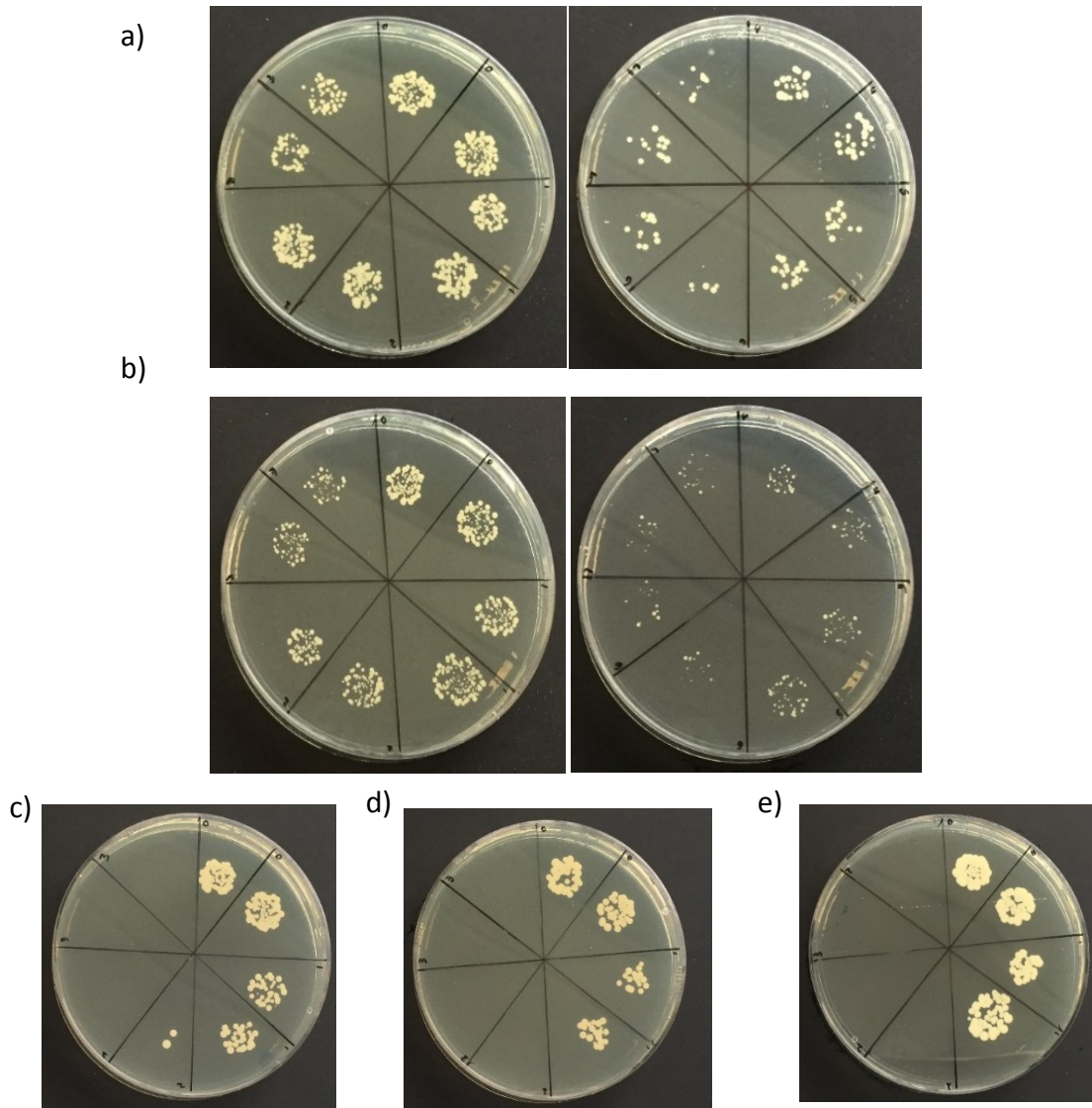


Figure 24. Spot inoculation of *C. albicans* onto thioglycollate agar plates (in duplicate) following 1 minute interval exposure to X1 (a), X2 (b), B3 (c), B4 (d) and B5 (e) zeolite samples at concentration of 0.5 mg/ml. Each sector on the plates above corresponds to one minute sampling time; the first sample (top) is taken directly after mixing (0 min).

The silver release data is provided in Table 11. The amount of released silver was higher for all zeolite beta samples despite their lower Ag loading, which could explain their higher activity. Daniel *et al.* has shown that there are distinct differences in the estimated number and strength of adsorption sites for Xe in silver-modified zeolites X and beta, suggesting that differences could be expected for their Ag release profiles.²⁰⁹ Extra-framework aluminium has also been speculated to hinder the silver release.¹⁰³ Additionally, smaller crystals may be aggregated to a larger extent in the testing medium to obstruct the release of silver and lower concentrations of Ag were measured for samples X1 and B1 compared to X2 and B2, respectively.

Table 11. ICP-OES results of Ag⁺ ions leaching from zeolite samples immersed in distilled water after the 7-minute tests using *E. coli*

Sample	Ag released (ppm)		
Concentration (mg L ⁻¹)	0.5	0.1	0.05
X1	0.05 ± 0.00	0.04 ± 0.01	0.02 ± 0.01
X2	0.15 ± 0.01	0.14 ± 0.01	0.11 ± 0.01
B1	1.71 ± 0.08	1.00 ± 0.04	1.01 ± 0.10
B2	2.19 ± 0.11	1.70 ± 0.07	1.52 ± 0.24
B3	2.78 ± 0.58	1.92 ± 0.11	1.08 ± 0.18

3.2.4 Conclusions

The effect of the zeolite structure and crystal size on the antimicrobial efficacy of two Ag zeolites, zeolite X and zeolite beta, was studied by a qualitative method allowing for a direct visual comparison of the antimicrobial activity of different samples. Zeolite beta was found to be more efficient compared to zeolite X and no viable cells of *E. coli* and *C. albicans* were observed within 2 min of incubation with both microorganisms using zeolite concentrations of 0.5 mg mL⁻¹. Introduction of mesoporosity in zeolite beta also resulted in an increase in the antibacterial activity. Reduction of crystal size resulted in an increase in the *E. coli* killing time as a result of the reduced Ag content released to the medium by the smaller crystals. The results reported here will be of interest when selecting silver zeolites for biomedical applications, particularly when fast antimicrobial response is required.

3.3 Silver zeolite-loaded silicone elastomers

A multidisciplinary approach has been applied to the preparation of antibacterial Ag zeolite/silicone elastomer composites aimed at products that satisfy a range of requirements, namely good mechanical properties after zeolite incorporation and strongly antibacterial. The antimicrobial effect of the silver zeolite containing polymers was tested against selected organisms. *S. epidermidis*, *E. coli* and *C. albicans* are amongst the organisms, which are recognised to be involved in medical device infections.

3.3.1 Zeolite characteristics

Initial experiments started with the preparation of small batches of zeolite Na-X. After confirmation of the phase purity and the degree of crystallinity, a large batch of zeolite Na-X was prepared and used for the preparation of all samples described in this section. The as-made zeolite was in a sodium form (Na-X). The NaX zeolite prepared had a Si/Al ratio of 1.4. SEM analysis indicated that the sample was highly crystalline and free from impurities of other phases (Figure 25 a and c). The crystal sizes ranged between 400 nm and 3.5 μm and a typical morphology for the FAU-type zeolite structure (Figure 25 a and c). The introduction of Ag and the functionalisation with organic silanes did not influence the morphology or the crystal size distribution of the zeolite samples (Figure 25 b and d) in accordance with previous studies.⁹¹

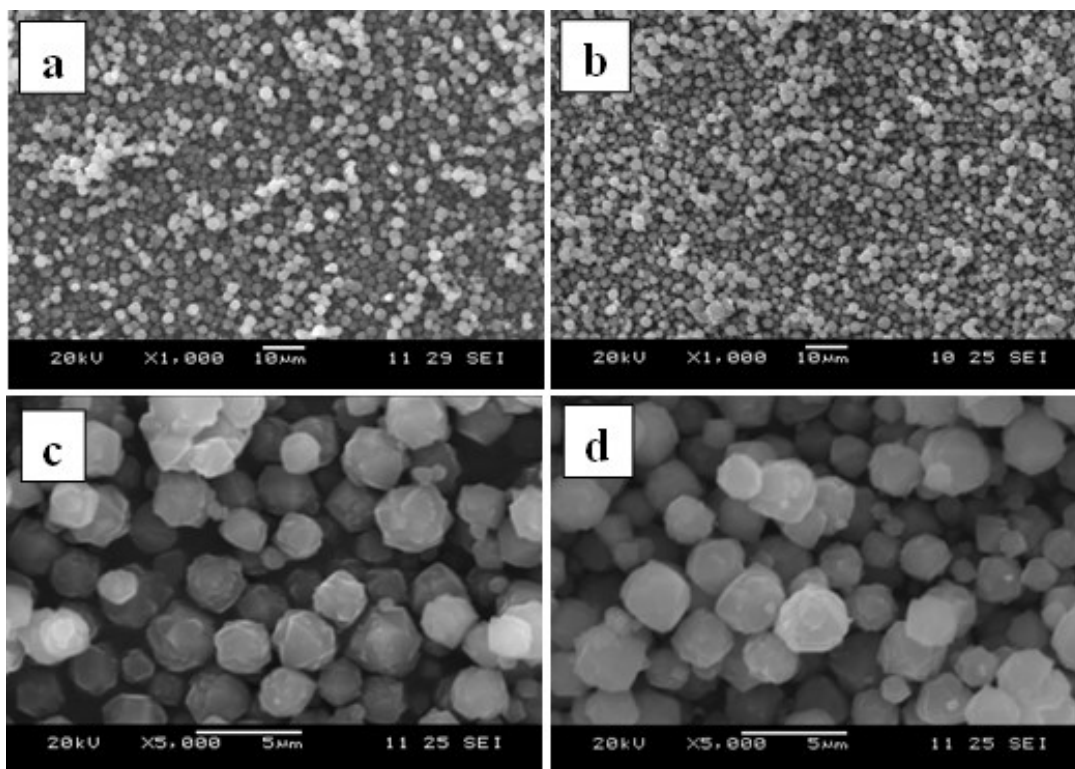


Figure 25. SEM images at two different magnification of (a and c) zeolite Na-X and (b and d) typical SEM images of organically modified AgX crystals displaying the morphology and crystal size.

The phase purity was further confirmed by XRD analysis (Figure 26). All Bragg peaks observed in the XRD patterns of all four samples could be indexed to the FAU-type zeolite structure.²¹⁰ Ag ion-exchange resulted in negligible change in the Bragg peak positions and widths, indicating high degree of crystallinity for all four samples. The substitution of Ag for Na only changed the relative intensity of some diffraction peaks, which was most pronounced for the (220), (311) and (331) faujasite peaks. In the XRD pattern of NaX, the intensity decreased in the order $I(220) > I(331) > I(311)$, whereas in the XRD pattern of all AgX zeolites, the order was $I(311) > I(220) > I(331)$. The relative intensity variations are related to the change in the charge-balancing cations from Na to Ag.⁸⁹ EDS analysis showed that

86% of the Na in NaX (15.9 wt%) was ion-exchanged with Ag in AgX (Table 12). The Si/Al ratio of 1.4 for NaX slightly increased as a result of the modification procedures to 1.5 for AgX and M-AgX and 1.7 for V-AgX, respectively, indicating that there may be a certain degree of Al leakage. However, EDX analysis does not allow quantification of the degree of Al leakage. The Ag content of zeolite samples decreased as a result of silane treatment (Table 12), and a C content of ca. 6 wt.% was detected in both M-AgX and V-AgX samples.

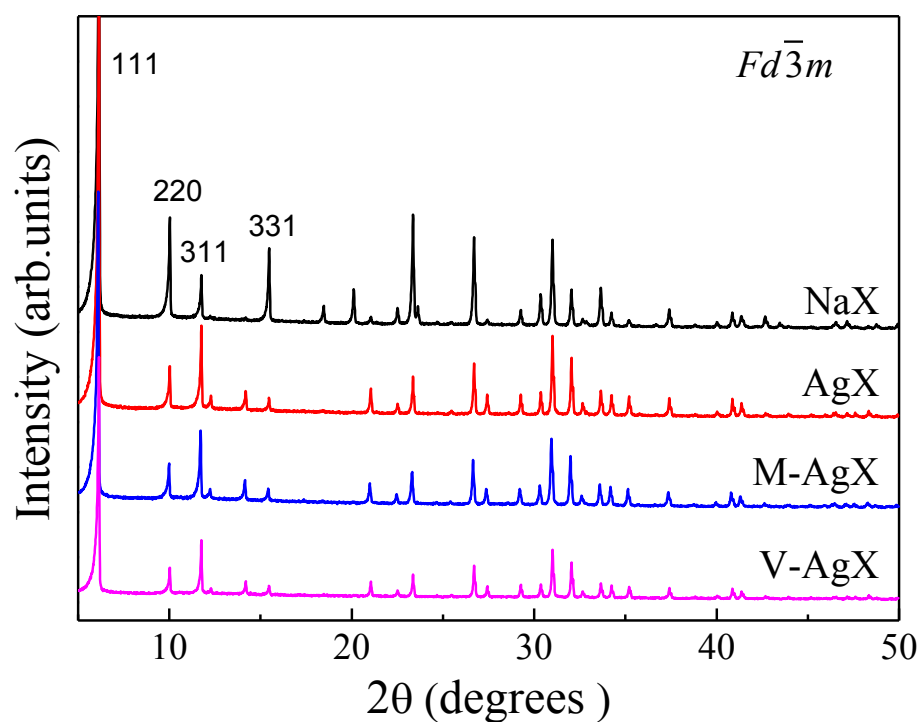


Figure 26. XRD patterns of Na-X and Ag-containing zeolite showing the phase of samples. Miller indices are given in $Fd\bar{3}m$.

Nitrogen adsorption isotherms, Brunauer–Emmett–Teller (BET) surface areas and micropore volumes for the Na-X and Ag-X samples further confirmed the results from the XRD study. The decrease in the degree of crystallinity was also

evident from the gas adsorption data (Figure 27 and Table 12). Nitrogen adsorption isotherms were all type I isotherms typical of microporous materials suggesting that the Ag ion-exchange and organic modification did not change the nature of the pore structure of the samples. However, there was a progressive decrease in the micropore volume in the order $\text{AgX} > \text{V-AgX} > \text{M-AgX}$. The external surface area of all zeolites was similar except for the M-AgX. Considering the XRD results, the decrease of the micropore volume is most likely due to the larger ionic radius of Ag^+ compared to Na^+ as well as inaccessibility of the nitrogen adsorbate gas to the pore structure of silane-modified samples and not due to loss of crystallinity.

Table 12. Ag content, BET surface area (S_{BET}), micropore volume (V_{μ}) and external surface area (S_{EXT}) of zeolite and modified zeolite samples.

Sample	Ag, wt%	$S_{\text{BET}} \text{ m}^2 \text{ g}^{-1}$	$V_{\mu} \text{ cm}^3 \text{ g}^{-1}$	$S_{\text{ext}} \text{ m}^2 \text{ g}^{-1}$
NaX	-	571	0.26	43.1
AgX	14.1	511	0.23	40.6
V- AgX	9.6	450	0.20	42.5
M- AgX	8.8	351	0.16	18.3

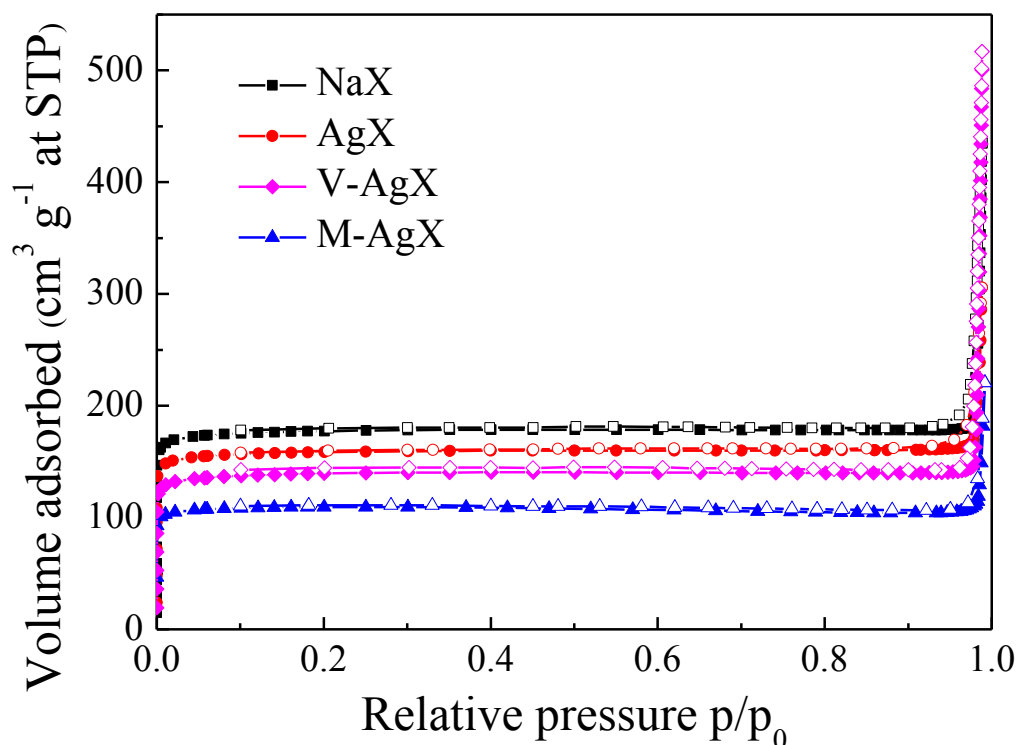


Figure 27. Nitrogen adsorption/desorption isotherms at $-196\text{ }^{\circ}\text{C}$ of NaX and Ag-containing zeolites samples demonstrating the nature of the samples' pore structure did not change with the introduction of silver.

The organic modification was further studied by DRIFTS analysis. DRIFTS spectra of Na-X, Ag-X, Ag-X/M and Ag-X/V samples are shown in Figure 28. First, all zeolite bands in the range $460\text{--}1100\text{ cm}^{-1}$ remained unchanged confirming preservation of the zeolite structure in the modified samples. The organic modification resulted in additional C–H bands in the range $1200\text{--}1500\text{ cm}^{-1}$, which were more evident in the spectrum of M-AgX, and also bands in the range $2800\text{--}3000\text{ cm}^{-1}$ for M-AgX.^{134, 211} In addition, a shoulder at 1700 cm^{-1} was present in spectrum of M-AgX, associated with the carbonyl C=O group of the M modifier.²¹²

The organic functionalisation was further proved by the ability to obtain dispersions of V-AgX and M-AgX in chloroform and their aggregation in distilled water (Figure 29). The modification of the Ag-X zeolite with silanes increased the zeolite hydrophobicity, which was confirmed by the zeolite low dispersibility in distilled water and high dispersibility in chloroform (Figure 29). The hydrophobicity of the modified samples is key for the next section in order to improve dispersion in the polymer.

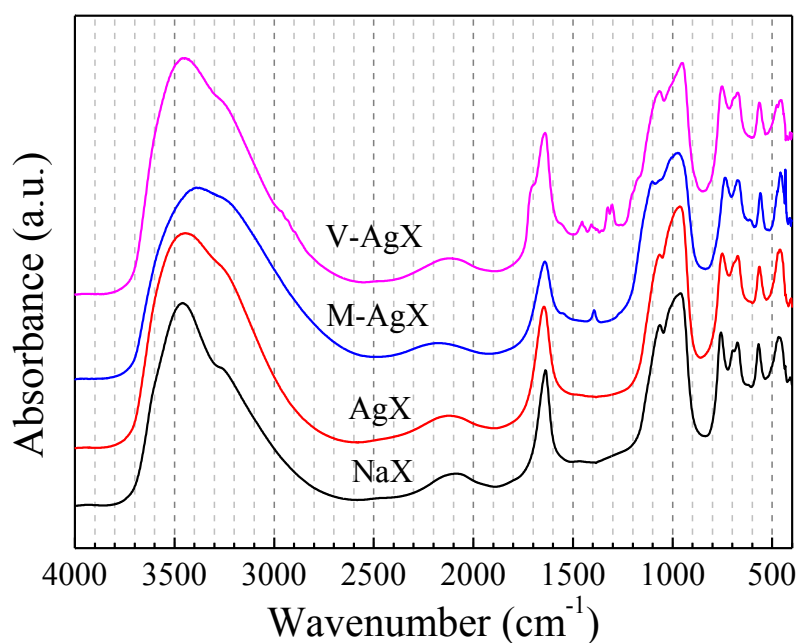


Figure 28. DRIFTS spectra of Na-X, Ag-X, Ag-X/M and Ag-X/V zeolites demonstrating the structure remained unchanged confirming preservation of the zeolite structure in the modified samples.



Figure 29. Digital images of: Left) V-AgX in distilled water and Right) V-AgX in chloroform showing dispersion of the vinylsilane modified zeolite in chloroform.

Figure 30a shows the Raman spectra of NaX, AgX, V-AgX, and M-AgX samples. The Raman spectra of the silane-modified samples V-AgX and M-AgX resembled the Raman spectrum of AgX, i.e. the influence of the organic modifier on the skeleton vibrations was negligible. All three Ag-exchanged samples showed the same spectral differences in the range of framework vibrations as compared to NaX: (i) slight shift of the main Raman peak near 510 cm^{-1} towards lower energies accompanied with a slight broadening (see Figure.30b) and (ii) additional weak peaks near 570 and 600 cm^{-1} .

The strongest peak in the Raman spectrum of zeolite X is generated by the double 6-membered rings (D6Rs) typical of FAU framework topology.²¹³ Previous single-crystal XRD analysis of Ag-exchanged FAU has revealed that a large part of the incorporated Ag^+ ions are accommodated in the D6Rs.²¹⁴ On the other hand, a lower-energy shift and broadening of the peak near 510 cm^{-1} along with appearance of a peak near 570 cm^{-1} due to the existence of single 4-membered rings (S4R) has been observed in amorphous FAU.^{213, 215} Raman scattering in the vicinity of 600 cm^{-1}

¹ is typical of small 3-membered rings in amorphous framework silicates.²¹⁶ Therefore, the Raman data presented here indicate that the incorporation of Ag in part induces local structural defects, but otherwise the overall zeolite framework topology is preserved. The Raman scattering in the range 3200-3600 cm⁻¹, originating from O-H bond stretching is suppressed in the spectrum of AgX. Thermogravimetric analysis showed a negligible reduction in the water content of AgX compared to NaX (Figure 31) indicating that this region of the Raman spectra was very sensitive to variations in the water content of samples. The level of photoluminescence background above 3000 cm⁻¹ was unfortunately too high for M-AgX and V-AgX to draw any conclusions about H₂O in the pores of these two samples. The comparison of far-IR spectra of AgX with the spectra of reference mechanical mixtures of zeolite NaX and monovalent and divalent silver oxides (Figure 32) indicate that indeed Ag enters the zeolite structure in a monovalent ionic form, in accordance with the results from single-crystal XRD analysis²¹³ and EXAFS analysis.²¹⁷

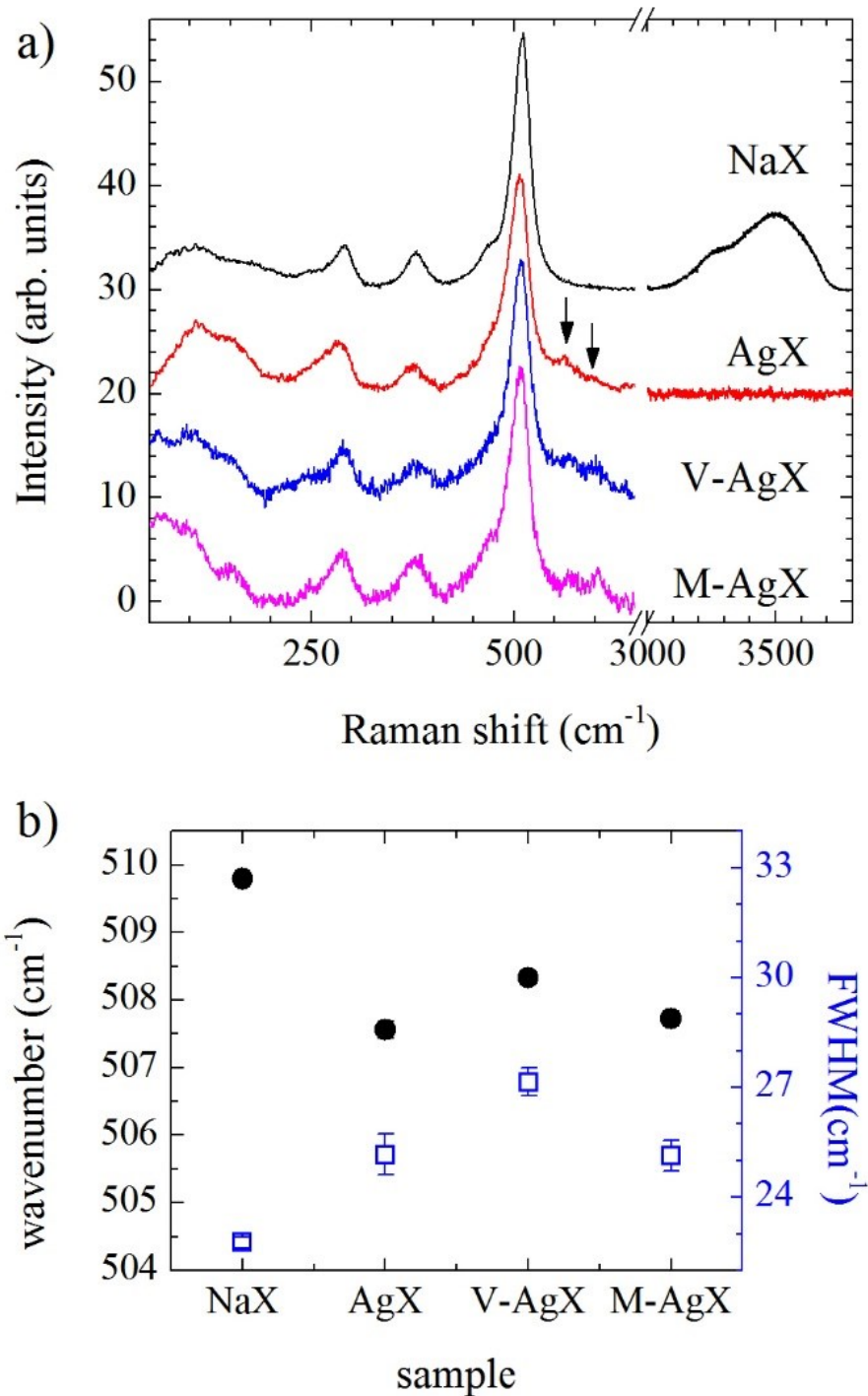


Figure 30. a) Raman spectra of NaX, AgX, V-AgX and M-AgX; spectra are vertically offset for clarity. The arrows mark the additional peaks observed in all Ag-exchanged samples. b) Position and FWHM of the strong peak near 510 cm⁻¹ as determined by fitting the spectra.

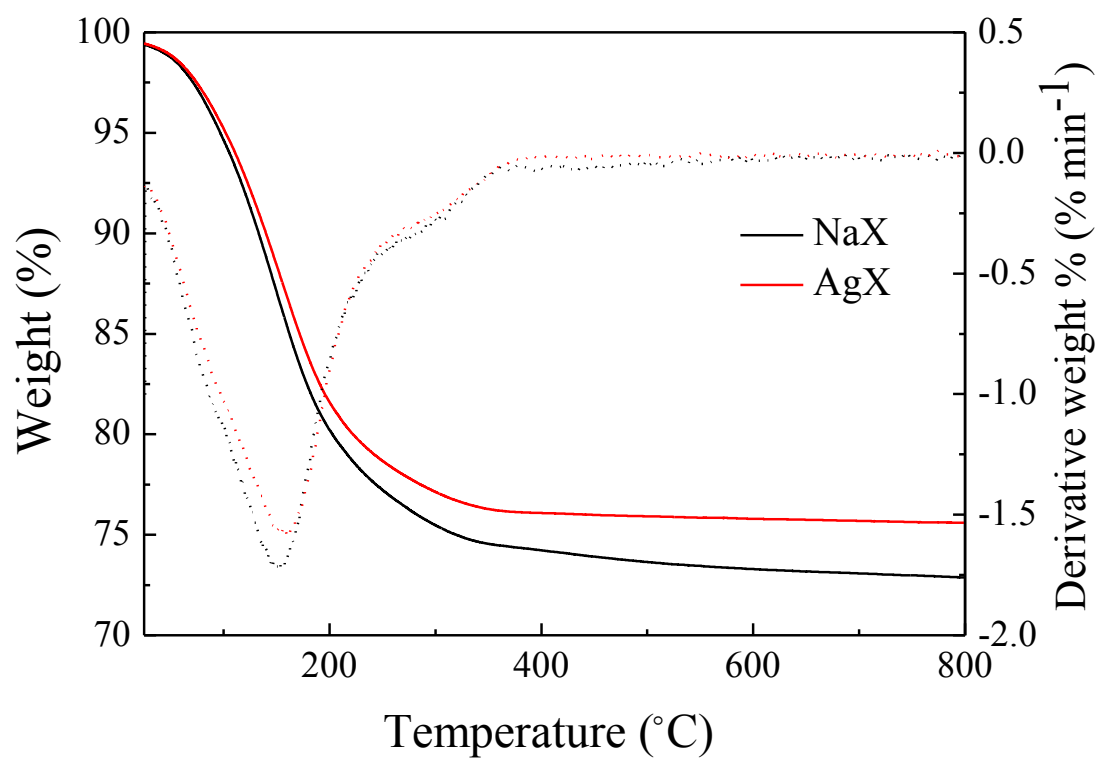


Figure 31. TGA curves of NaX and AgX samples demonstrating percentage mass loss against time.

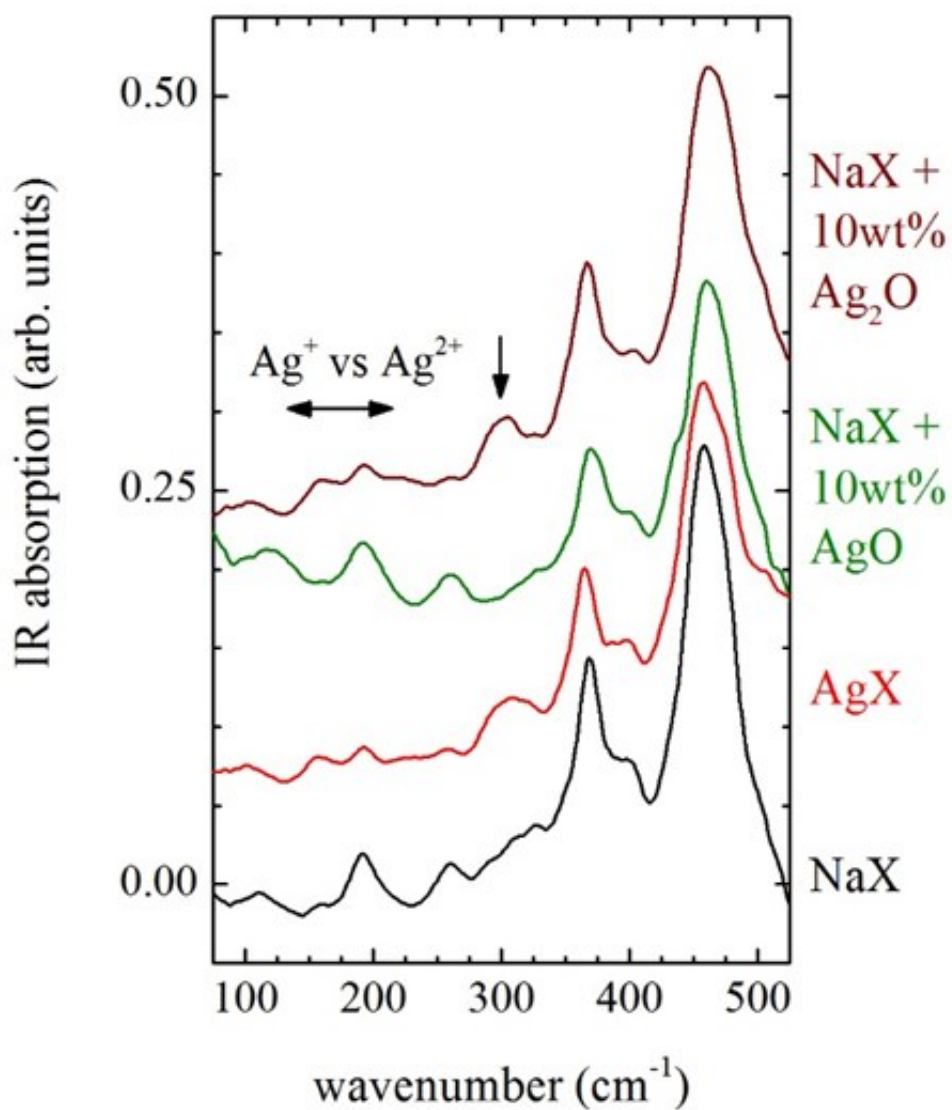


Figure 32. Far-IR absorption spectra of zeolite X (NaX) and Ag-exchanged zeolite X (AgX) as well as of reference mechanical mixtures of zeolite X with 10 wt.% Ag(I) oxide (NaX + 10 wt.% Ag₂O) and Ag(II) oxide (NaX + 10 wt.% AgO). The arrows mark the spectral bands that can discriminate monovalent and divalent Agⁿ⁺. Spectra are vertically offset for clarity.

3.3.2 Silicone elastomers

Na-X, Ag-X and organically functionalised Ag-X zeolites were used as additives in silicone elastomers. Zeolite and modified zeolite samples were added to silicone elastomers at 2 wt.% loading. Digital images of the obtained polymers are shown in Figure 33. The addition of the filler to the silicone elastomer presented a number of challenges. First, NaX and AgX without silane treatment was poorly dispersed in the matrix; large aggregates were noticeable.

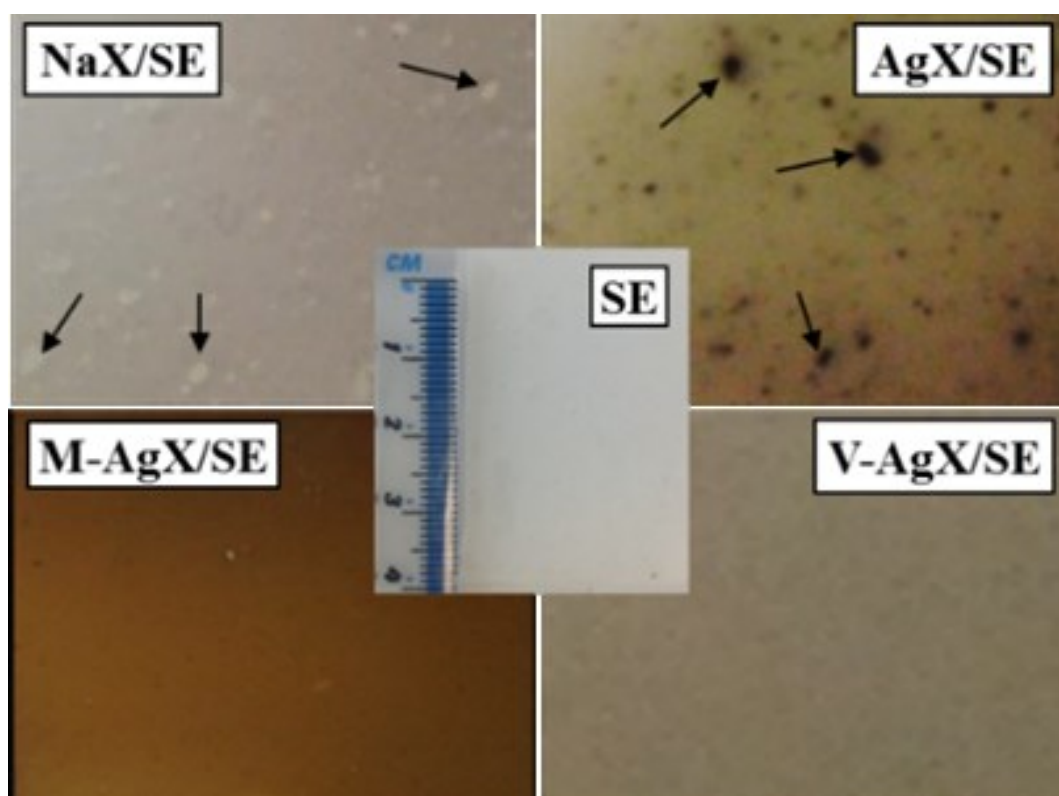


Figure 33. Digital images of silicone elastomers containing NaX, AgX, M-AgX and V-AgX zeolites showing the dispersion throughout the polymer. The middle image shows the neat SE (control). The arrows point to zeolite aggregates present in samples NaX/SE and AgX/SE.

Treatment of the NaX and AgX with the silanes, however lead to a significant increase in dispersion quality. This is consistent with the good dispersion observed in chloroform (Figure 29) and is a reflection of effective hydrophobisation of the zeolite surface. The colour of all elastomers containing Ag zeolite particles was darker compared to the neat SE. However, SE / Ag-X appeared yellow-brownish with brown aggregates visible throughout the polymer. Both of the coupling agent containing samples exhibited a brown discolouration due to the presence of silver, however the colour was homogeneous as opposed to the colour of SE / Ag-X. The brown discolouration was stronger in the M-AgX/SE in comparison to V-AgX/SE, approaching the overall appearance of NaX/SE. Since the amount of Ag in M-AgX/SE is slightly larger than that in V-AgX/SE (Table 12), the concentration of Ag cannot be the sole reason for the colour differences observed between M-AgX/SE and V-AgX/SE. Brownish discolouration of polymers upon addition of Ag has been observed before and attributed to the reduction of silver within the polymer, this effect has not been fully investigated.¹²¹ A combined computational and experimental study of the electronic structure of d¹⁰-ion-exchanged zeolites has demonstrated that the colour of evacuated (H₂O-free) silver containing sodium zeolite X changes to yellowish/reddish due to electronic transition between Ag⁺ and the lone pair of adjacent O from the four-membered rings in the absence of H₂O.²¹⁷ The reduction of H₂O in the zeolite pores during the preparation of the silicone elastomers could be the reason for the brownish colourisation observed in AgX/SE. In the case of M-AgX/SE and V-AgX/SE, organic functionalisation may have partially prevented the water from leaving the zeolite channels during preparation thus reducing the degree of colourisation, this was particularly true for the V-AgX/SE sample. Also, it was found that in the presence of

coupling agents, it was difficult to separate the silicone elastomer bond composite from the two mould plates after preparation. Therefore, introducing a melinex polyethylene film above and below the mould eased the removal and reduced the number of defects. The SEM images of cryo-fractured SE/zeolite composite fracture surfaces (Figure 34) supported visual observation of poor zeolite dispersion (Figure 33). Zeolite aggregates and poor filler-matrix adhesion are apparent in NaX/SE and AgX/SE (Figure 34a). In contrast, composites based on the organo-silane treated zeolite showed good filler dispersion and good filler – matrix adhesion (Figure 34b).

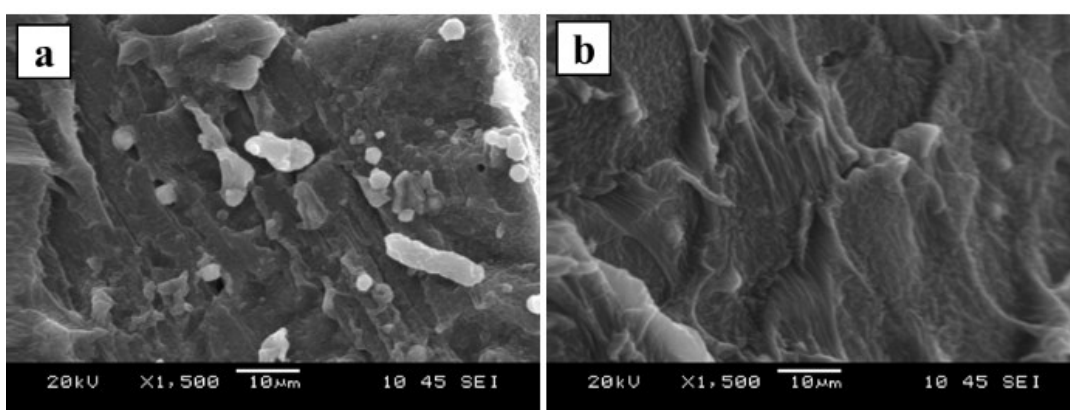


Figure 34. Typical SEM images of cryo-fractured surfaces of SE/zeolite composite containing: (a) unmodified zeolite (NaX or AgX) and (b) organo-silane modified Ag zeolite (M-AgX and V-AgX gave similar images), demonstrating the importance of the presence of a coupling agent.

Mechanical testing results are presented in Table 13. The mechanical testing of the samples provided some insight into both the stiffness and the filler-matrix interaction related to the coupling agent. The addition of the zeolite in the absence of a coupling agent resulted in reduction in the stiffness. There were significant differences in the tensile strength and elongation of break. The unfilled silicone

elastomer matrix and the composites based on silane treated zeolites showed similar values of tensile strength and elongation break, indicating good filler-matrix adhesion. The composites based on unmodified NaX and AgX had lower tensile strength and elongation at break due to poor dispersion of the zeolite particles and weak filler-matrix adhesion. Poor dispersion of the unmodified AgX and NaX was confirmed by the SEM analysis of SE cross-sections (Figure 34).

Table 13. Mechanical testing data of SE samples prepared in this work. Demonstrating no deterioration in the mechanical properties of composite samples compared to these of the neat silicone elastomer was observed.

Sample	Tensile Strength (MPa) \pm SD	Break % \pm SD
SE	5.98 \pm 0.56	661.6 \pm 65.00
SE / Na-X	4.01 \pm 0.78	557.5 \pm 91.55
SE / Ag-X	4.50 \pm 0.26	523.1 \pm 42.86
SE / Ag-X / M	5.89 \pm 0.31	649.5 \pm 21.00
SE / Ag-X / V	5.63 \pm 0.51	694.4 \pm 42.45

The hexane swelling characteristics are given in Table 14. The degree of swelling was lower when organo-silane modified NaX or AgX were added to SE; this is entirely consistent with increased filler – matrix interaction. Silicone/Na-X and Silicone/Ag-X showed the highest level of swelling in comparison with silicone (poor filler-matrix interaction). The high level of swelling can be related to reduced

filler-matrix adhesion which is constant with the inferior mechanical properties and the visible presence of aggregates. The composite based on silane treated zeolites exhibit a similar level of swelling to that of the unfilled matrix confirming the improved filler-matrix adhesion the presence of a coupling agent. These results indicated that the coupling agents improved the compatibility between the zeolite and the polymer and resulted in high quality SE/zeolite composites.

Table 14. The interaction between the interfaces can be explained from their Swelling degree of:(a) Silicone, (b) Silicone/Na-X, (c) Silicone/Ag-X, (d) Silicone/Ag-X/M and (e) Silicone/Ag-X/V.

Sample	Swelling level on hexane %
Silicone	1.77
Silicone/Na-X	3.74
Silicone/Ag-X	3.09
Silicone/Ag-X/M	1.88
Silicone/Ag-X/V	1.79

3.3.3 Antimicrobial assessment of silicone elastomers loaded with AgX

The SE samples were tested over a 24 hour period for their antimicrobial activity, with samples taken at time periods of 0, 5 and 24 hours. All the SE samples were tested against *E. coli* (ATCC 8739), *S. epidermidis* (NTCC 11046) and *C. albicans* (NCYC 1363). The SE and NaX/SE did not show any antibacterial activity in all tests. Figure 35 shows the antimicrobial activity of the samples against *E. coli*. SE / Ag-X exhibited the highest level of antimicrobial activity after 5 h of exposure.

This may be due to the higher Ag content in this sample (Table 12). All SE samples containing Ag showed at least a 3 log reduction in the number of *E. coli* cells on the surface in comparison to the positive controls. No viable cells were detected after 24 h of exposure. It should be noted that for the intended applications the long-term antibacterial activity is more relevant. Thus, the 24 h killing time indicates that the materials prepared are well-suited for fabrication of antibacterial medical devices.

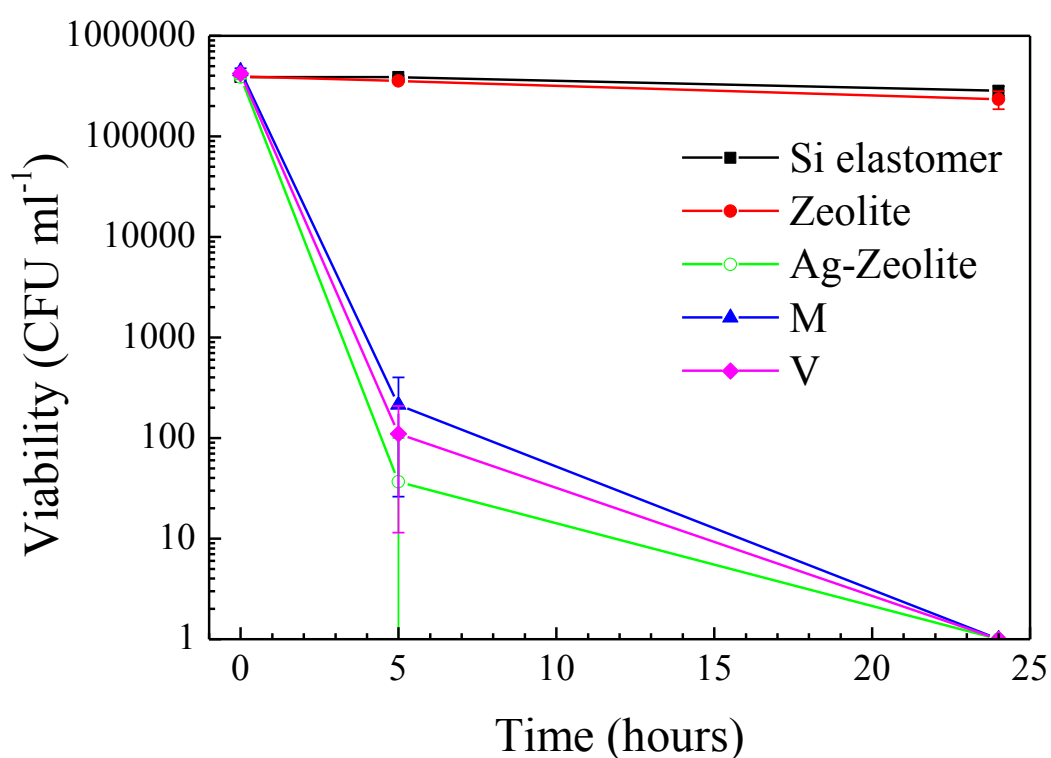


Figure 35. Antimicrobial testing of Silicone elastomer (Si elastomer), NaX/SE (zeolite), AgX/SE (Ag-zeolite), V-AgX/SE (V) and M-AgX/SE (M) against *E. coli*, demonstrating the successful conferment of antimicrobial activity to the SE after addition of the silver.

Figure 36 shows the antimicrobial efficiency of the samples against *S. epidermidis*. There were some variations in the killing efficiency of *S. epidermidis* after 5 hours for the different Ag containing samples, but these were not significant ($p > 0.05$) unlike test with *E. coli*. The bactericidal mechanism of silver ions against *E. coli* and *S. aureus* has been studied by Feng *et al.*⁷⁵ The authors attributed the inhibitory effect of Ag^+ to loss of replication abilities of the DNA molecules and inactivation of the bacterial proteins as a result of a reaction between the silver ions and the protein thiol groups. In addition, similar morphological changes were observed in the two types of bacteria but the Gram-positive *S. aureus* demonstrated a stronger defence system against Ag^+ . These results may explain the greater reduction in the number of viable *E. coli* cells after 5 h of incubation compared to that of *S. epidermidis* on SE containing functionalised Ag-zeolites. This was not observed for SE/Ag zeolite composites, probably because of local fluctuations in Ag concentration in test pieces as a result of the presence of aggregates in this sample (Figure 33). The SE samples containing Ag^+ challenged with *S. epidermidis* showed at least a 2 log reduction in the viable bacterial cells compared to the positive controls after 5 h exposure. The composite based on silane treated Ag zeolites, gave similar levels of performance throughout the 24 hours course. It seems that the Gram-positive *S. epidermidis* was more resistant compared to the Gram-negative *E. coli* because of the log reduction difference, which may be explained by the presence of the extra cell wall affecting penetration of the silver thus taking longer to achieve the same antibacterial effect.⁷⁵ Since the Ag^+ containing samples reduced the viability of *E. coli* and *S. epidermidis* and as no antimicrobial effect was observed in the controls (Ag^+ free samples), it suggests that Ag^+ were responsible for reducing the viable bacterial cell count.

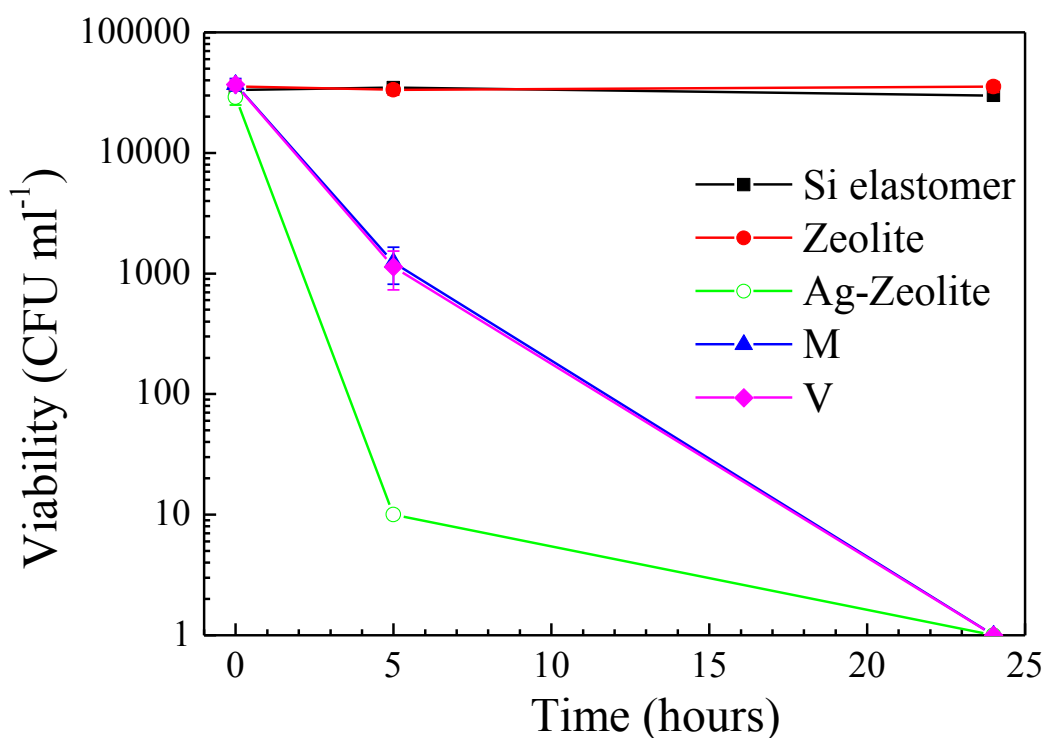


Figure 36. Antimicrobial testing of Silicone elastomer (Si elastomer), NaX/SE (zeolite), AgX/SE (Ag-zeolite), V-AgX/SE (V) and M-AgX/SE (M) against *S. epidermidis*, demonstrating the successful conferment of antimicrobial activity to the SE after addition of the silver.

The same procedure was applied to challenge with *C. albicans* but the growth medium was performed in Sabouraud dextrose liquid medium (Oxoid, UK). The antimicrobial activity of the samples against the yeast *C. albicans* was determined after 0, 24 and 48 h of incubation (Figure 37). *C. albicans* proved to be less sensitive to the action Ag⁺ containing samples than bacteria. A small decline in the number of viable cells was observed over the first 24 h for all test samples, although this was only significant when comparing V-AgX/SE at 0 h to 24 h ($p \approx 0.014$). At the 48 h sampling time, an increase of *C. albicans* on the test surfaces was apparent, although

again only significant when comparing V-AgX/SE at 24 h to 48 h. The reason for this slight increase may be because *C. albicans* reproduces by budding followed by release of daughter cells, which could have led to the higher colony count. The results in Figure 36 suggest that the Ag⁺ concentration released from the polymers is not high enough to kill the yeast. Eukaryotic yeast cells are larger and more complex than prokaryotic bacterial cells, and are less sensitive to many antimicrobial agents. Ferreira *et al.* found that Ag-containing FAU-type zeolites displayed higher minimum inhibitory concentrations for yeasts compared to bacteria.⁸⁹ It is therefore likely that an increase in the Ag-zeolite loading in the SE could also lead to greater efficacy against *C. albicans*. However, this was not an objective of the present study. However, it seems that *C. albicans* as a fungus is more resistant to the Ag⁺ containing samples than Gram-negative *E. coli* and Gram positive *S. epidermidis*. The structure of the cell wall of *C. albicans* may explain the need for greater amounts of Ag⁺-zeolite to reduce the number of viable cells¹¹⁹. An attempt was made to determine the concentrations of Ag released from the different surfaces prepared after immersion in distilled water. Silver concentrations were determined to be around 0.005 ppm for all surfaces and no trends could be established for the influence of sample type or the exposure time on the concentrations of released Ag. Greulich *et al.* have reported that silver ions can be toxic not only to bacterial but also to human cells in the concentration range 0.5 to 5 ppm of silver.⁸³

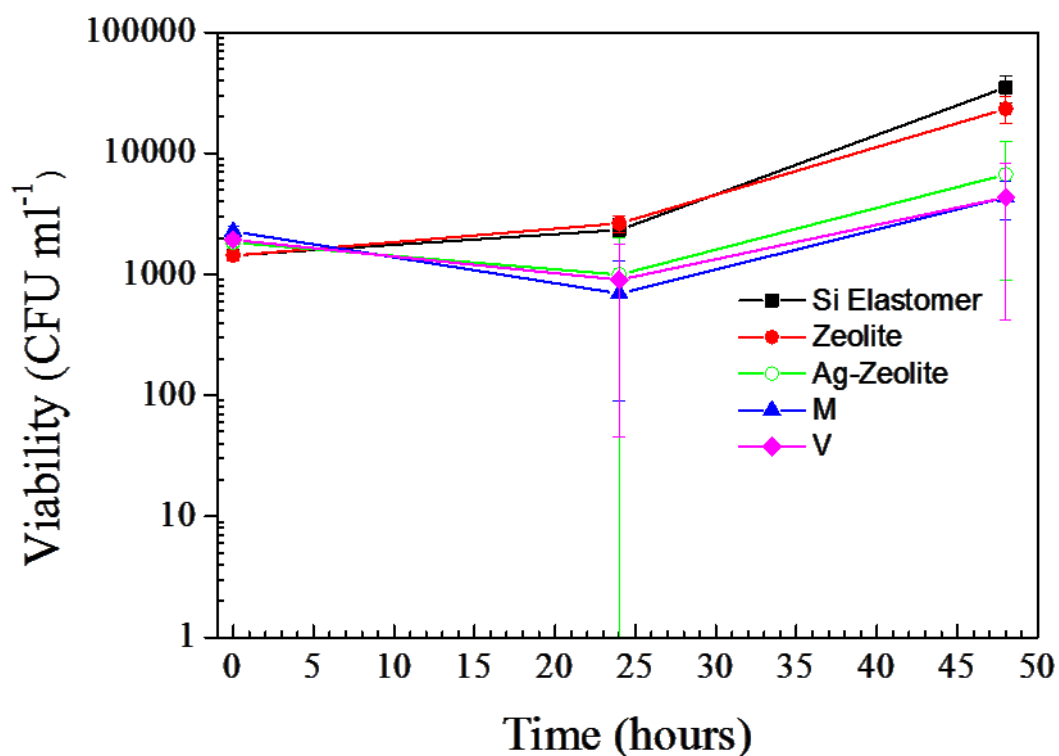


Figure 37. Antimicrobial testing of Silicone elastomer (Si elastomer), NaX/SE (zeolite), AgX/SE (Ag-zeolite), V-AgX/SE (V) and M-AgX/SE (M) against *C. albicans*, demonstrating the successful conferment of antimicrobial activity to the SE after addition of the silver.

3.3.4 Conclusions

A multidisciplinary approach was applied to the development of antibacterial silicone elastomers (SE)/zeolite composites. Silver zeolite X was prepared and incorporated into silicone elastomers after organo-silane modification. Raman spectroscopy revealed that Ag ion-exchange of the zeolites introduced local structural defects, however the overall zeolite structure was preserved. Far-IR analysis indicated that Ag was present in monovalent form. Organo-silane

modification of the zeolite was found to be essential for retention of composite mechanical properties, relative to the unfilled matrix. The latter, together with reduced swelling in hexane and SEM evidence, indicated that organo-silane modification lead to improved filler-matrix interaction. Reduction of ionic Ag to metallic Ag led to discolouration of the SE/Ag zeolite composites. Organo-silane modification led to a decrease in the extent of discolouration; interestingly this effect was strongest with the vinyl silane. The antibacterial tests revealed 4 to 3-log reductions in the viability of *E. coli* and *S. epidermidis* (after 24 h of incubation), respectively, on contact with SE/Ag zeolite composites. *C. albicans* was less sensitive to the test materials than the bacteria tested. A higher concentration of agent might prove more effective against this microorganism. The composites prepared could potentially be used for medical devices featuring long-term antibacterial activity to prevent infections.²¹⁸ The present work and previous research clearly demonstrate that a multidisciplinary approach is required for preparation and evaluation of antimicrobial polymers containing inorganic fillers in order to avoid compromising key aspects, e.g., zeolite characteristics, polymers mechanical properties and physical appearance or use of reliable antimicrobial tests.

3.4 Silver zeolite-loaded dental acrylic resins

In this section the characteristics and antimicrobial properties of Ag zeolite loaded dental acrylic resins were investigated. The organically functionalised Ag-X zeolites described in the silicone elastomer work were used as additives. 3-(trimethoxysilyl)propyl methacrylate was selected for organic functionalisation of the zeolite. The high level of silver (14 wt.%) within the zeolite enabled the preparation of antibacterial composites containing low levels of zeolite (2 wt.%, 0.7 wt.%, 0.4 wt.% and 0.2 wt.%). The antimicrobial effect of the silver zeolite containing polymers was tested against *E. coli* and *C. albicans*. The sustained Ag release over long periods of time were studied. Colour measurements were conducted before and after Ag release experiments in order to provide further insight into discolouration problems associated with silver-containing materials. In an attempt to overcome discolouration, dental acrylic samples containing 3-(trimethoxysilyl)propyl methacrylate functionalised Na-X zeolite (Ag free) at 2 wt.% and 1 wt.% were submersed in a solution of 0.01 M AgNO₃. The samples were tested for their antibacterial activity against *E. coli*.

3.4.1. Dental acrylic resins

Organically functionalised Ag-X zeolites were used as additives in dental acrylic resin (DA). Ag exchanged zeolites were added to dental acrylic resin at 0.2 wt.%, 0.4 wt.%, 0.7 wt.% and 2 wt.% loadings. Digital images of the composites obtained are shown in Figure 38. The organically functionalised zeolite was well distributed through the matrix with no visible aggregation in the polymer sample. The samples appeared homogeneous. The colour of all resins containing Ag zeolite

particles was darker compared to the neat DA. The brown discolouration was stronger and more pronounced with higher loadings of Ag-X. DA / Ag 0.2 wt.% seems to be considerably less coloured, approaching the overall appearance of DA.



Figure 38. Digital images DA acrylic resins; from left to right: DA (control), DA containing Ag-zeolite at 0.2 wt.% loading, DA containing Ag-zeolite at 0.4 wt.%, DA containing Ag-zeolite at 0.7 wt.% and DA containing Ag-zeolite at 2 wt.% loading.

Colour measurements were conducted to further analyse the colour changes observed (Table 15). For each specimen, three repeated measurements were taken to determine the colourimetric values, i.e. L^* (brightness), a^* (red-green proportion) and b^* (yellow-blue proportion). The differences to the zero value were calculated from the means of the colourimetric values ΔL^* , Δa^* and Δb^* . From that difference, the total colour difference ΔE ($\Delta E = [(\Delta L^*)^2 + (\Delta a^*)^2 + (\Delta b^*)^2]^{1/2}$) values were calculated and compared among the samples.^{150, 219} Visual evaluation of the specimens observed an increase in discolouration with an increase in Ag-X loading. However, no trend was observed between increasing levels of silver-zeolite and the calculated ΔE values (Table 15). Nonetheless a negative trend can be identified when

comparing a^* values to the control. The colour difference (ΔE) of tested samples ranged from 11.52 to 20.03 compared with control. It is well known that discolouration is a common problem for silver-containing materials because of Ag reduction. Our approach seems to offer a solution to that problems as indicated by the colour measurements performed.

Table 15. Colour measurement test resulting from DA and DA containing Ag-zeolite. The colour difference results from the difference in the Ag-zeolite loadings.

Sample	L*	a*	b*	ΔE^*
DA	47.71	15.11	6.70	-
Ag2wt.%	31.25	5.62	3.73	19.23
Ag0.7wt.%	37.01	11.16	5.10	11.52
Ag0.4wt.%	29.29	7.72	3.99	20.03
Ag0.2wt.%	32.74	12.00	8.23	15.37

Mechanical testing results are presented in Table 16. The mechanical testing of the samples provided some insight into both the stiffness and the interaction in coupling agent and the polymer. The addition of the zeolite in the absence of a coupling agent resulted in reduction in the stiffness. There were significant differences among the dental resin in the tensile strength. DA (control) and DA prepared by addition of the organically modified Ag-X showed similar tensile strength. Both values were lower for the non-functionalised samples indicating that silane modification indeed improved the dispersion of the filler within the polymer.

These results indicated that the coupling agents improved the compatibility between the zeolite and the polymer and resulted in high quality DA/ zeolite composites.

Table 16. Mechanical testing data of dental acrylic resin samples prepared in this work. Demonstrating no deterioration in the mechanical properties of composite samples compared to these of the neat dental acrylic resin was observed.

Sample	Flexural modulus (MPa) \pm SD	Flexural Strength (MPa) \pm SD
DA	2.12 \pm 0.24	90.10 \pm 2.38
DA / Na-X	2.09 \pm 0.15	81.15 \pm 5.06
DA / Ag-X	2.14 \pm 0.20	80.60 \pm 6.67
DA / Ag-X / M	2.35 \pm 0.23	85.20 \pm 3.30

3.4.2 Antimicrobial testing of dental acrylic samples

DA, DA / Ag-X (2 wt.%), DA / Ag-X (0.7 wt.%), DA / Ag-X (0.4 wt.%), and DA / Ag-X (0.2 wt.%) were tested against *E. coli* (ATCC 8739, Figure 39) and *C. albicans* (NCYC 1363, Figure 40). The DA samples were tested over a 24 hours period for their antimicrobial activity, with samples taken at sampling periods of 0, 1, 2, 3, 5, 16 and 24 hours. The DA (control) did not show any antibacterial activity in all tests. Figure 39 shows the antimicrobial efficiency of the samples against *E. coli*. DA / Ag-X (2 wt.%) and DA / Ag-X (0.7 wt.%), exhibited the highest level of antimicrobial activity after 1 h of exposure. No viable cells were detected after 2 hours with DA / Ag-X (2 wt.%) and DA / Ag-X (0.7 wt.%). This may be due to the

higher Ag content in this sample. All DA samples containing Ag showed at least a 3 log reduction in the number of *E. coli* cells on the surface in comparison to the positive control after 6 h exposure. There were some variations in the killing efficiency of *E. coli* after 2 hours for the DA / Ag-X (0.4 wt.%) and DA / Ag-X (0.2 wt.%) samples, but these were not significant. No viable cells were detected after 24 h of exposure. Since the Ag⁺ containing samples reduced the viability of *E. coli* and as no antimicrobial effect was observed in the controls (Ag⁺ free samples), it suggests that Ag⁺ were responsible for reducing the viable bacterial cell count.

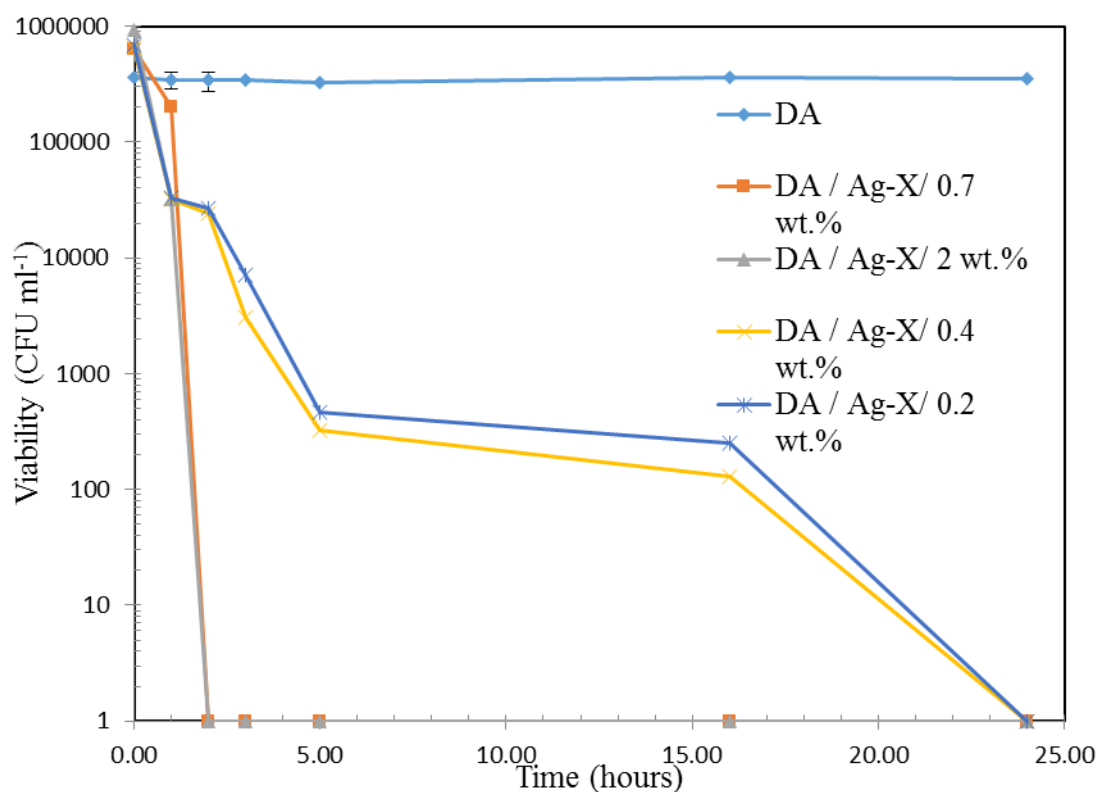


Figure 39. Antimicrobial testing of DA (Dental resin), DA / Ag-X (2 wt.%), DA / Ag-X (0.7 wt.%), DA / Ag-X (0.4 wt.%), and DA / Ag-X (0.2 wt.%) against *E. coli*, demonstrating the successful conferment of antimicrobial activity to the DA after addition of the silver.

The same procedure was applied to *C. albicans* but the growth medium was in Sabouraud dextrose liquid medium (Oxoid, UK). Figure 40 shows the antimicrobial efficiency of the samples against *C. albicans*. DA / Ag-X (2 wt.%) and DA / Ag-X (0.7 wt.%), exhibited the highest level of antimicrobial activity, with no viable cells detected after 6 h of exposure. A small decline in the number of viable cells was observed over the 24 h for DA / Ag-X (0.2 wt.%) and DA / Ag-X (0.4 wt.%). *C. albicans* proved to be less sensitive to the action Ag⁺ containing samples than bacteria in the case of DA / Ag-X (0.2 wt.%) and DA / Ag-X (0.4 wt.%). The reason for this slight decrease in number of viable cells, this may be due to the lower Ag content in this sample. Also it may be due to the low Ag⁺ concentration released from the polymers, which is not high enough to kill this yeast. The complex cellular organization of eukaryotic cells and/or the structure of the cellular wall may explain the need for greater amounts of Ag to inhibit their growth.

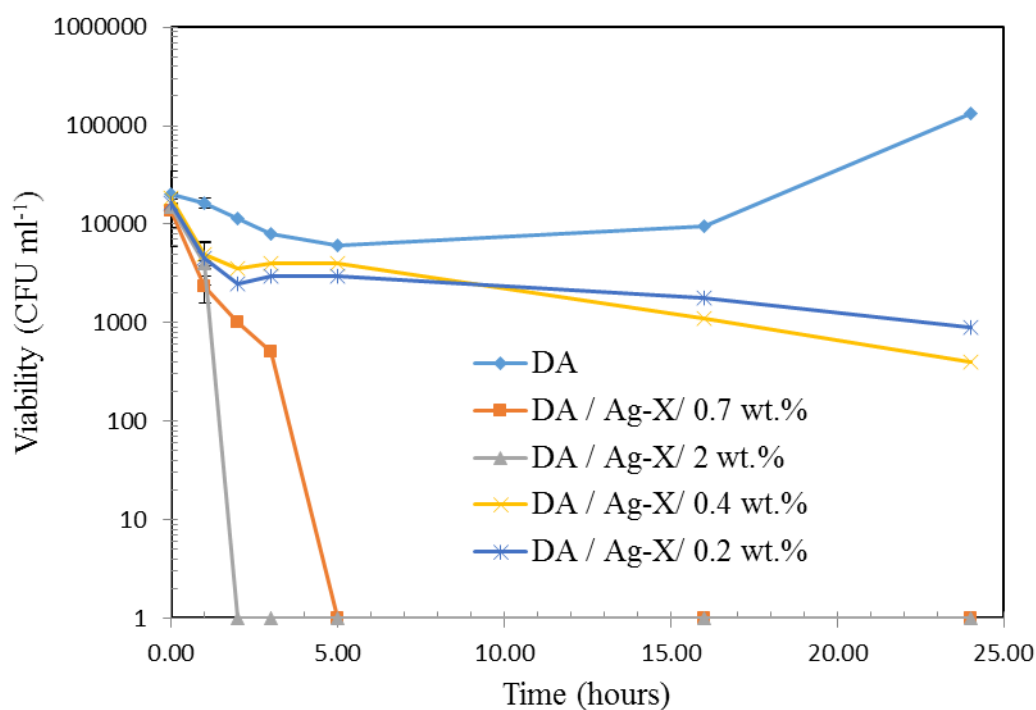


Figure 40. Antimicrobial testing of DA (Dental resin), DA / Ag-X (2 wt.%), DA / Ag-X (0.7 wt.%), DA / Ag-X (0.4 wt.%), and DA / Ag-X (0.2 wt.%) against *C. albicans*, demonstrating the successful conferment of antimicrobial activity to the DA after addition of the silver.

The concentration of Ag released from the different surfaces prepared after immersion in distilled water or artificial saliva were determined during a duration of 54 days. The Ag concentration was determined after the following time intervals 4, 8, 12, 26, 40 and 54 days of incubation at 37 °C. The Ag release in distilled water (Figure 41) or artificial saliva (Figure 42) are shown. The Ag released from AgX surfaces was generally higher in artificial saliva compared to distilled water with a maximum of 0.031 ppm for the 2 wt.% sample tested at day 8. The corresponding Ag concentration in distilled water was 0.015 ppm. The concentration of Ag released from the Ag-charged surfaces over 20 days immersion in sterile distilled water was 0.4-06 ppm for the 2 wt.% sample and 0.3-0.4 ppm for the 1 wt.% sample. The amount of silver released increased with an increase in Ag zeolite loading. All four materials produced their highest concentrations after 8 days. Longer immersion times showed a diminished amount of silver released in silver (0.2, 0.4 wt.%) within zeolite dental resin.

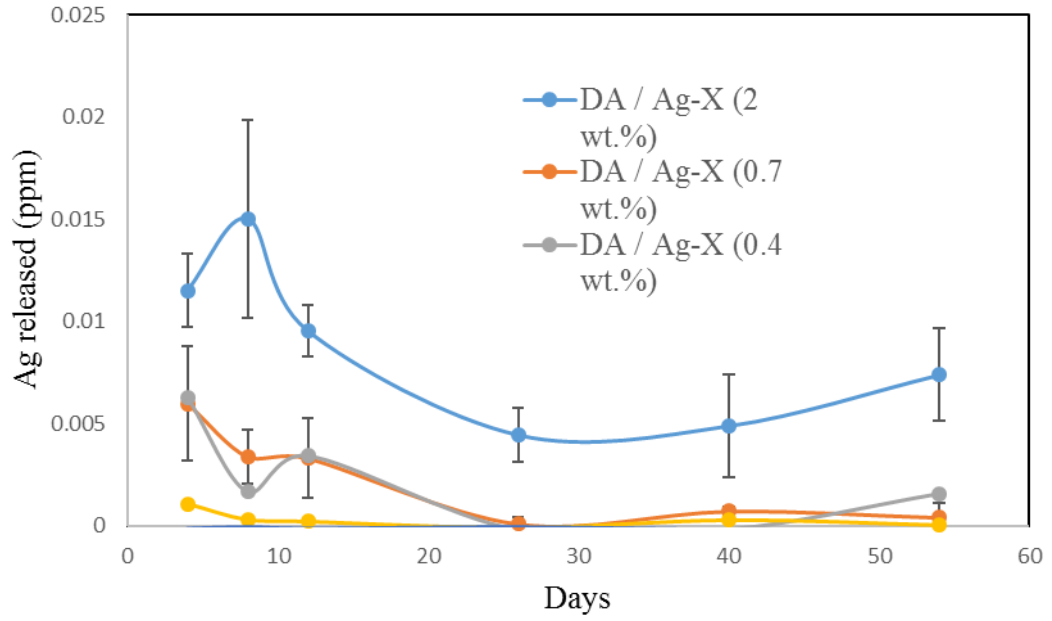


Figure 41. ICP-OES results of Ag^+ ions leaching from DA and DA containing Ag-zeolite composites immersed in 20 ml distilled water.

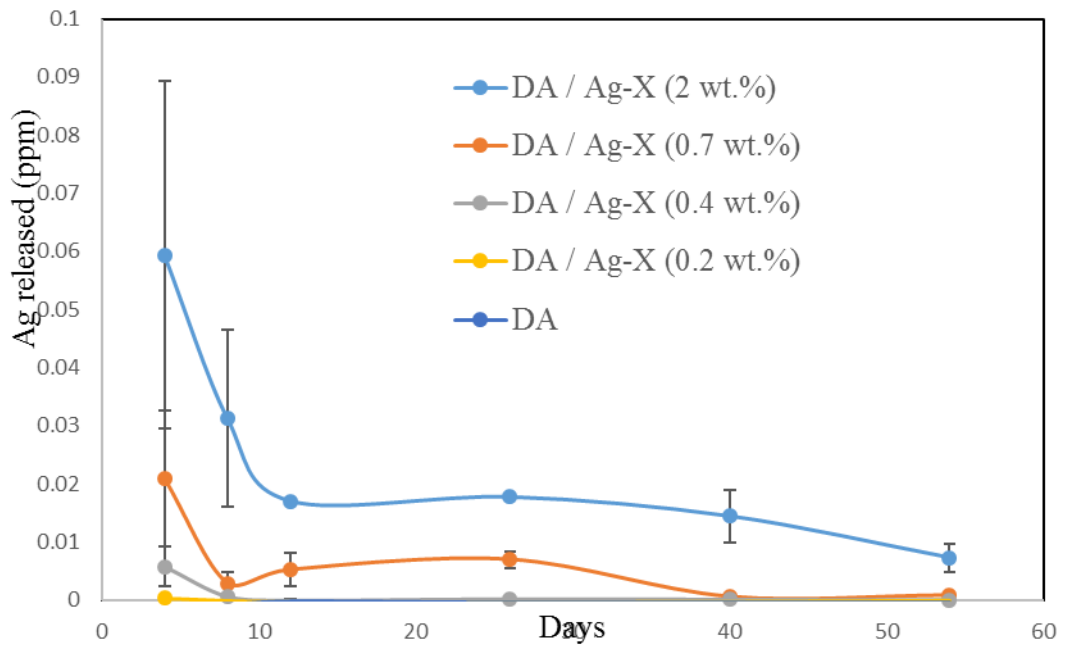


Figure 42. ICP-OES results of Ag^+ ions leaching from DA and DA containing Ag-zeolite composites immersed in 20 ml artificial saliva.

Colour measurements were conducted to study the effect of Ag release on discolouration (Table 17, Figure 43). The colour difference (ΔE) of tested samples ranged from 11.52 to 20.03 compared with control, whereas after the Ag release test for 54 days, ΔE ranged from 11.56 to 15.85. A significant decrease in ΔE was observed, suggesting that Ag contributes to the discolouration observed.

Table 17. Colour measurement test of DA and DA containing Ag-zeolite before and after Ag release test.

Sample	Before Ag release test				After Ag release test			
	L*	a*	b*	* ΔE	L*	a*	b*	* ΔE
DA	47.71	15.11	6.70	-	47.71	15.11	6.70	-
Ag2wt.%	31.25	5.62	3.73	19.23	35.28	5.36	5.36	15.85
Ag0.7wt.%	37.01	11.16	5.10	11.52	38.24	8.51	6.11	11.56
Ag0.4wt.%	29.29	7.72	3.99	20.03	34.45	9.62	6.94	14.35
Ag0.2wt.%	32.74	12.00	8.23	15.37	38.24	12.73	13.18	11.72

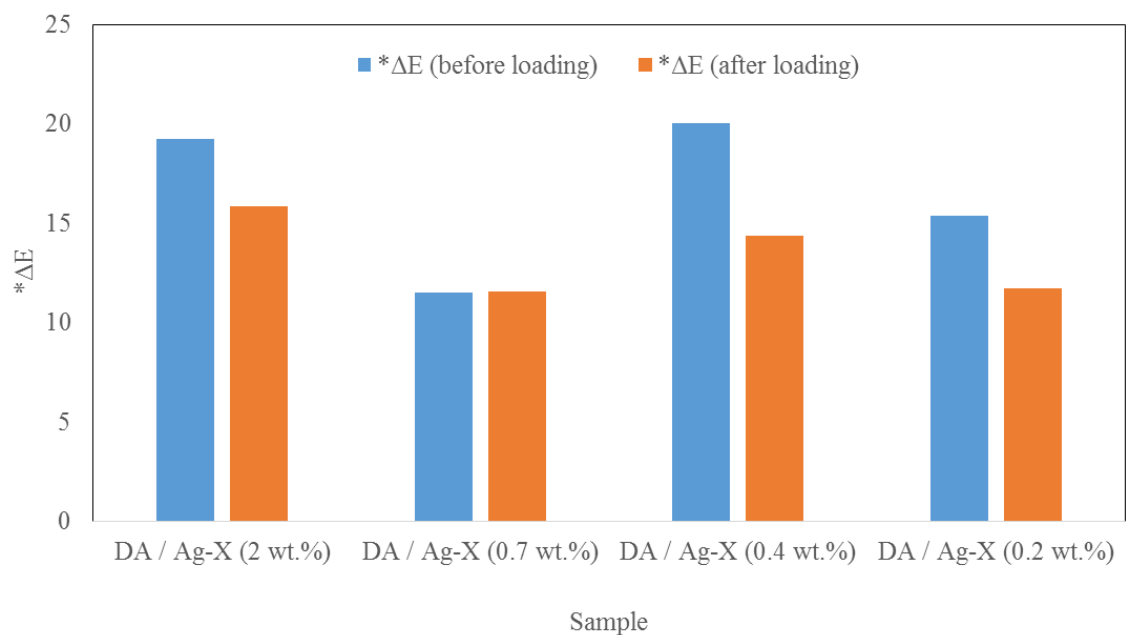


Figure 43. Colour difference (*ΔE) resulting from DA and DA containing Ag-zeolite before and after Ag release test.

The DA and silver containing DA were tested for antibacterial efficiency after the Ag release for 54 days. The antibacterial activity of dental resin and Ag containing dental resin was tested against *E. coli* (Figure 44). The DA and Ag containing DA demonstrated that polymers retained their antibacterial activity after 54 days submersion in distilled water. They were capable of killing *E. coli* upon repeated exposure. It can be seen that these polymers containing Ag at 2 and 0.7 wt.% are extremely antimicrobial, killing all *E. coli* bacteria after 24 h incubation. Ag release concentration after 54 days for DA / Ag-X (2 wt.%) is 0.006 ppm. In comparison, DA / Ag-X (0.2 wt.%) ag release concentration after 54 days Ag release test is no Ag was detected. The DA / Ag-X (0.4 wt.%) and DA / Ag-X (0.2 wt.%) showed reduced antibacterial efficiency against *E. coli*. This can attributed to no Ag release from the sample. As no antibacterial activity was observed with the DA,

silver ions released from zeolite NaX were responsible for the efficacy of killing a large number of bacteria in a very short period of time.

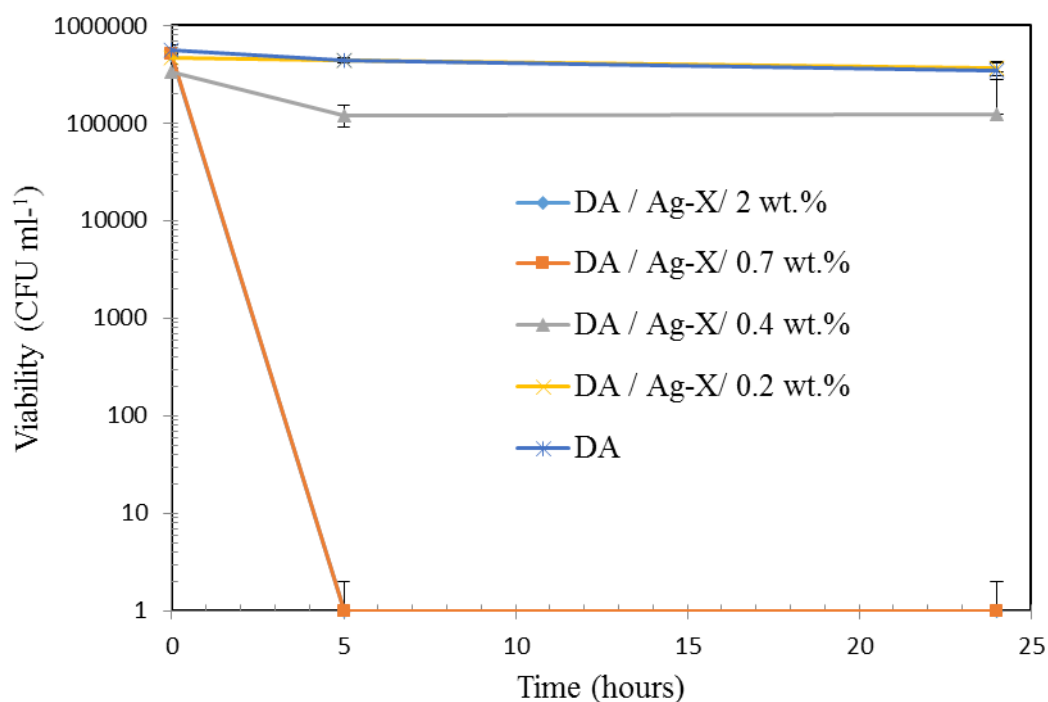


Figure 44. Antimicrobial testing of DA (Dental resin), DA / Ag-X (2 wt.%), DA / Ag-X (0.7 wt.%), DA / Ag-X (0.4 wt.%), and DA / Ag-X (0.2 wt.%) against *E. coli*, after 54 days submersion in distilled water.

3.4.3 Ag charged NaX dental acrylic samples

The dental acrylic resin contained 2 wt.% and 1 wt.% 3-(trimethoxysilyl)propyl methacrylate function NaX zeolite (Ag free). The samples were submersed in 20 ml of 0.01 M silver nitrate solution at room temperature for 24 h. The samples were washed several times with distilled water after submersion. The concentration of Ag released from the different surfaces prepared after immersion in

distilled water were determined during a duration of 20 days at 37 °C (Table 18). During the test period, the silver release values for DA containing zeolite-silane at 2 wt.% loading ranged from 0.43 to 0.6 ppm. Silver release values in DA containing zeolite-silane at 1 wt.% loading ranged from 0.26 to 0.39 ppm. The amount of silver released increased with an increase in zeolite-silane loading. DA containing zeolite-silane at 2 wt.% loading produced the highest concentration of Ag after 20 days. Longer immersion times showed a reduced amount of silver release.

Table 18. ICP-OES results of Ag⁺ ions leaching from DA and DA containing zeolite-silane composites immersed in 20 ml distilled water charged from AgNO₃ solution.

Duration (Days)	Ag release (ppm)	
	DA / M-AgX 2wt.%	DA / M-AgX 1wt.%
1	0.60 ± 0.07	0.39 ± 0.06
20	0.43 ± 0.09	0.26 ± 0.01

The DA samples were tested over a 24 hours period for their antimicrobial activity, with samples taken at time periods of 0, 5 and 24 hours. All the DA samples were tested against *E. coli* (ATCC 8739). The DA (control) did not show any antibacterial activity in all tests. Figure 45 shows the antimicrobial efficiency of the samples against *E. coli*. DA containing zeolite-silane at 2 wt.% and DA containing zeolite-silane at 1 wt.%, exhibited similar antimicrobial activity. No viable cells were detected after 5 hours with DA containing zeolite-silane at 2 wt.% and DA containing zeolite-silane at 1wt.%. The antibacterial efficiency can be attributed to

the high Ag release in both samples. Since the Ag⁺ containing samples reduced the viability of *E. coli* and as no antimicrobial effect was observed in the controls (Ag⁺ free samples), it suggests that Ag⁺ were responsible for reducing the viable bacterial cell count.

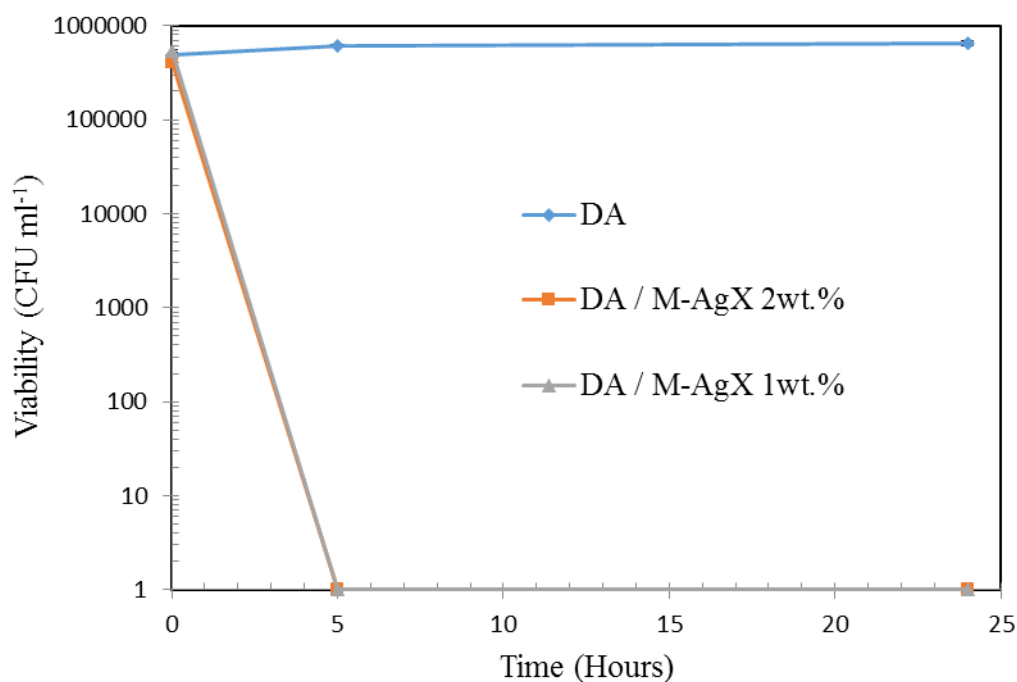


Figure 45. Viable bacterial cell counts of *E. coli* in the presence of DA and DA containing zeolite-silane charged from AgNO₃ solution.

Colour measurements were conducted before and after submersion of DA containing silane-zeolite (M-NaX) in AgNO₃ solution (Table 19). The colour difference (ΔE) of tested samples ranged from 4.03 to 10.51 compared with control, whereas after the AgNO₃ submersion, ΔE ranged from 1.87 to 6.64. A significant decrease in observed in ΔE , the results suggest that Ag contribute to the discolouration observed. No visible colour change was observed visually before and after submersion in AgNO₃ solution (Figure 46).

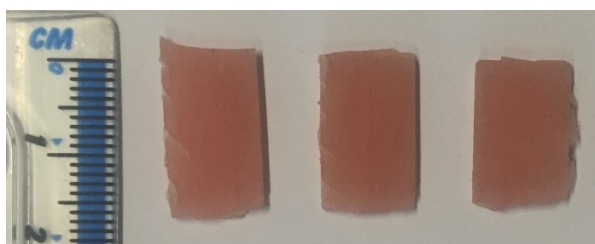


Figure 46. Digital image of DA acrylic resins; from left to right: DA (control), DA containing zeolite-silane at 2 wt.% loading (before charging) and c) DA containing zeolite-silane at 2 wt.% loading (after charging).

Table 19. Colour measurement test resulting from DA and DA containing zeolite-silane composites before and after immersion in 20 ml AgNO₃ solution.

Sample	L*	a*	b*	*ΔE
DA	47.71	15.11	6.7	-
DA / M-NaX 2 wt.% (Before charging)	47.25	11.62	4.73	4.03
DA / M-AgX 2 wt.% (After charging)	48.52	14.18	5.30	1.87
DA / M-NaX 1 wt.% (Before charging)	39.25	9.62	3.73	10.51
DA / M-AgX 1 wt.% (After charging)	42.68	10.99	5.37	6.64

3.4.4 Conclusions

Functionalised Ag zeolite was incorporated into dental acrylic resin at loadings of 2 wt.%, 0.7 wt.%, 0.4 wt.% and 0.2 wt.%. The antibacterial tests revealed a 3 log reductions in viability of *E. coli*, when in contact with Ag-zeolite dental acrylic. *C. albicans* was more resistant, the lower Ag loadings had reliably less effect, although the two highest loadings showed good efficiency against this more challenging organism. Mechanical properties indicated that organo-silane modification was essential for good filler-matrix adhesion. At the most effective Ag-zeolite loadings a noticeable brown discolouration was imparted to the composites. Ag release from dental acrylic in artificial saliva was significantly higher than Ag release in distilled water during the early periods of leaching. Colour measurements showed a pronounced decrease in ΔE after a 54 days leaching period.

Ag was charged into DA resins containing NaX zeolites and ion-exchanged within the zeolite, which has successfully solved the discolouration and Ag-containing resins with a similar colour to that of the original polymer were obtained. The Ag-charged samples showed similar activity against *E. coli* to that of samples loaded with AgX. The results in this work show that Ag-based antimicrobial dental acrylic resins with long-term activity and convenient Ag replenishment can be successfully prepared using zeolites. The materials have the potential to increase the life-time of denture acrylic resins and to improve the oral health of patients with prosthetic devices.

Chapter 4. Conclusions

This project studied different aspects of the antimicrobial properties of Ag zeolites in powder form such as the influence of the form of silver, metallic or ionic, the zeolite type and crystal size and the presence of mesoporosity. As part of the work, a suitable screening technique was developed, allowing quick comparison of the antimicrobial efficacy of samples of similar nature. The results indicated that silver in metallic form was slightly more efficient compared to silver in ionic form, however the difference could not justify the additional complex preparation steps with the reduction of Ag-exchanged zeolites. Reduction of crystal size resulted in a decrease in the killing efficiency against *E. coli* and *C. albicans*. Zeolite beta showed higher antibacterial efficiency than zeolite X despite the lower Ag content in that sample, which was attributed to the higher concentration of silver released from zeolite beta samples to the medium. Introduction of mesoporosity in zeolites also resulted in an increase in the antibacterial activity. The difference in the killing abilities of the different samples were not sustainable and could be as little as 1 min between samples. However, the results are of importance for applications where quick killing is needed. Cytotoxicity measurements using PBMCs indicated that Ag zeolite X was more toxic compared to Ag beta, particularly the nanosized sample. All samples except the latter showed insignificant differences compared to untreated cells at concentrations of 0.1 mg mL^{-1} and below. During our method development, we showed that the use of reliable antimicrobial tests were of paramount importance for the results. For instance, neutralisation of Ag to halt its activity after incubation was essential for the reliability of the results. The results reported here will be of interest when selecting silver zeolites for biomedical applications, particularly when fast antimicrobial response is required.

Another aim of this thesis was to apply a multidisciplinary approach on the preparation and antimicrobial assessment of antimicrobial polymers contacting Ag zeolites. The works on silicone elastomers and dental acrylic resins showed that Ag zeolites can successfully be incorporated into polymers to introduce antimicrobial activity. Organic modification of the zeolites was found to be essential in order to improve the compatibility between the zeolite and the polymer matrix and improved filler-matrix interactions were found. The polymers showed discolouration when Ag zeolites were added to uncured polymers. This problem could be solved to a certain extent by the selection of the organic modifier. A more elegant approach was to introduce the silver post-synthetically to polymers loaded with Na zeolites. The materials prepared using this approach had a similar colour to that of the original polymer as determined by colour measurement tests. The Ag zeolite containing dental acrylic resin retained antibacterial activity after a 54 days leaching period after two cycles of antibacterial testing. The results showed the surface will be able to prevent multiple colonisations of surfaces. The antimicrobial silicone elastomer and acrylic resins reported here will be of interest for potential medical devices and denture applications.

Chapter 5. Future work

The initial antimicrobial screening investigated Ag zeolite in powder form. Zeolite beta showed higher activity than zeolite X despite the lower Ag content in that sample, which was attributed to the higher concentration of silver released from zeolite beta samples to the medium. Investigating more zeolites would provide a better understanding of the zeolites antimicrobial properties. In addition, the introduction of mesoporosity had a beneficial effect on the antimicrobial efficacy. Mesoporous zeolite beta contained a large amount of amorphous material. It would be beneficial to test materials having the same crystallinity but different mesoporosity to determine the influence of mesoporosity on antibacterial activity. Cytotoxicity measurements using peripheral blood mononuclear cells indicated that Ag zeolite X was more toxic compared to Ag beta, particularly the nanosized sample. Testing the effect of incorporating Ag-zeolite into a polymer on cytotoxicity would be of great interest for potential future applications of these materials.

The antimicrobial Ag zeolite/polymer composites prepared showed high antimicrobial efficiency against bacteria and fungi; testing against other microorganisms would provide an insight into how effective they are as a general biocidal material. Further analysis of the Ag zeolite containing polymers antimicrobial properties needed to provide an insight, in particular the long term behaviour of the polymers (e.g., is Ag stable within the polymers, will there be Ag migration within the materials, etc.). The growth of biofilms on the surfaces are also worth investigating.

The antimicrobial testing (viable plate count method used in this study) of the polymers was fundamental and focused on proof of concept. The plate count method does not explore the antibacterial agent effect on bacteria, which may be

bacteriostatic (kills organisms) or bactericide (inhibits the growths of organism).. SEM can be used to determine whether cells lysis had occurred. Lysis of bacteria would confirm cells are being killed by antibacterial agents rather than experiencing growth inhibition. Exploring other techniques to test the antimicrobial efficiency (e.g., live dead stain) is necessary to obtain a broader view of its ability to prevent colonisation. Using a live dead stain would allow for the determination of the number of viable bacterial cells remaining on the polymer surface.

The effect of charging dental resins loaded with Ag-free zeolites from AgNO₃ solution, focused on the proof of concept. The results proved promising, although further work needs to be carried out, for instance to study the cytotoxicity of the materials as well as their activity towards more microorganisms associated with oral diseases. Applying the same protocol to silicone elastomers, and determining the antibacterial efficiency would also be worthwhile testing.

References

1. D. W. Breck, *Zeolite Molecular Sieve*, Wiley-Interscience, New York, 1974.
2. R. Szostak, *Handbook of Molecular Sieves*, Van Nostrand Reinhold, New York, 1992.
3. <http://www.iza-structure.org/databases/>.
4. D. H. Everett, *Pure Appl. Chem.*, 1972, 31, 577.
5. L. V. C. Rees, *Zeolites*, 1992, 12, 767.
6. R. M. Barrer, *Zeolites and Clay Minerals as Sorbents and Molecular Sieves*, Academic press, London, 1978.
7. C. M. Baerlocher, L. B.; Olson, D. H., *Atlas of Zeolite Framework Types*, Elsevier, Amsterdam, 6th edition edn., 2007.
8. M. W. Anderson, K. S. Pachis, F. Prebin, S. W. Carr, O. Terasaki, T. Ohsuna and V. Alfredsson, *Journal of the Chemical Society, Chemical Communications*, 1991, DOI: 10.1039/C39910001660, 1660-1664.
9. C.-n. Wu and K.-j. Chao, *Journal of the Chemical Society, Faraday Transactions*, 1995, 91, 167-173.
10. N. Hanif, M. W. Anderson, V. Alfredsson and O. Terasaki, *Physical Chemistry Chemical Physics*, 2000, 2, 3349-3357.
11. F. Schüth, *Current Opinion in Solid State and Materials Science*, 2001, 5, 389-395.
12. F. Taulelle, *Solid State Sciences*, 2001, 3, 795-800.
13. W. Fan, M. Ogura, G. Sankar and T. Okubo, *Chemistry of Materials*, 2007, 19, 1906-1917.
14. V. P. Valtchev and K. N. Bozhilov, *The Journal of Physical Chemistry B*, 2004, 108, 15587-15598.
15. N. D. Hould, S. Kumar, M. Tsapatsis, V. Nikolakis and R. F. Lobo, *Langmuir*, 2010, 26, 1260-1270.
16. L. Tosheva and V. P. Valtchev, *Chemistry of Materials*, 2005, 17, 2494-2513.
17. S. C. Larsen, *The Journal of Physical Chemistry C*, 2007, 111, 18464-18474.
18. W. Song, G. Li, V. H. Grassian and S. C. Larsen, *Environmental Science & Technology*, 2005, 39, 1214-1220.
19. B. Louis, A. I. Vicente, C. Fernandez and V. Valtchev, *The Journal of Physical Chemistry C*, 2011, 115, 18603-18610.
20. J. Perez-Ramirez, C. H. Christensen, K. Egeblad, C. H. Christensen and J. C. Groen, *Chemical Society Reviews*, 2008, 37, 2530-2542.
21. D. P. Serrano, J. M. Escola and P. Pizarro, *Chemical Society Reviews*, 2013, 42, 4004-4035.
22. V. Valtchev and L. Tosheva, *Chemical Reviews*, 2013, 113, 6734-6760.
23. W. Song, R. E. Justice, C. A. Jones, V. H. Grassian and S. C. Larsen, *Langmuir*, 2004, 20, 8301-8306.
24. Y. Tao, H. Kanoh, L. Abrams and K. Kaneko, *Chem Rev*, 2006, 106, 896-910.
25. K. Egeblad, C. H. Christensen, M. Kustova and C. H. Christensen, *Chemistry of Materials*, 2008, 20, 946-960.
26. M. Farcasiu and T. F. Degnan, *Industrial & Engineering Chemistry Research*, 1988, 27, 45-47.
27. W. O. Haag, R. M. Lago and P. B. Weisz, *Faraday Discussions of the Chemical Society*, 1981, 72, 317-330.
28. P. B. Weisz, *Industrial & Engineering Chemistry Research*, 1995, 34, 2692-2699.

29. G.-T. Vuong, V.-T. Hoang, D.-T. Nguyen and T.-O. Do, *Applied Catalysis A: General*, 2010, 382, 231-239.
30. V. Georgieva, A. Vicente, C. Fernandez, R. Retoux, A. Palčić, V. Valtchev and S. Mintova, *Crystal Growth & Design*, 2015, 15, 1898-1906.
31. B. J. Schoeman, J. Sterte and J.-E. Otterstedt, *Journal of the Chemical Society, Chemical Communications*, 1993, DOI: 10.1039/c39930000994, 994-995.
32. S. Mintova and V. Valtchev, *Stud. Surf. Sci. Catal.*, 1999, 125, 141.
33. B. J. Schoeman and J. Sterte, *KONA Powder and Particle Journal*, 1997, 15, 150-158.
34. Y. Huang, K. Wang, D. Dong, D. Li, M. R. Hill, A. J. Hill and H. Wang, *Microporous and Mesoporous Materials*, 2010, 127, 167-175.
35. Y. Kim, J. Jeong, J. Hwang, S. Kim and W. Kim, *Journal of Porous Materials*, 2009, 16, 299-306.
36. H. Yin, T. Zhou, Y. Liu, Y. Chai and C. Liu, *Journal of Porous Materials*, 2012, 19, 277-281.
37. G. Lischke, E. Schreier, B. Parltitz, I. Pitsch, U. Lohse and M. Woettke, *Applied Catalysis A: General*, 1995, 129, 57-67.
38. K. Wang, X. Wang and G. Li, *Microporous and Mesoporous Materials*, 2006, 94, 325-329.
39. E.-P. Ng, D. Chateigner, T. Bein, V. Valtchev and S. Mintova, *Science*, 2012, 335, 70-73.
40. M. A. Camblor, A. Corma and S. Valencia, *Journal of Materials Chemistry*, 1998, 8, 2137-2145.
41. B. J. Schoeman, E. Babouchkina, S. Mintova, V. P. Valtchev and J. Sterte, *Journal of Porous Materials*, 2001, 8, 13-22.
42. O. Larlus, S. Mintova, S. T. Wilson, R. R. Willis, H. Abrevaya and T. Bein, *Microporous and Mesoporous Materials*, 2011, 142, 17-25.
43. S. Mintova, V. Valtchev, T. Onfroy, C. Marichal, H. Knözinger and T. Bein, *Microporous and Mesoporous Materials*, 2006, 90, 237-245.
44. D. E. Kuechl, A. I. Benin, L. M. Knight, H. Abrevaya, S. T. Wilson, W. Sinkler, T. M. Mezza and R. R. Willis, *Microporous and Mesoporous Materials*, 2010, 127, 104-118.
45. G. Majano, L. Delmotte, V. Valtchev and S. Mintova, *Chemistry of Materials*, 2009, 21, 4184-4191.
46. C. T. Kresge, M. E. Leonowicz, W. J. Roth, J. C. Vartuli and J. S. Beck, *Nature*, 1992, 359, 710-712.
47. D. P. Serrano, J. Aguado, J. M. Escola, J. M. Rodriguez and A. Peral, *Journal of Materials Chemistry*, 2008, 18, 4210-4218.
48. D. P. Serrano, J. Aguado, G. Morales, J. M. Rodríguez, A. Peral, M. Thommes, J. D. Epping and B. F. Chmelka, *Chemistry of Materials*, 2009, 21, 641-654.
49. Z. Xue, T. Zhang, J. Ma, H. Miao, W. Fan, Y. Zhang and R. Li, *Microporous and Mesoporous Materials*, 2012, 151, 271-276.
50. S. Svelle, L. Sommer, K. Barbera, P. N. R. Vennestrøm, U. Olsbye, K. P. Lillerud, S. Bordiga, Y.-H. Pan and P. Beato, *Catalysis Today*, 2011, 168, 38-47.
51. J. Y. Ying and J. García-Martínez, Google Patents, 2011.
52. J. Garcia-Martinez, M. Johnson, J. Valla, K. Li and J. Y. Ying, *Catalysis Science & Technology*, 2012, 2, 987-994.
53. J. Garcia-Martinez, Google Patents, 2010.
54. J. Y. Ying and J. García-Martínez, Google Patents, 2011.
55. J. Garcia-Martinez, Google Patents, 2011.
56. J. Garcia-Martinez and M. M. Johnson, Google Patents, 2012.

57. R. Chal, T. Cacciaguerra, S. van Donk and C. Gerardin, *Chemical Communications*, 2010, 46, 7840-7842.
58. S. Chernousova and M. Epple, *Angewandte Chemie (International ed. in English)*, 2013, 52, 1636-1653.
59. A. B. Lansdown, *Curr Probl Dermatol*, 2006, 33, 17-34.
60. J. W. Alexander, *Surg Infect (Larchmt)*, 2009, 10, 289-292.
61. K. Vasilev, J. Cook and H. J. Griesser, *Expert Rev Med Devices*, 2009, 6, 553-567.
62. D. W. Brett, *Ostomy/wound management*, 2006, 52, 34-41.
63. S. W. P. Wijnhoven, W. J. G. M. Peijnenburg, C. A. Herberts, W. I. Hagens, A. G. Oomen, E. H. W. Heugens, B. Roszek, J. Bisschops, I. Gosens, D. Van De Meent, S. Dekkers, W. H. De Jong, M. van Zijverden, A. J. A. M. Sips and R. E. Geertsma, *Nanotoxicology*, 2009, 3, 109-138.
64. B. Nowack, H. F. Krug and M. Height, *Environmental Science & Technology*, 2011, 45, 1177-1183.
65. T. V. Duncan, *Journal of Colloid and Interface Science*, 2011, 363, 1-24.
66. J. W. Wiechers and N. Musee, *J Biomed Nanotechnol*, 2010, 6, 408-431.
67. L. Rizzello and P. P. Pompa, *Chemical Society Reviews*, 2014, 43, 1501-1518.
68. J. R. Morones, J. L. Elechiguerra, A. Camacho, K. Holt, J. B. Kouri, J. T. Ramirez and M. J. Yacaman, *Nanotechnology*, 2005, 16, 2346-2353.
69. S. Eckhardt, P. S. Brunetto, J. Gagnon, M. Priebe, B. Giese and K. M. Fromm, *Chemical Reviews*, 2013, 113, 4708-4754.
70. J. M. Schierholz, N. Yücel, A. F. E. Rump, J. Beuth and G. Pulverer, *International journal of antimicrobial agents*, 19, 511-516.
71. X. Chen and H. J. Schluesener, *Toxicology Letters*, 2008, 176, 1-12.
72. C. Marambio-Jones and E. M. V. Hoek, *Journal of Nanoparticle Research*, 2010, 12, 1531-1551.
73. H. Lara, N. Ayala-Nunez, L. Ixtepan-Turrent and C. Rodriguez-Padilla, *Journal of Nanobiotechnology*, 2010, 8, 1.
74. S. L. Percival, P. G. Bowler and D. Russell, *J Hosp Infect*, 2005, 60, 1-7.
75. Q. L. Feng, J. Wu, G. Q. Chen, F. Z. Cui, T. N. Kim and J. O. Kim, *Journal of Biomedical Materials Research*, 2000, 52, 662-668.
76. I. Sondi and B. Salopek-Sondi, *Journal of Colloid and Interface Science*, 2004, 275, 177-182.
77. J. S. Kim, E. Kuk, K. N. Yu, J. H. Kim, S. J. Park, H. J. Lee, S. H. Kim, Y. K. Park, Y. H. Park, C. Y. Hwang, Y. K. Kim, Y. S. Lee, D. H. Jeong and M. H. Cho, *Nanomedicine*, 2007, 3, 95-101.
78. R. F. Phalen, R. C. Mannix and R. T. Drew, *Environmental Health Perspectives*, 1984, 56, 23-34.
79. Sato, Sueki and Nishijima, *British Journal of Dermatology*, 1999, 140, 158-163.
80. S. Saint, D. L. Veenstra, S. D. Sullivan, C. Chenoweth and A. Fendrick, *Archives of Internal Medicine*, 2000, 160, 2670-2675.
81. L. H. Catsakis and V. I. Sulica, *Oral Surg Oral Med Oral Pathol*, 1978, 46, 371-375.
82. P. L. DRAKE and K. J. HAZELWOOD, *Annals of Occupational Hygiene*, 2005, 49, 575-585.
83. C. Greulich, D. Braun, A. Peetsch, J. Diendorf, B. Siebers, M. Epple and M. Koller, *RSC Advances*, 2012, 2, 6981-6987.
84. T. Kihara, Y. Zhang, Y. Hu, Q. Mao, Y. Tang and J. Miyake, *Journal of Bioscience and Bioengineering*, 2011, 111, 725-730.
85. A. Petushkov, J. Intra, J. B. Graham, S. C. Larsen and A. K. Salem, *Chem Res Toxicol*, 2009, 22, 1359-1368.

86. S. Laurent, E. P. Ng, C. Thirifays, L. Lakiss, G. M. Goupil, S. Mintova, C. Burtea, E. Oveisi, C. Hebert, M. de Vries, M. M. Motazacker, F. Rezaee and M. Mahmoudi, *Toxicology Research*, 2013, 2, 270-279.
87. S. Mintova, M. Jaber and V. Valtchev, *Chemical Society Reviews*, 2015, 44, 7207-7233.
88. S. E. Lehman and S. C. Larsen, *Environmental Science: Nano*, 2014, 1, 200-213.
89. L. Ferreira, A. M. Fonseca, G. Botelho, C. A. Aguiar and I. C. Neves, *Microporous and Mesoporous Materials*, 2012, 160, 126-132.
90. K. Kawahara, K. Tsuruda, M. Morishita and M. Uchida, *Dental Materials*, 2000, 16, 452-455.
91. K. K. Krishnani, Y. Zhang, L. Xiong, Y. Yan, R. Boopathy and A. Mulchandani, *Bioresource Technology*, 2012, 117, 86-91.
92. B. Kwakye-Awuah, C. Williams, M. A. Kenward and I. Radecka, *Journal of applied microbiology*, 2008, 104, 1516-1524.
93. A. Top and S. Ülkü, *Applied Clay Science*, 2004, 27, 13-19.
94. Y. Inoue, M. Kogure, K. Matsumoto, H. Hamashima, M. Tsukada, K. Endo and T. Tanaka, *Chemical & pharmaceutical bulletin*, 2008, 56, 692-694.
95. L. Tosheva, A. Brockbank, B. Mihailova, J. Sutula, J. Ludwig, H. Potgieter and J. Verran, *Journal of Materials Chemistry*, 2012, 22, 16897-16905.
96. R. S. Bedi, R. Cai, C. O'Neill, D. E. Beving, S. Foster, S. Guthrie, W. Chen and Y. Yan, *Microporous and Mesoporous Materials*, 2012, 151, 352-357.
97. P. Lalueza, M. Monzón, M. Arruebo and J. Santamaría, *Materials Research Bulletin*, 2011, 46, 2070-2076.
98. Y. Matsumura, K. Yoshikata, S. Kunisaki and T. Tsuchido, *Applied and environmental microbiology*, 2003, 69, 4278-4281.
99. R. Guerra, E. Lima, M. Viniestra, A. Guzmán and V. Lara, *Microporous and Mesoporous Materials*, 2012, 147, 267-273.
100. C. Chiericatti, J. C. Basílico, M. L. Z. Basílico and J. M. Zamaro, *Microporous and Mesoporous Materials*, 2014, 188, 118-125.
101. Y. Zhou, Y. Deng, P. He, F. Dong, Y. Xia and Y. He, *RSC Advances*, 2014, 4, 5283-5288.
102. L. Ferreira, C. Almeida-Aguiar, P. Parpot, A. M. Fonseca and I. C. Neves, *RSC Advances*, 2015, 5, 37188-37195.
103. P. Saint-Cricq, Y. Kamimura, K. Itabashi, A. Sugawara-Narutaki, A. Shimojima and T. Okubo, *European Journal of Inorganic Chemistry*, 2012, DOI: 10.1002/ejic.201200476, 3398-3402.
104. S. Demirci, Z. Ustaoglu, G. A. Yilmazer, F. Sahin and N. Bac, *Applied Biochemistry and Biotechnology*, 2014, 172, 1652-1662.
105. G. A. Sotiriou and S. E. Pratsinis, *Environ Sci Technol*, 2010, 44, 5649-5654.
106. D. Jiraroj, S. Tungasmita and D. N. Tungasmita, *Powder Technology*, 2014, 264, 418-422.
107. L. Lv, Y. Luo, W. J. Ng and X. S. Zhao, *Microporous and Mesoporous Materials*, 2009, 120, 304-309.
108. S. Sabbani, D. Gallego-Perez, A. Nagy, W. James Waldman, D. Hansford and P. K. Dutta, *Microporous and Mesoporous Materials*, 2010, 135, 131-136.
109. Z.-m. Xiu, Q.-b. Zhang, H. L. Puppala, V. L. Colvin and P. J. J. Alvarez, *Nano Letters*, 2012, 12, 4271-4275.
110. O. Choi, K. K. Deng, N.-J. Kim, L. Ross Jr, R. Y. Surampalli and Z. Hu, *Water Research*, 2008, 42, 3066-3074.

111. C. N. Lok, C. M. Ho, R. Chen, Q. Y. He, W. Y. Yu, H. Sun, P. K. Tam, J. F. Chiu and C. M. Che, *Journal of biological inorganic chemistry : JBIC : a publication of the Society of Biological Inorganic Chemistry*, 2007, 12, 527-534.
112. D. Campoccia, L. Montanaro and C. R. Arciola, *Biomaterials*, 2013, 34, 8533-8554.
113. V. V. Singh, B. Jurado-Sánchez, S. Sattayasamitsathit, J. Orozco, J. Li, M. Galarnyk, Y. Fedorak and J. Wang, *Advanced Functional Materials*, 2015, 25, 2147-2155.
114. S. Husain and W. J. Koros, *Journal of Membrane Science*, 2007, 288, 195-207.
115. R. Mahajan and W. J. Koros, *Industrial & Engineering Chemistry Research*, 2000, 39, 2692-2696.
116. R. Kumar, S. Howdle and H. Münstedt, *Journal of Biomedical Materials Research Part B: Applied Biomaterials*, 2005, 75B, 311-319.
117. D. R. Monteiro, L. F. Gorup, A. S. Takamiya, A. C. Ruvollo-Filho, E. R. de Camargo and D. B. Barbosa, *International journal of antimicrobial agents*, 2009, 34, 103-110.
118. K. Kamişoğlu, E. A. Aksoy, B. Akata, N. Hasirci and N. Baç, *Journal of Applied Polymer Science*, 2008, 110, 2854-2861.
119. P. Kaali, E. Strömberg, R. E. Aune, G. Czél, D. Momcilovic and S. Karlsson, *Polymer Degradation and Stability*, 2010, 95, 1456-1465.
120. D. Zampino, T. Ferreri, C. Puglisi, M. Mancuso, R. Zacccone and R. Scaffaro, in *Ivth International Conference on Times of Polymers*, eds. D. Acierno, A. Damore and L. Grassia, 2008, vol. 1042, pp. 240-242.
121. D. L. Boschetto, L. Lerin, R. Cansian, S. B. C. Pergher and M. Di Luccio, *Chemical Engineering Journal*, 2012, 204-206, 210-216.
122. H. Pehlivan, D. Balköse, S. Ülkü and F. Tihminlioglu, *Composites Science and Technology*, 2005, 65, 2049-2058.
123. A. Fernández, E. Soriano, P. Hernández-Muñoz and R. Gavara, *Journal of Food Science*, 2010, 75, E186-E193.
124. D. Zampino, T. Ferreri, C. Puglisi, M. Mancuso, R. Zacccone, R. Scaffaro and D. Bennardo, *J Mater Sci*, 2011, 46, 6734-6743.
125. K. Taptim and N. Sombatsompop, *Journal of Vinyl and Additive Technology*, 2013, 19, 113-122.
126. L. A. Casemiro, C. H. Gomes Martins, C. Pires-de-Souza Fde and H. Panzeri, *Gerodontology*, 2008, 25, 187-194.
127. S. Khoonsap and S. Amnuaypanich, *Journal of Membrane Science*, 2011, 367, 182-189.
128. J. Y. Lee, S. H. Lee and S. W. Kim, *Materials Chemistry and Physics*, 2000, 63, 251-255.
129. D. Metin, F. Tihminlioglu, D. Balköse and S. Ülkü, *Composites Part A: Applied Science and Manufacturing*, 2004, 35, 23-32.
130. T. Sano, M. Hasegawa, S. Ejiri, Y. Kawakami and H. Yanagishita, *Microporous Materials*, 1995, 5, 179-184.
131. A. F. Ismail, T. D. Kusworo and A. Mustafa, *Journal of Membrane Science*, 2008, 319, 306-312.
132. B. Moermans, W. D. Beuckelaer, I. F. J. Vankelecom, R. Ravishankar, J. A. Martens and P. A. Jacobs, *Chemical Communications*, 2000, DOI: 10.1039/B007435G, 2467-2468.
133. H. Wang, B. A. Holmberg and Y. Yan, *Journal of Materials Chemistry*, 2002, 12, 3640-3643.
134. P. Wei, X. Qu, H. Dong, L. Zhang, H. Chen and C. Gao, *Journal of Applied Polymer Science*, 2013, 128, 3390-3397.
135. D. Bastani, N. Esmaeili and M. Asadollahi, *Journal of Industrial and Engineering Chemistry*, 2013, 19, 375-393.

136. M. D. Khare, S. S. Bukhari, A. Swann, P. Spiers, I. McLaren and J. Myers, *Journal of Infection*, 2007, 54, 146-150.
137. Y. Abe, M. Ishii, M. Takeuchi, M. Ueshige, S. Tanaka and Y. Akagawa, *J Oral Rehabil*, 2004, 31, 568-573.
138. Y. Abe, M. Ueshige, M. Takeuchi, M. Ishii and Y. Akagawa, *Int J Prosthodont*, 2003, 16, 141-144.
139. J. Marra, A. G. Paleari, L. S. Rodriguez, A. R. P. Leite, A. C. Pero and M. A. Compagnoni, *Journal of Applied Oral Science*, 2012, 20, 643-648.
140. K.-Y. Nam, *The Journal of Advanced Prosthodontics*, 2014, 6, 207-214.
141. M. Z. Kassaee, A. Akhavan, N. Sheikh and A. Sodagar, *Journal of Applied Polymer Science*, 2008, 110, 1699-1703.
142. H. el-Charkawi, E. A. el-Said, H. M. Safouh and N. el-Raghi, *Egypt Dent J*, 1994, 40, 785-790.
143. T. Matsuura, Y. Abe, Y. Sato, K. Okamoto, M. Ueshige and Y. Akagawa, *Journal of Dentistry*, 1997, 25, 373-377.
144. H. Nikawa, T. Yamamoto, T. Hamada, M. B. Rahardjo, H. Murata and S. Nakanoda, *J Oral Rehabil*, 1997, 24, 350-357.
145. S. Imazato, Y. Kinomoto, H. Tarumi, M. Torii, R. R. Russell and J. F. McCabe, *J Dent Res*, 1997, 76, 768-772.
146. N. S. Yadav, S. Saraf, S. K. Mishra and P. Hazari, *J Nat Sci Biol Med*, 2015, 6, 340-342.
147. C. Fan, L. Chu, H. R. Rawls, B. K. Norling, H. L. Cardenas and K. Whang, *Dent Mater*, 2011, 27, 322-328.
148. L. S. Acosta-Torres, I. Mendieta, R. E. Nunez-Anita, M. Cajero-Juarez and V. M. Castano, *Int J Nanomedicine*, 2012, 7, 4777-4786.
149. D. T. Castro, R. D. Holtz, O. L. Alves, E. Watanabe, M. L. Valente, C. H. Silva and A. C. Reis, *J Appl Oral Sci*, 2014, 22, 442-449.
150. K.-Y. Nam, C.-H. Lee and C.-J. Lee, *Gerodontology*, 2012, 29, e413-e419.
151. T. R. Schneid, *Spec Care Dentist*, 1992, 12, 245-250.
152. J. Clayden, Greeves, N., Warren, S., and Wothers, *Organic Chemistry*, Oxford University Press., Oxford, 2007.
153. D. R. Paul and J. E. Mark, *Progress in Polymer Science*, 2010, 35, 893-901.
154. W. Li, F. Liu, L. Wei and T. Zhao, *European Polymer Journal*, 2006, 42, 580-592.
155. K. J. Saunders, *Organic Polymer Chemistry*, Chapman and Hall, London, Second Edition edn., 1988.
156. P. Jerschow, *Silicone Elastomers. Rapra Review Reports, Report 137: Volume 12, Number 5, 2001*, RAPRA, 2001.
157. J. F. M. a. A. W. G. Walls, *Applied dental materials*, Wiley-Blackwell, 9th ed edn., 2008.
158. K. J. Anusavice, *Philips' Science of Dental Materials*, Elsevier, St. Louis, Missouri, 2003.
159. R. O. Darouiche, *Clin Infect Dis*, 2001, 33, 1567-1572.
160. D. Kregiel, J. Berlowska, U. Mizerska, W. Fortuniak, J. Chojnowski and W. Ambroziak, *World J Microbiol Biotechnol*, 2013, 29, 1197-1206.
161. N. Clarkson and L. V. Evans, *Biofouling*, 1995, 9, 129-143.
162. S. Ye, A. McClelland, P. Majumdar, S. J. Stafslie, J. Daniels, B. Chisholm and Z. Chen, *Langmuir*, 2008, 24, 9686-9694.
163. B. Gottenbos, H. C. van der Mei, F. Klatter, P. Nieuwenhuis and H. J. Busscher, *Biomaterials*, 2002, 23, 1417-1423.
164. H.-S. Yang and E.-S. Park, *Macromolecular Materials and Engineering*, 2006, 291, 621-628.

165. S. L. Steffensen, M. H. Vestergaard, M. Groenning, M. Alm, H. Franzyk and H. M. Nielsen, *Eur. J. Pharm. Biopharm.*, 2015, 94, 305-311.
166. M. C. McBride, R. Karl Malcolm, A. David Woolfson and S. P. Gorman, *Biomaterials*, 2009, 30, 6739-6747.
167. L. L. Wang, T. Sun, S. Y. Zhou and L. Q. Shao, *Acta Physica Polonica A*, 2014, 125, 248-250.
168. D. R. Monteiro, L. F. Gorup, A. S. Takamiya, E. R. de Camargo, A. C. Filho and D. B. Barbosa, *J Prosthodont*, 2012, 21, 7-15.
169. D. T. de Castro, R. D. Holtz, O. L. Alves, E. Watanabe, M. L. da Costa Valente, C. H. Lovato da Silva and A. C. dos Reis, *Journal of Applied Oral Science*, 2014, 22, 442-449.
170. Y. Xie, C. A. S. Hill, Z. Xiao, H. Militz and C. Mai, *Composites Part A: Applied Science and Manufacturing*, 2010, 41, 806-819.
171. H. Demir, D. Balköse and S. Ülkü, *Polymer Degradation and Stability*, 2006, 91, 1079-1085.
172. D. E. Newbury, *Advanced scanning electron microscopy and x-ray microanalysis*, New York ; London, 1986
173. R. Schneider, 2011, pp. 293-310.
174. C. Hammond, *The basics of crystallography and diffraction*, Oxford, Third edition edn., 1942.
175. B. D. Cullity, *Elements Of X Ray Diffraction* Addison-Wesley Publishing Company, Inc., 1956.
176. T. J. Bandosz, *Journal of the American Chemical Society*, 2005, 127, 7655-7656.
177. F. J. H. Douglas A. Skoog , Stanley R. Crouch, *Principles of instrumental analysis*, David Harris, Sixth edition edn., 1998.
178. M. M. Beasley, E. J. Bartelink, L. Taylor and R. M. Miller, *Journal of Archaeological Science*, 2014, 46, 16-22.
179. J. R. Ferraro, K. Nakamoto and C. W. Brown, in *Introductory Raman Spectroscopy (Second Edition)*, ed. J. R. F. N. W. Brown, Academic Press, San Diego, 2003, pp. 1-94.
180. N. B. Colthup, L. H. Daly and S. E. Wiberley, in *Introduction to Infrared and Raman Spectroscopy (Third Edition)*, eds. N. B. Colthup, L. H. Daly and S. E. Wiberley, Academic Press, San Diego, 1990, pp. xi-xii.
181. P. Larkin, in *Infrared and Raman Spectroscopy*, ed. P. Larkin, Elsevier, Oxford, 2011, pp. ix-x.
182. H. Jans, X. Liu, L. Austin, G. Maes and Q. Huo, *Analytical Chemistry*, 2009, 81, 9425-9432.
183. R. Bottom, in *Principles and Applications of Thermal Analysis*, Blackwell Publishing Ltd, 2008, pp. 87-118.
184. J. M. Hollas and I. NetLibrary, *Modern spectroscopy*, Wiley, Chichester, 2004.
185. P. W. J. M. Boumans, *Inductively coupled plasma emission spectroscopy; Pt.1, Methodology, instrumentation and performance*, Wiley, New York, 1987.
186. J. R. Davis, *Tensile testing*, Second Edition edn., 2004.
187. G. M. Swallowe, *Mechanical Properties and Testing of Polymers*, Kluwer academic publishers, The Netherlands, 1999.
188. S. HOGG, *Essential microbiology* wiley, The university of Glamorgan, uk.
189. R. D. Inman, K. V. Gallegos, B. D. Brause, P. B. Redecha and C. L. Christian, *The American journal of medicine*, 1984, 77, 47-53.
190. M. T. McCann, B. F. Gilmore and S. P. Gorman, *J Pharm Pharmacol*, 2008, 60, 1551-1571.

191. J. N. Simon Baker, Naveed Khan, Richard Killington, *Microbiology*, Taylor & Francis, 2007.
192. T. M. Hamill, B. F. Gilmore, D. S. Jones and S. P. Gorman, *Expert Review of Medical Devices*, 2007, 4, 215-225.
193. J. E. Stajich, M. L. Berbee, M. Blackwell, D. S. Hibbett, T. Y. James, J. W. Spatafora and J. W. Taylor, *Current Biology*, 2009, 19, R840-R845.
194. M. J. McCullough, B. C. Ross and P. C. Reade, *International journal of oral and maxillofacial surgery*, 1996, 25, 136-144.
195. L. H. G. Emanuel Goldman, *Practical Handbook of Microbiology*, CRC Press, Third Edition edn., 2015.
196. R. M. Atlas, *Principles of microbiology*, Mosby, University of Louisville, Louisville, Kentucky, 1995.
197. L. M. Schwartz and B. A. Osborne, *Immunology Today*, 1993, 14, 582-590.
198. T. L. Riss, R. A. Moravec and A. L. Niles, *Methods Mol Biol*, 2011, 740, 103-114.
199. M. Ansari, A. Aroujalian, A. Raisi, B. Dabir and M. Fathizadeh, *Advanced Powder Technology*, 2014, 25, 722-727.
200. J. Zhu, Y. Zhu, L. Zhu, M. Rigutto, A. van der Made, C. Yang, S. Pan, L. Wang, L. Zhu, Y. Jin, Q. Sun, Q. Wu, X. Meng, D. Zhang, Y. Han, J. Li, Y. Chu, A. Zheng, S. Qiu, X. Zheng and F.-S. Xiao, *Journal of the American Chemical Society*, 2014, 136, 2503-2510.
201. B. Dong, S. Belkhair, M. Zaarour, L. Fisher, J. Verran, L. Tosheva, R. Retoux, J. P. Gilson and S. Mintova, *Nanoscale*, 2014, 6, 10859-10864.
202. S. Belkhair, M. Kinninmonth, L. Fisher, B. Gasharova, C. M. Liauw, J. Verran, B. Mihailova and L. Tosheva, *RSC Advances*, 2015, 5, 40932-40939.
203. R. J. Garland, N. El-Shanti, S. E. West, J. P. Hancock, N. J. Goulden, C. G. Steward and A. W. Rowbottom, *Scandinavian Journal of Immunology*, 2002, 55, 61-69.
204. N. Al-Shanti and C. E. Stewart, *Journal of Cellular Biochemistry*, 2012, 113, 923-933.
205. X.-W. Zhang and C. Q. and Bin Xu, *Anti-Cancer Drugs*, 1999, 10, 569-576.
206. R. C. Tilton and B. Rosenberg, *Applied and environmental microbiology*, 1978, 35, 1116-1120.
207. Zhengbing Cao, Xinbo Sun, Yuyu Sun and Hao Fong, *Journal of Bioactive and Compatible Polymers*, 2009, 24, 350-367.
208. S. Y. Liau, D. C. Read, W. J. Pugh, J. R. Furr and A. D. Russell, *Lett Appl Microbiol*, 1997, 25, 279-283.
209. C. Daniel, A. Elbaraoui, S. Aguado, M.-A. Springuel-Huet, A. Nossov, J.-P. Fontaine, S. Topin, T. Taffary, L. Deliere, Y. Schuurman and D. Farrusseng, *The Journal of Physical Chemistry C*, 2013, 117, 15122-15129.
210. W. H. Baur and *Am. Mineral*, 1964, 49, 697-704.
211. S. Yi, Y. Su and Y. Wan, *Journal of Membrane Science*, 2010, 360, 341-351.
212. Q. Y. a. Y. Zhou, *J. Inorg. Organomet. Polym*, 2009, 19, 215-222.
213. S. Inagaki, K. Thomas, V. Ruaux, G. Clet, T. Wakihara, S. Shinoda, S. Okamura, Y. Kubota and V. Valtchev, *ACS Catalysis*, 2014, 4, 2333-2341.
214. S. Y. Kim, Y. Kim and K. Seff, *The Journal of Physical Chemistry B*, 2003, 107, 6938-6945.
215. J. Catafesta, F. Alabarse, C. Levelut, A. Isambert, P. Hebert, S. Kohara, D. Maurin, J.-L. Bantignies, O. Cambon, G. Creff, P. Roy, J.-B. Brubach, T. Hammouda, D. Andrault and J. Haines, *Physical Chemistry Chemical Physics*, 2014, 16, 12202-12208.
216. L. Tosheva, B. Mihailova, V. Valtchev and J. Sterte, *Microporous and Mesoporous Materials*, 2000, 39, 91-101.
217. S. G. Aspromonte, M. D. Mizrahi, F. A. Schneeberger, J. M. R. López and A. V. Boix, *The Journal of Physical Chemistry C*, 2013, 117, 25433-25442.

218. A. Muñoz-Bonilla and M. Fernández-García, *Progress in Polymer Science*, 2012, 37, 281-339.
219. M. Hashiguchi, Y. Nishi, T. Kanie, S. Ban and E. Nagaoka, *Dent Mater J*, 2009, 28, 307-314.

Appendices

Appendix 1

Publications and presentations based on the results presented in this thesis

1. S. Belkhair, M. Kinninmonth, C. Liauw, J. Verran and L. Tosheva, Functionalised silver-zeolites for antibacterial applications, 36th BZA meeting, Keele, 8-10 April 2013 (Poster presented).
2. S. Belkhair, M. Kinninmonth, C. Liauw, J. Verran and L. Tosheva, Functionalised silver-zeolites for antibacterial applications, Manchester Metropolitan University Annual Research Student conference, April 2013 (Poster presented).
3. B. Dong, S. Belkhair, M. Zarrour, L. Fisher, J. Verran, L. Tosheva and S. Mintova, Ultra-small silver-EMT nanoparticles: synthesis and antibacterial properties, 6th International FEZA Conference, Leipzig, 8-11 September 2014 (Poster presented)
4. S. Belkhair, M. Kinninmonth, L. Fisher, C. Liauw, J. Verran and L. Tosheva, Functionalised silver-zeolites for polymer composite fabrication, 6th International FEZA Conference, Leipzig, 8-11 September 2014. (Poster presented)
5. S. Belkhair, B. Dong, M. Zaarour, L. Fisher, J. Verran, L. Tosheva, R. Retoux, J. P. Gilson and S. Mintova, Silver confined within zeolite EMT nanoparticles: preparation and antibacterial properties, *Nanoscale*, 2014, 6, 10859-10864.
6. S. Belkhair, M. Kinninmonth, L. Fisher, B. Gasharova, C. M. Liauw, J. Verran, B. Mihailova and L. Tosheva, Silver zeolite-loaded silicone elastomers: a multidisciplinary approach to synthesis and antimicrobial assessment, *RSC Advances*, 2015, 5, 40932-40939.

Cite this: *Nanoscale*, 2014, 6, 10859

Silver confined within zeolite EMT nanoparticles: preparation and antibacterial properties†

B. Dong,^{ab} S. Belkhair,^c M. Zaarour,^a L. Fisher,^c J. Verran,^c L. Tosheva,^{ac} R. Retoux,^d J.-P. Gilson^a and S. Mintova^{a*}

The preparation of pure zeolite nanocrystals (EMT-type framework) and their silver ion-exchanged (Ag^+ -EMT) and reduced silver (Ag^0 -EMT) forms is reported. The template-free zeolite nanocrystals are stabilized in water suspensions and used directly for silver ion-exchange and subsequent chemical reduction under microwave irradiation. The high porosity, low Si/Al ratio, high concentration of sodium and ultrasml crystal size of the EMT-type zeolite permitted the introduction of a high amount of silver using short ion-exchange times in the range of 2–6 h. The killing efficacy of pure EMT, Ag^+ -EMT and Ag^0 -EMT against *Escherichia coli* was studied semi-quantitatively. The antibacterial activity increased with increasing Ag content for both types of samples (Ag^+ -EMT and Ag^0 -EMT). The Ag^0 -EMT samples show slightly enhanced antimicrobial efficacy compared to that of Ag^+ -EMT, however, the differences are not substantial and the preparation of Ag nanoparticles is not viable considering the complexity of preparation steps.

Received 9th June 2014
Accepted 16th July 2014

DOI: 10.1039/c4nr03169e

www.rsc.org/nanoscale

Introduction

The introduction of antimicrobials to a vast range of materials, including medical devices, food packaging, clothing and toiletries, for purposes of reducing infection or deterioration, or for hygienic and mechanical reasons has been widely researched. Antibacterial inorganic materials present important advantages over traditionally used organic agents due to their chemical and thermal stability allowing for flexible processing during preparation of nanocomposites, alloys, coatings and other complex structures.^{1,2} Amongst them, silver, with its broad spectrum of antimicrobial properties, has become one of the most intensively studied systems.³ There have been a certain degree of controversy in mechanistic studies of silver toxicity because of the huge variations in antibacterial tests/silver systems used.⁴ The antibacterial effect of silver has been associated with the release of silver ions in aqueous solutions causing plasmolysis after entering the bacterial cell and partial disruption of the cytoplasmic membrane and affecting the DNA

replication ability.⁵ Direct damage of the bacterial cell walls and accumulation of silver in the membrane have been demonstrated by Sondi and Salopek-Sondi.⁶ The bactericidal effect of silver nanoparticles has also been found to be dependent on the nanoparticle size.⁷ Silver nanoparticles with sizes below 10 nm were found to directly interact with bacterial cells. Further, it has been demonstrated that the activity of silver nanoparticles was due to the aerobic release of silver ions and that Ag^0 did not have any bactericidal properties.^{8–10}

In many cases, slow release of silver ions over long periods of time is required to ensure sustainable antibacterial efficacy conforming to the requirements of the specific application. For long-term antibacterial applications, silver is usually incorporated into matrices, such as zeolites. Zeolites are microporous crystalline aluminosilicates, composed of TO_4 tetrahedra ($T = \text{Si}$ or Al) linked to each other by oxygen ions. Each AlO_4 tetrahedron brings a net negative charge, which is balanced by a cation. The channels or interconnected voids of the framework are occupied by cations, which can readily be exchanged by silver via ion-exchange post-synthesis treatment. Recently, a procedure to optimise the ion-exchange conditions to yield a high silver loading in the zeolite was reported.¹¹ In aqueous medium, silver ions can be released and act as an antimicrobial.¹² The stabilisation of Ag within the zeolite matrix has resulted in enhanced antifungal activity in comparison with free Ag ions.¹³ The antibacterial properties of Ag-zeolites have been found to depend on various factors such as the physical form of the zeolite host (e.g., powder, granules or pellets),¹⁴ the zeolite pore architecture¹⁵ and the silver form (Ag^+ or Ag^0).¹⁶ Although several studies have reported the antibacterial properties of

*Laboratoire Catalyse & Spectrochimie, University of Caen, CNRS, 6, boulevard du Maréchal Juin, 14050 Caen Cedex, France. E-mail: svetlana.mintova@ensicam.fr

^aState Key Laboratory on Integrated Optoelectronics, College of Electronic Science and Engineering, Jilin University, Changchun 130012, P. R. China^cFaculty of Science and Engineering, Manchester Metropolitan University, Chester St, Manchester, M1 5GQ, UK. E-mail: L.tosheva@mmu.ac.uk^dCRISMAT, ENSICAM, University of Caen, 6, boulevard du Maréchal Juin, 14050 Caen Cedex, France

† Electronic supplementary information (ESI) available: Zeta potential data of Ag-EMT suspensions, pore-size distributions and antibacterial data for Ag-EMT 2 h samples. See DOI: 10.1039/c4nr03169e

Cite this: *RSC Adv.*, 2015, 5, 40932

Silver zeolite-loaded silicone elastomers: a multidisciplinary approach to synthesis and antimicrobial assessment†

Sama Belkhair,^a Malcolm Kirminmonth,^a Leanne Fisher,^a Biliana Gasharova,^b Christopher M. Liauw,^a Joanna Verran,^a Boriana Mihailova^c and Lubomira Tosheva^{a*}

A multidisciplinary approach has been applied to the preparation of antibacterial Ag zeolite/silicone elastomer composites aimed at products that satisfy a range of requirements, namely good mechanical properties after zeolite incorporation and strongly antibacterial. Zeolite X was synthesised and used as antibacterial agent after ion-exchange with silver. The high level of silver (14 wt%) within the zeolite enabled the preparation of antibacterial composites containing a relatively low level of zeolite (2 wt%). The composites showed strong efficacy against *Escherichia coli* and *Staphylococcus epidermidis*. Organic functionalization of the zeolite with organo-silanes prior blending with the matrix usefully improved composite mechanical properties and reduced color development in Ag zeolite containing silicone elastomers. Organo-silane modification did not substantially affect the antibacterial performance of the materials; the number of viable cells of both Gram-positive and Gram-negative bacteria was reduced to beyond detection limits within 24 hours of incubation. Efficacy of the Ag zeolite containing composites against the yeast *Candida albicans* was found to be substantially less than observed with the two bacteria. This study demonstrates that evaluation of polymer composites needs to be performed via a multidisciplinary approach in order to avoid compromising a particular aspect of the materials' design, characteristics or performance, including the use of reliable testing methods to determine the latter.

Received 4th March 2015
Accepted 29th April 2015
DOI: 10.1039/c5ra03856a
www.rsc.org/advances

Introduction

The use of medical devices has become an essential part of modern day medicine and as a consequence, microbial infections resulting from bacterial adhesion and colonization to biomaterial surfaces is of major concern. The continuously increasing levels of antibiotic resistance have prompted research into adding therapeutic antimicrobials to medical devices with long-term activity to prevent infections.¹ Zeolites are excellent candidates for such applications. They can be exchanged with metal antimicrobials, they are chemically and thermally stable, their pore structure facilitates the slow release of antibacterial metals and also there is a possibility for regeneration upon metal depletion by secondary ion-exchange.

Silver is a well-known antibacterial agent with an ability to act on a broad spectrum of organisms.² Silver is also the most popular metal of choice for preparation of antibacterial zeolites. The Ag leaching and the antimicrobial activity of Ag-exchanged zeolite A over a 12 month period has been studied by Yan and co-workers.³ The study demonstrated that Ag zeolite coatings retained their antibacterial activity after 12 months submersion in distilled water and that they were capable of killing *Escherichia coli* (*E. coli*) upon repeated exposures. The killing efficacy of Ag zeolites has been found to depend not only on the silver content but also on the geometry of zeolite pores.⁴ Zeolites with a three-dimensional pore system showed superior antibacterial activity compared to one-dimensional zeolites, probably due to the hindered release of Ag in the latter. Further, the antibacterial properties of Ag exchanged into zeolites having the same structure (FAU-type) have been found to differ depending on the Si/Al ratio.⁵ Ag-exchanged zeolite Y (Si/Al ratio = 2.83) displayed lower minimum inhibitory concentration against bacteria compared to zeolite X (Si/Al ratio = 1.64), both containing similar Ag loading of 9.7 wt% and 9.8 wt%, correspondingly. This result was attributed to the presence of metallic silver in zeolite X. The bactericidal activity of Ag zeolites has also been found to depend on the zeolite physical form, namely powders or zeolite aggregates.⁶ Although Ag zeolites of very low Ag

*Faculty of Science and Engineering, Manchester Metropolitan University, Chester St, Manchester, M1 5GD, UK. E-mail: Ltosheva@mmu.ac.uk; Fax: +44 (0)161 2476940; Tel: +44 (0)161 2471426

^bInstitute for Photon Science and Synchrotron Radiation, Karlsruhe Institute of Technology, P.O. Box 3640, Karlsruhe 76021, Germany

^cMineralogisch-Petrographisches Institut, Universität Hamburg, Grindelallee 48, D-20146 Hamburg, Germany

† Electronic supplementary information (ESI) available: Nitrogen adsorption isotherms and DRIFT spectra of NaX, AgX and silane-modified AgX samples. See DOI: 10.1039/c5ra03856a